Receptor mediated gene delivery using targeted liposomes and Quantum Dots

Dissertation
zur Erlangung des Doktorgrades
der Mathematisch-Naturwissenschaftlichen Fakultäten
der Georg-August-Universität zu Göttingen

vorgelegt von
Valeria Sigot
aus Rosario, Argentinien

Göttingen, 2008

D7

Referent: Prof. Dr. Hans-Joachim Fritz

Korreferent: Prof. Dr. Rüdiger Hardeland

Tag der mündlichen Prüfung: 02.07.08

Summary

The design of liposomal carriers for gene or drug delivery is an active field in current biomedical research. An important issue is the targeting of the carriers to specific cell types for which the therapeutical approach is intended.

The combination of liposomes and imaging probes such as Quantum Dots (QDs) in a single nanoparticle offers an excellent tool for increasing the understanding of the mechanisms of liposome uptake thereby increasing the efficiency of gene or drug delivery.

In the research developed in this thesis, biotinylated lipid particles (BLP) were loaded with plasmid DNA and labeled on the surface with QDs functionalized with the ligand EGF (Epidermal Growth Factor). In a second and novel approach, BLP were loaded with a red emitting QD_{655} and surface coated with a green emitting QD_{525} tagged with the EGF ligand. This latter approach was intended to monitor the specificity of BLP binding and uptake in live cells by fluorescence confocal microscopy. Both types of BLP were targeted to A431 cells, a cancer cell line that overexpresses the EGF receptor (EGFR). Furthermore, BLP formulations differing in the content of the protective polymer PEG (polyethylene glycol) were tested in order to optimize the intracellular delivery of plasmid DNA or QDs.

The colocalization of green emitting QD_{525} and red emitting QD_{655}, allowed the immediate discrimination of the targeted BLP from the untargeted counterparts, as well as the presence of free EGF-QD_{525} complexes during live cell imaging. EGFR-targeted BLP showed increased binding and accelerated uptake as compared to EGF-free BLP. Cellular binding of targeted BLP was further associated with the perinuclear localization of QDs in clusters which persisted over days, indicating the difficulty in releasing the encapsulated nanoparticles from endo-lysosomal vesicles. On the other hand, targeted BLP with encapsulated plasmid carrying the reporter gene for the Green Fluorescent Protein (GFP) showed enhanced transfection of A431 cells compared to that exhibited by non-targeted particles for all lipid formulations tested, indicating the occurrence of plasmid release in the cytoplasm. No targeting effect, however, was evident in cells devoid of EGF receptor or in the receptor occupied by competing free ligand, indicating that enhanced EGFR-targeted delivery is primarily mediated via a ligand/receptor interaction.

From a therapeutic point of view, the specificity displayed by the BLP labeled with two colors of QDs and targeted to tumor cells overexpressing the EGF receptor may provide a platform for testing the specific delivery of tumorigenic drugs. This approach was also intended to elucidate the fate of lipid particles in real time, taking advantages of the photostability and bright fluorescence of QDs.

The designed BLP will provide refined information about the still poorly understood trafficking processes and the subcellular barriers to gene or drug delivery via liposomal carriers.

Table of contents

Abbreviations 1

1. Introduction and aims of the thesis 3

1.1. Molecular therapy 5
1.1.1. Gene delivery 5
1.2. Viral and non-viral gene delivery systems 6
1.2.1. Viral vectors 6
1.2.2. Non-viral vectors 7
1.3. Lipid-based delivery systems 8
1.3.1. Components of lipid-based nanoparticles 8
1.3.2. Sterically Stabilized Liposomes 9
1.3.3. Stabilized Plasmid-Lipid Particles (SPLP) 10
1.4. Cell mechanisms of liposome uptake 11
1.4.1. Receptor-mediated endocytosis as a route for targeted liposomal delivery 13
1.4.2. EGF receptor targeted delivery systems 14
1.5. Fluorescent nanoparticles in live-cell imaging 14
1.5.1. Applications for lipid-based delivery systems 14
1.5.2. Long-term imaging using Quantum Dots 15
1.5.3. Ligand tagged Quantum Dots 16
1.6. Aims and organization of the thesis 18

2. Materials and methods 21

2.1. Reagents 23
2.1.1. Lipids 23
2.1.2. Biotin and biotin-related reagents 24
2.1.3. Buffers 24
2.1.4. Quantum Dots 24
2.1.5. Labeled proteins and organic fluorophores 24
2.1.6. Plasmid DNA 25
2.1.7. *bis*-PNA (*bis* Peptide Nucleic Acid) 25
2.1.8. Restriction endonucleases and DNA standards 25
2.2. Cell lines, media and labware 25
2.3. Miscellaneous 25
2.4. Equipments and softwares 26
2.5. Preparation of Biotinylated Lipid Particles (BLP) 27
2.5.1. Detergent dialysis technique 27
2.5.2. Ultracentrifugation in sucrose density gradient 28
2.5.3. Particle size analysis by Dynamic Light Scattering 28
2.5.4. DNA quantitation 29
2.5.5. Biotin quantitation 30
2.5.6. Transmission Electron Microscopy 31
2.6. Labeling and targeting of BLP 32
2.6.1. EGF-QDs preformed complexes 32
2.6.2. EGF-QDs coupling to BLP 32
2.7. Live-cell experiments 33
2.7.1. Cell culture 33
2.7.2. Experimental conditions for the incubation of A431 cells with BLP 33
2.7.3. Incubation of EGF-QDs and Transferrin-Alexa$_{488}$ complexes with A431 cells 33
2.7.4. Competitive binding assay 34
2.7.5. Experimental conditions for targeted gene delivery by BLP 34
2.8. Confocal fluorescence microscopy 35
2.8.1. Simultaneous detection of two different colors of QDs 35
2.8.2. Colocalization analysis 35
2.9. Quantitative GFP expression analysis 36

2.9.1. Epi-fluorescence microscopy 36
2.9.2. Flow cytometry 37
2.10. *bis*-PNA:DNA Hybrids 38
2.10.1. Plasmid DNA amplification and purification 38
2.10.2. Biotinylation of *bis*-PNA 38
2.10.3. Cy5 labeling of *bis*-PNA 38
2.10.4. Hybridization of *bis*-PNA to pEGFP-C1 plasmid 38
2.10.5. QD labeling of Hybrids 39
2.10.6. Restriction fragment analysis by gel electrophoresis 39
2.10.7. Conjugation of QD-Hybrids to biotin coated magnetic beads 40
2.11. Atomic Force Microscopy analysis 40
2.11.1. Sample preparation for scanning 41

3. Results: "Characterization of Biotinylated Lipid Particles" 43

3.1. Encapsulation of plasmid DNA and QDs in BLP 45
3.1.1. BLP formulations 45
3.1.2. Time course formation of BLP during detergent dialysis 46
3.1.3. BLP-DNA purification from non-encapsulated DNA 47
3.1.4. Effect of PEG content in DNA encapsulation efficiency and particle size 49
3.1.5. BLP size analysis by AFM 50
3.1.6. Encapsulation of QDs in BLP by the detergent dialysis method 51
3.1.7. Characterization of fluorescent BLP-QDs 52

4. Results: "Cell uptake of EGFR targeted and QDs-labeled BLP" 55

4.1. Targeting and labeling of BLP 57
4.1.1. Cell uptake of targeted BLP-QDs 58
4.1.2. Intracellular distribution of internalized BLP 59
4.1.3. Time course of BLP internalization 60
4.1.4. EGFR targeted BLP follow the route of EGF-QDs complexes 62
4.1.5. Intracellular fate of QDs encapsulated in targeted BLP 64
4.2. Receptor specificity of targeted BLP 65
4.2.1. Competitive assay 65
4.2.2. Interaction of BLP with EGFR-negative cells 66
4.3. Delivery and transfection abilities of targeted and QDs labeled BLP-DNA 67
4.3.1. Intracellular fate of dual-labeled and targeted BLP-DNA 67
4.3.2. Transfection competency of dual-labeled and targeted BLP-DNA 69
4.3.3. BLP targeting in a two-step procedure 70

5. Results: "Single Quantum Dot labeling of plasmid DNA" 73

5.1. *bis*-PNA strand invasion of supercoiled plasmids 75
5.2. Quantum Dot labeling of biotin-*bis*-PNA: plasmid DNA Hybrids 77
5.2.1. Specificity of single QD labeling revealed by AFM 78
5.2.2. Visualization of Hybrids and QD:Hybrids complexes on magnetic beads 79

6. Discussion 83

6.1. PEGylated and Biotinylated Lipid Particles 86
6.2. Single step conjugation for targeting and labeling of BLP 87
6.3. Non-covalent Quantum Dot labeling of plasmid DNA 90
6.4. Rational liposome design 91

7. Conclusions 93

References 97

Acknowledgments 105

Publications related to this thesis project 106

Lebenslauf 107

Abbreviations

AFM	Atomic Force Microscopy
a.u.	arbitrary units
BLP	Biotinylated Lipid Particles
bp	base pair
BP	Band pass filter (optics)
BSA	Bovine serum albumin
CCD	Charged-coupled device
CHO	Chinese hamster ovary cell line
CLSM	Confocal Laser Scanning Microscopy
cmc	critical micellar concentration
DIC	Differential interference contrast
DLS	Dynamic Light Scattering
DMEM	Dulbecco modified Eagle medium
DNA	Deoxyribonucleic acid
DOPE	Dioleoyl-L-a-phosphatidylethanolamine
DOTAP	1,2-Dioleoyloxy-3-(trimethylammonio)-propane
DSPE	Distearoyl-L-a-phosphatidylethanolamine
EDTA	Ethylenediamine tetraacetic acid
EGF	Epidermal growth factor
EGFR	Epidermal growth factor receptor
ex./em.	excitation/emission wavelengths
FCS	Fetal calf serum
g	gravitational field centrifugation unit
GFP	Green fluorescent protein
HBS	HEPES buffered saline
HEPES	N-(2-hydroxyethyl)piperazine-N´-(2-ethanesulfonic acid)
kDa	kilodalton
LB	Luria Bertani growth medium
LP	Long pass filter (optics)
mM, µM, nM	millimolar, micromolar, nanomolar
min, h	minute, hour
MWCO	Molecular Weight Cut-off
NA	Numerical aperture
OGP	Octylglucopyranoside
PBS	Phosphate buffered saline
pdi	Polydispersity index
PEG	Polyethyleneglycol

PEG-Cer-C20	PEG-Ceramide bioconjugate with an arachidoyl acyl group
PEG-Cer-C8	PEG-Ceramide bioconjugate with an octanoyl acyl group
PEG-DSGS	PEG-[succinoyl]-1,2-distearoyl-*sn*-glycerol
pH	Negative decadic logarithm of the hydrogen ion (H+) concentration
PNA	Peptide nucleic acid
QD	Quantum dot
RT	Room temperature
SPLP	Stabilized Plasmid Lipid Particles
StAv	Streptavidin
t	time
TEM	Transmission Electron Microscopy
UV	Ultraviolet

1. Introduction and aims of the thesis

1.1. Molecular therapy

The genomic information obtained through the Human Genome Project has accelerated enormously the analysis of the functions of various disease relevant genes as well as the design of therapeutic molecules and delivery systems (Hicks, 2003; Austin, 2004).

Biomolecules, such as sense and antisense oligonucleotides, small interference RNAs and peptides, as well as entire genes (cDNA) and proteins are essential tools in the development of molecular therapies (Shi and Hoekstra, 2004; Wagner, 2007). However, the potential of such information-rich macromolecules for therapeutic use has been limited by the difficulties in delivering them specifically to target tissues *in vivo* and in discriminating between disease-affected and normal cells.

A variety of viral and non-viral vehicles have been conceived to effect the encapsulation, *in vivo* cell targeting and intracellular delivery of therapeutic macromolecules (Maurer *et al.*, 1999; Gupta *et al.*, 2005; Torchilin, 2006). However, the hostile extracellular environment constitutes a primary challenge in the systemic delivery of gene or drug carriers to intracellular targets. This presents a number of barriers, such as extreme pH, proteases and nucleases and the immune defence and scavenger systems (Figure 1.1). Once the carrier reaches the target tissue, the efficient cell binding, uptake and delivery of the cargo into and within subcellular compartments is critical for gaining the desired therapeutic effect. At this stage, the cell membrane is the main physical barrier due to the poor permeability of the lipid bilayer, where the diffusion rate is highly dependent on the size and hydrophobicity of the molecular carrier. Therefore, the rational design of intracellular gene/drug delivery vehicles requires a better understanding of the cell membrane barrier (Belting *et al.*, 2005).

1.1.1. Gene delivery

The realization that nucleic acids could be used as therapeutic agents to alter the expression and function of proteins in the body has given an immense boost to transfection biology. Gene therapy is a part of the growing field of molecular medicine gaining significance in the treatment of human diseases. By delivering genes into cells to regulate or supplement defective genetic loci, the morbidity of inherited and acquired diseases can be alleviated (Civin, 2000; Edelstein *et al.*, 2007).

In most procedures to date, nucleic acids have been encapsulated in vehicles that both protect the therapeutic gene and allow its extracellular and intracellular trafficking. Most DNA delivery systems operate at one of three general levels: DNA condensation and complexation, endocytosis, and nuclear membrane translocation (Luo and Saltzman, 2000). Negatively charged DNA molecules are usually condensed and/or complexed with cationic lipids or polymers before the delivery into cells. These complexes are taken up by cells usually through an endocytic mechanism, which determines subsequent DNA release, trafficking, lifetime and function in the cell (Guy *et al.*, 1995).

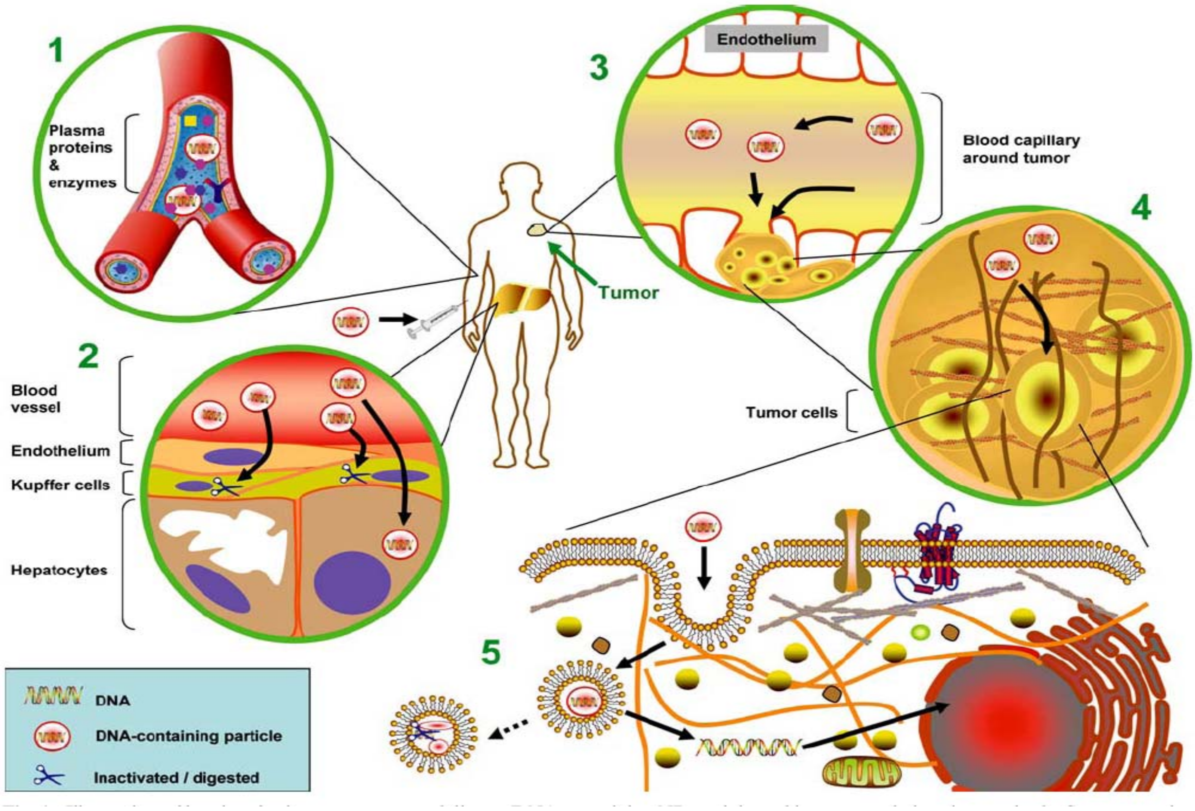
1
Plasma proteins & enzymes
2
Blood vessel
Endothelium
Kupffer cells
Hepatocytes
3
Endothelium
Blood capillary around tumor
Tumor
4
Tumor cells
5
DNA
DNA-containing particle
Inactivated / digested

Figure 1.1: Illustration of barriers for systemic gene delivery. DNA-containing nanoparticles are injected intravenously into human body. Serum proteins may bind to the particles, crosslink them and increase the particle size. This can result in rapid particle elimination (Insert 1). The Kupffer cells (RES) may take up particles, leading to rapid nanoparticles elimination from circulation and decrease their access to the hepatocytes (Insert 2). Circulating nanoparticles may extravasate in tumor tissue through the leaky tumor vessels (Insert 3). Particles then need to pass through the crowded extracellular matrix to contact the cell surface (Insert 4). When the particles are internalized into cells, DNA must escape from the endosome and find its way into the nucleus (Insert 5). Adapted from (Weijun Li, 2007).

1.2. Viral and non-viral gene delivery systems

1.2.1. Viral vectors

Viruses in nature have evolved an exceptional ability for delivering their genome into cells, responding to changes in the cellular environment and gaining access to their desired intracellular compartments (Vives *et al.*, 2006).

A number of different viruses, such as retrovirus, adenovirus, adeno-associated virus and herpes virus have been widely studied in gene transfer systems attracting the most attention in the field of transduction (Zhang and Godbey, 2006). Retroviral vectors were the first viral vectors to enter clinical trials and continue to be attractive candidates for applications where integration of the transgene is required (Cornetta K, 2008).

Virus-based vectors are modified by removing certain viral genes associated with pathogenic function. Other approaches mimic the viral machinery required for cell binding and internalization by coupling modified proteins from the viral capside to the surface of therapeutic carriers (Boeckle and Wagner, 2006). In fact, more than 70% of recent clinical protocols involving gene therapy use recombinant virus-based vectors for DNA delivery (Cornetta K, 2008). However, these delivery systems are restricted by their limited DNA carrying capacity, toxicity and potential oncogenicity, factors that hamper their routine use in basic research laboratories (Anderson, 1998; Boeckle and Wagner, 2006).

1.2.2. Non-viral vectors

Synthetic non-viral vectors have many potential advantages over viral ones, including a size-independent delivery of nucleic acids ranging from oligonucleotides to artificial chromosomes, significantly reduced toxicity and immunogenicity, and lower potential for oncogenicity (Luo and Saltzman, 2000). Additionally, they involve less demanding quality controls, and less complex pharmaceutical and regulatory requirements. However, these reagents still demonstrate reduced transfection efficiencies and transient levels of gene expression compared to the viral vehicles (Lechardeur *et al.*, 2005; Mehier-Humbert and Guy, 2005).

Non-viral approaches include physical methods for introducing naked DNA directly into the cell, such as particle bombardement, microinjection and electroporation (Chou *et al.*, 2004; Mehier-Humbert and Guy, 2005). The drawbacks of these systems are the limited number of cells that can be treated and the possible physical damage to the cell membrane.

Widespread approaches involve chemical methods to enable the cellular uptake of insoluble or highly charged macromolecules. Chemical carriers are based on peptides, lipids and phospholipids mixtures as well as polymers (Kramer et al., 2004; Kneuer et al., 2006) which form complexes with the cargo molecules such as drugs or DNA. In these delivery systems, the cargo does not get into contact with the cell surface molecules, so that unspecific interactions are omitted. Chemical carriers enhance the uptake of macromolecules by facilitating either direct cell translocation (Merkleb, 2004) or endocytosis (Hoekstra et al., 2007). Lipid or polymer-based delivery systems have now become the major tools to introduce not only nucleic acids but also proteins, peptides and nanoparticles into cultured cells.

The scope of non-viral delivery systems have been expanded by the incorporation of environment-sensitive polymers, carefully designed to take advantage of intracellular changes in pH and temperature in order to achieve a controlled release of the therapeutic molecule (Heath *et al.*, 2007). Furthermore, to achieve active transport of DNA through the nuclear pore complex, nuclear localizing signal (NLS) peptides have been widely used (Branden *et al.*, 2001; Simonson *et al.*, 2005). In most cases, NLS is conjugated with a gene carrier such as polyethylenimine (PEI) or with DNA directly.

1.3. Lipid-based delivery systems

The most studied and widespread non-viral approaches for deliverying DNA have been those based on lipids. A breakthrough was achieved when Felgner reported for the first time that complexes of plasmid DNA and the cationic lipid dioleyl-trimethylammmonium chloride (DOTMA) at a 1:1 molar ratio with dioleoylphosphatidylethanolamine (DOPE), were avidly internalized by cells and caused profound expression of the plasmid (Felgner *et al.*, 1987).

Cationic lipid/nucleic acid complexes or lipoplexes have been the subject of intensive investigation in recent years. The main focus has been the characterization of the molecular mechanisms of lipid-vector and cell membrane interaction, essential for overcoming intracellular barriers (Felgner and Ringold, 1989; Simoes *et al.*, 2005; Wasungu and Hoekstra, 2006; Hoekstra *et al.*, 2007).

Originally developed for the transfection of DNA, lipid vectors have become the major tools for introducing not only a variety of nucleic acids but also proteins, peptides and nanoparticles into cells *in vitro* and *in vivo* (Maurer *et al.*, 1999; Audouy and Hoekstra, 2001; Torchilin *et al.*, 2003).

The other major field of lipid-based delivery systems arose from the observation that phospholipids in aqueous systems can form closed bilayered structures, known as liposomes (Lasic and Papahadjopoulos, 1995). These particles comprising an outer lipid layer membrane surrounding and internal aqueous space can be loaded with therapeutic biomolecules (Mayer *et al.*, 1989). Liposomes can encapsulate and facilitate the delivery of plasmid DNA containing therapeutic genes with sizes of several kilobases (Fenske and Cullis, 2005).

Liposomes represent a flexible platform for encapsulation since they can range from multilamellar vesicles (MLVs) with diameters of several microns to small unilamellar vesicles (SUV) of about 20 nm. For biomedical applications, particles with the greatest utility have diameters of ~100 nm, large enough to carry a significant payload but small enough to ‘slip’ between leaky endothelial junctions escaping the immune system surveillance (Szoka and Papahadjopoulos, 1980).

1.3.1. Components of lipid-based nanoparticles

Usually, the nanosized lipid particles are constructed from a combination of synthetic and natural lipids, lipopolymers and pH or reduction-sensitive components. For most of these lipid-based particles, cationic lipids are the key elements used to package the DNA (Zuidam and

Barenholz, 1999). An added advantage of the cationic lipids is that they can bind to negatively charged mammalian cell membranes inducing the uptake of the associated nucleic acid into cells. Neutral lipids such as the fusogenic lipid 1,2-dioleoyl-sn-glycero-3-phosphoethanolamine (DOPE) and cholesterol are usually used as helper lipids which may increase transfection activity of the DNA-containing lipid-based carrier (Hafez and Cullis, 2001). For example, DOPE has a phosphoethanolamine head group whose size is smaller than its hydrophobic diacyl chain facilitating membrane fusion and disruption, and consequently the DNA release (Zuhorn *et al.*, 2005).

1.3.2. Sterically Stabilized Liposomes

The fast and efficient clearance of conventional liposomes from the circulation by macrophages has seriously compromised their application for the treatment of a wide range of diseases involving other organs. The incorporation of the hydrophilic and biocompatible polymer polyethylene glycol (PEG) improved the lifespan of liposomes in the bloodstream and reduced cell toxicity, leading to a renewed interest in liposomal carriers during the 90' (Lasic *et al.*, 1991). PEG has been covalently linked to natural and synthetic lipids, which were subsequently incorporated into liposome formulations (Bhadra *et al.*, 2002). The PEG polymer acts like a shield protecting the encapsulated therapeutic agent from enzymatic degradation, rapid renal clearance and interactions with cell surface proteins, thereby minimizing adverse immunological effects (Woodle and Lasic, 1992). Figure 1.2 schematically depicts a conventional liposome and the advanced sterically stabilized liposome surface-coated with PEG.

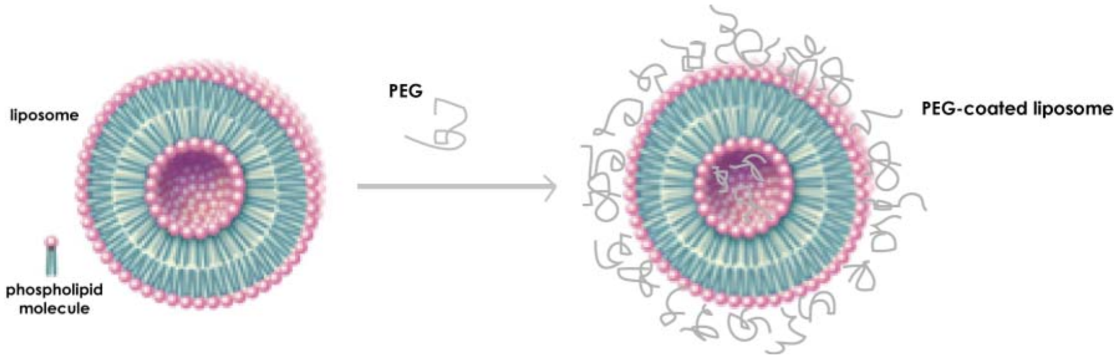

Figure 1.2: Schematic representation of a conventional liposome and a sterically stabilized PEG-liposome. Adapted from Encyclopedia Britannica (online).

'Pegylation' is now established as the method of choice for improving the pharmacokinetics and pharmacodynamics of liposomes. However, once the liposomal carrier reaches the cell surface, pegylation may interfere for instance with the endocytic mechanism of uptake by either lowering the binding affinity to cell receptors or by preventing the intermembrane contact between liposomal surface and endosomal

membranes, required to release the cargo in the cytoplasm (Shi *et al.*, 2002; Song *et al.*, 2002). Therefore, PEG-lipids included in liposomal formulations should dissociate from the complex, once the liposome is in close contact with endosomes upon internalization. This has been accomplished by incorporating a short acyl chain lipid-PEG to the liposome formulation with the ability to promote within minutes the lipid transfer from the liposome bilayer (Harvie *et al.*, 2000). Alternatively, by adding a cleavable, pH-sensitive PEG analogue in which the polymer moiety is cleaved off upon exposure to the acidic environment of certain endosomal compartments (Kirpotin *et al.*, 1996; Guo and Szoka, 2001; Shi *et al.*, 2002; Choi *et al.*, 2003; Guo *et al.*, 2003).

Current development is focused on combining long-term circulating (Lasic *et al.*, 1999) and targeted liposomes (Sofou and Sgouros, 2008). The later feature, achieved by incorporating a suitable ligand or antibody to the liposome surface, is essential for improving the specificity for target cells.

1.3.3. Stabilized Plasmid-Lipid Particles (SPLP)

Employing a detergent dialysis technique (Hofland *et al.*, 1996), plasmid DNA has been encapsulated with a 50-70% efficiency in small particles (~70 nm) stabilized by PEG-Ceramide lipids (Wheeler *et al.*, 1999). These nanocarriers, known as a Stabilized Plasmid Lipid Particles (SPLP), have been further improved by several groups by adding pH-sensitive lipids and ceramides with shorter carbon chains to confer endosamal escape capabilities (Mok *et al.*, 1999; Wheeler *et al.*, 1999; Fenske *et al.*, 2002; Li *et al.*, 2005).

The first generation SPLP developed by Wheeler et al. contained a high percentage of the helper lipid DOPE (84 mol%), low levels of cationic lipid dioleyl-dimethylammonium chloride DODAC (6 mol%) and quite high levels (10 mol%) of PEG-Ceramide with an arachidoyl acyl group (PEG-Cer-C20). The release half-life ($t_{1/2}$) of PEG-Cer-C20 from SPLP was 13 days, becoming an intractable steric barrier to transfection. The length of the ceramide lipid anchor determined the time that the PEG conjugate remained associated with the bilayer. When PEG-Cer-C20 was replaced by PEG-Cer-C8 with an octanoyl acyl group, the $t_{1/2}$ was reduced to 1.2 min, considerably increasing the transfection of cells in vitro (Mok *et al.*, 1999). This first generation of SPLP was improved by Szoka and coworkers (Choi *et al.*, 2003; Li *et al.*, 2005) by adding a pH sensitive PEG-lipid to trigger plasmid release in the acidic endosomal environment. The key design feature of such PEG-lipids is that the pH triggerable PEG-linker should be completely stable at pH 7 and sufficiently destabilized at pH 5.5, as to irreversibly dissociate within at least 1 hour, essential requirement to ensure quantitative release of nucleic acid from the lipid particle.

As mentioned above, entrapment of plasmid DNA in SPLP was accomplished by a detergent dialysis procedure (Hofland *et al.*, 1996) by which reconstituted liposomes consist of unilamellar vesicles regardless of the rate of detergent removal (Figure 1.3). As the detergent is being removed, a series of micelle-micelle interactions are initiated to minimize the unfavourable energy resulting from the exposure of lipids to the aqueous medium (Figure 1.3 I). At a critical micelle size, the amplitude of the bending is sufficient to cause bilayer closure (Figure 1.3 II) and plasmid encapsulation (Figure 1.3 III). One of the most important aspects of SPLP is their great structural integrity with negligible variation in size or DNA encapsulation after 5 months at 4 °C.

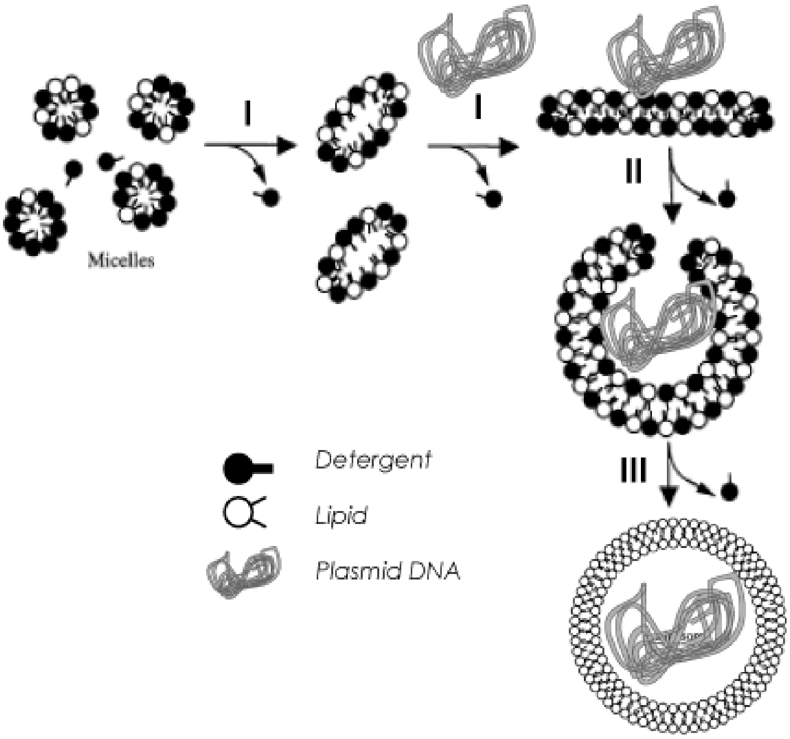

Figure 1.3: Schematic representation of SPLP formation during detergent dialysis. Detergent removal from lipid-detergent micelles causes the transformation of small micelles into larger ones **(I)**, which bend upon further detergent removal to form curved mixed micelles and trapp the plasmid DNA **(II)**. The bilayer becomes continuous forming the stable plasmid-lipid particles **(III)**. Adapted from (Jean-Louis Rigaud, 1998).

SPLP have been designed for long-term circulation in vivo but given the severity of the extracellular environment, only a modest detectable transfection in animals post i.v.-administration has been reported (Monck *et al.*, 2000). SPLP systems are now under evaluation in Phase I clinical trials (Protiva, unpublished data).

1.4. Cell mechanisms of liposome uptake

The cellular uptake of liposomes is generally believed to be mediated by adsorption of liposomes onto the cell surface and subsequent endocytosis. As previously described, the rate limiting steps in this process are the efficiency of cell surface association, internalization, release of loaded drug/genes from intracellular compartments such as endosomes, transfer to the cytosol and eventually, translocation into the nucleus.

Liposomal carriers can adsorb specifically and non-specifically to the cell surface (Figure 1.4 a, b), in some cases promoting a direct delivery of the therapeutic agent into the cytoplasm (Figure 1.4 c, d). Additionally, in order to increase the initial cell binding, delivery carriers have been modified with cationic moieties to increase the electrostatic interaction of the vehicle with the negatively charged cell membrane (Figure 1.4 e, c). Constructs that are more sophisticated involve the covalent binding of a ligand or antibody to the liposome carrier to promote the specific receptor-mediated or antigen-mediated endocytosis, respectively (Figure 1.4 a). If uptake occurs via endocytosis (Figure 1.4 f), receptor or non-receptor mediated, the liposomes end up in endosomal compartments.

In the case of receptor-mediated endocytosis, internalized vesicles and their content are sorted mainly to the lysosomal compartment for degradation of the ligands and the loaded cargo (Figure 1.4 f, g). This also accomplishes the downregulation of activated receptors (Shepherd, 1989). However, the majority of targeted deliveries aim to avoid lysosomal trafficking in an effort to protect the drug molecule or biomolecules from enzymatic degradation.

Lysosomes, as well as the endoplasmatic reticulum (ER), Golgi apparatus, and endosomes are, to a variable degree topologically continuous with the exterior of the cell, i.e. the exit of macromolecules from any of these compartments requires passage through a lipid bilayer.

In general, the endocytosis mechanisms can be divided into clathrin-dependent and clathrin-independent. There is a close relation between particle size and the preferred internalization pathway, although the correlation is not absolute. Rejman et al. proposed that particles <200 nm are taken up via the clathrin-dependent mechanism whereas larger particles (250-500 nm) enter the cell through caveolin 1-rich vesicles (Rejman *et al.*, 2004). This correlation, between particle size and uptake pathway, is indeed plausible since some of these pathways are constrained to the size of their vesicles – e. g. clathrin-coated and caveolae-derived vesicles (Pelkmans *et al.*, 2004).

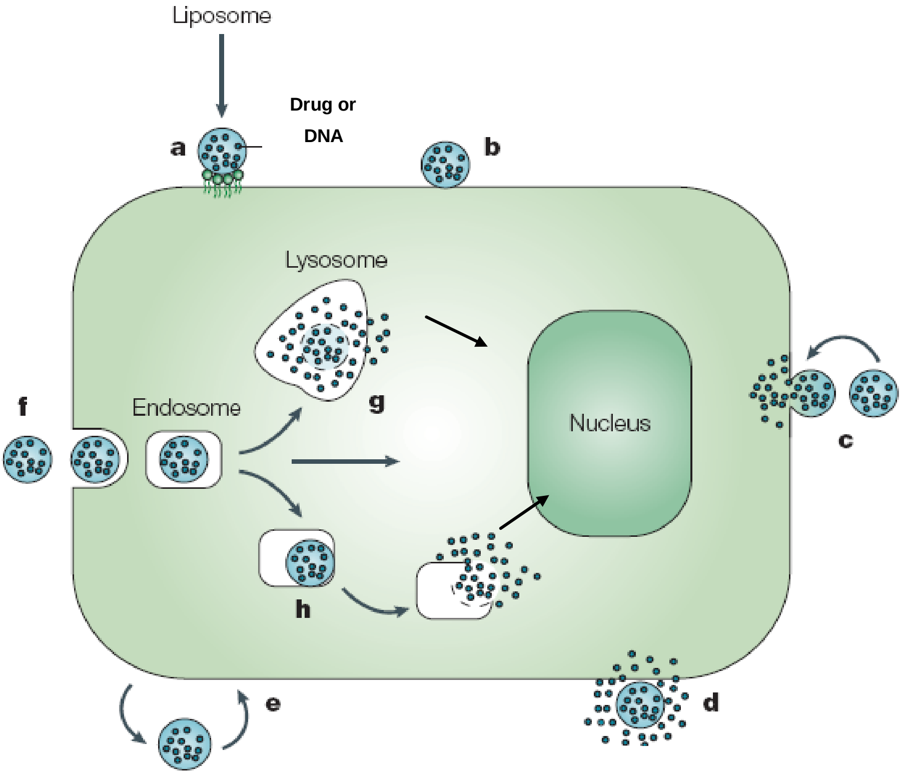

Figure 1.4: Liposome uptake and intracellular fate: DNA or drug loaded liposomes can specifically (**a**) or nonspecifically (**b**) adsorb onto the cell surface. Liposomes can also fuse with the cell membrane (**c**), and release their content into the cytoplasm, or can be destabilized by certain cell membrane components when adsorbed on the surface (**d**) so that the released drug can enter the cell via micropinocytosis. Liposomes can undergo the direct transfer or protein-mediated exchange of lipid components with the cell membrane (**e**) or be subjected to a specific or nonspecific endocytosis (**f**). In the case of endocytosis, liposomes can be directed into lysosomes (**g**) or, in route to the lysosome, they can provoke endosome destabilization (**h**), which results in the liberation of the therapeutic agent into the cell cytoplasm (Adapted from (Torchilin, 2005).

Clathrin-mediated endocytosis serves as the main mechanism of internalization for macromolecules and plasma membrane constituents for most cell types and it is the most investigated vesicular pathway for targeted drug delivery. This is initiated by the formation of clathrin-coated pits, which are subsequently pinched off and internalized. The clathrin coat is removed and multiple vesicles fuse originating the early and late endosomes that ultimately fuse with lysosomes (Mousavi *et al.*, 2004).

1.4.1. Receptor-mediated endocytosis as a route for targeted liposomal delivery

Targeting is usually achieved by conjugating a high affinity ligand to the carrier that provides preferential accumulation of the latter for instance, in a tumor-bearing organ, in the tumor itself, in individual cancer cells or intracellular organelles. In most cases the targeting moieties (ligands or antibodies) are directed toward specific receptors or antigens exposed on the plasma membrane (Kato and Sugiyama, 1997). The overexpression of receptors or antigens in many human cancers lends itself to efficient drug uptake via receptor-mediated endocytosis. Folate and Transferrin are widely applied ligands for liposome targeting because their cognate receptors are frequently overexpressed in a range of tumour cells (Kakudo *et al.*, 2004; Hilgenbrink and Low, 2005). Liposomes tagged with various monoclonal antibodies have been delivered to many targets (Park *et al.*, 2001).

The performance of non-viral vector could be certainly optimized by targeting them into distinct cellular internalization pathways, considering that not every pathway may be equally effective in releasing a therapeutic biomolecule in the cytosol. This step is critical for nucleic acid delivery to increase the possibility of nuclear transport and the ultimate expression of the delivered genes (Bareford and Swaan, 2007).

1.4.2. EGF receptor targeted delivery systems

The epidermal growth factor receptor (EGFR, ErbB) is a 170 kDa protein that is distributed randomly on the surface of cells, excluding hematopoietic cells. Its ligand, EGF, is a 53 aminoacid-peptide that mediates cellular signal events regulating cell proliferation, differentiation, cell cycle progression, adhesion, invasion, angiogenesis and inhibition of apoptosis. Following binding of the EGF, the EGFR functions either as a homodimer through the complexation of two identical EGFR molecules or as an heterodimer by associating with one of the three other ErbB family members; in either case the resulting dimerization then initiates the cellular internalization (Bublil and Yarden, 2007).

The EGFR is a tempting target for gene delivery since it is overexpressed in a wide variety of human tumors found in cancers of head and neck, breast, colon, ovary, lung, prostate and liver (Johnston *et al.*, 2006). Enhanced EGFR expression is associated with tumor invasiveness, resistance to chemotherapy and radiation therapy and clinically correlates with poor prognosis and lower patient survival (Rubin Grandis and V. A.; Wagener, 1998). Squamous cell carcinoma of the head and neck is a cancer commonly associated with EGFR overexpression (>90%), which appears to play a role in the unregulated growth of these cells (Cohen, 2006). EGFR has been used to target drugs and toxins loaded in therapeutic liposomes (Kullberg *et al.*, 2003; Mamot *et al.*, 2005) and lipoplexes (Shir *et al.*, 2006).

1.5. Fluorescent nanoparticles in live-cell imaging

1.5.1. Applications for lipid-based delivery systems

The use of multifunctional nanoprobes for molecular and cellular imaging is already showing great promise, providing new insights into approaches such as gene therapy and drug delivery.

Underlying the rational design of gene or drug loaded delivery vectors is the recognition of the individual steps of a particular internalization pathway. Live-cell imaging and single-particle tracking using confocal fluorescence microscopy have shed light on the intracellular dynamics and bottlenecks of the drug/gene delivery process (Payne, 2007; Zhang *et al.*, 2007).

1.5.2. Long-term imaging using Quantum Dots

Continuous cell imaging has been dramatically improved with the introduction in the last decade of fluorescent probes such as Quantum Dots (QDs), colloidal nanocrystals with unique optical properties that make them outstanding fluorescent labels for long-term and multicolor imaging (Alivisatos *et al.*, 2005; Michalet *et al.*, 2005).

QDs commonly consist of a cadmiumselenide (CdSe) or cadmiumtelluride (CdTe) core enclosed within a zincsulfide (ZnS) passivation shell. The cadmium-based core is toxic to cells, but the ZnS shell isolates it from the cell rendering the core non-toxic at functionally useful concentrations. Peptides, polyethylene glycol (PEG) or other biocompatible polymers, also provide protection and specific sites for bioconjugation (Figure 1.5, *left top panel*).

The main advantages of QDs over organic fluorophores are the greater photostability and the excitation wavelengths range that extends above 500 nm. This latter feature reduces cell phototoxicity, essential for long-term fluorescence imaging. Because the molar extinction coefficients ($0.5–2 \times 10^6$ $M^{-1}cm^{-1}$) of QDs are about 10–50 times larger than those of organic dyes, the QDs absorption rates will be 10–50 times greater than those of organic dyes at the same excitation photon flux. Because of the corresponding increased rate of light emission, single QDs appear 10–20 times brighter than organic dyes (Li *et al.*, 2007). Furthermore, the emission wavelengths of QDs are size-tunable (Figure 1.5, *left bottom panel*). For example, QDs of approximately 2 nm in the core diameter produce a blue emission, whereas QDs of approximately 7 nm in diameter emit red light. Therefore, multiple colors QDs can be generated by controlling the size of the nanoparticle during the synthesis. Although QDs absorption spectra are broad, emission spectra are narrow (Figure 1.5, *right panel*) without the extension to the red characteristic of organic dyes. This feature allows for simultaneous detection of multiple color QDs upon illumination with single light source (Smith et al., 2004).

Despite these features, QDs biocompatibility remains a critical issue to use in humans and a possible limitation to their in vivo applications (C. Kirchner and H.E. Gaub, 2005).

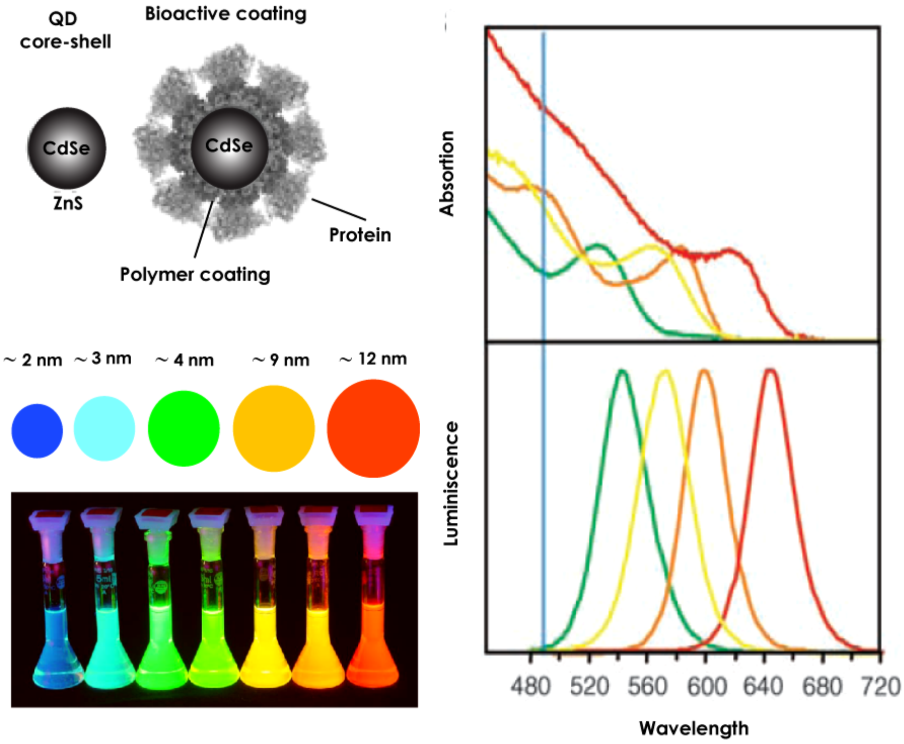

Figure 1.5: Scheme of Quantum Dots nanoparticles. Left top panel: QDs of CdSe core are surrounded by a ZnS shell and coated with biocompatible polymers**. Left bottom panel:** Size-tunable fluorescence emission. **Right panel:** Absorption (upper curves) and emission (lower curves) spectra of four CdSe/ZnS QDs samples. The blue vertical line indicates the 488-nm line of an argon-ion laser, which can be used to efficiently excite all four types of QDs simultaneously. Adapted from (Daniele Gerion, 2001).

1.5.3. Ligand tagged Quantum Dots

QDs have to be functionalized to act as useful, specific fluorescent labels. The targeting moiety attached to the QD surface determines the mode of entry into cells and their intracellular localization. Selective staining of plasma membrane and intracellular organelles was achieved using QD-labeled antibodies, receptor ligands or targeting peptides (Figure 1.5, *left top*)(Michalet *et al.*, 2005; Al-Jamal and Kostarelos, 2007). Dynamic processes such as diffusion of membrane receptors (Dahan *et al.*, 2003) or antigen uptake by cells (Cambi *et al.*, 2007) have been tracked with ligand and antigen tagged QDs, respectively.

The cell binding of EGF tagged QDs has been extensively investigated in the laboratory in which this thesis work was carried out. It has been demonstrated that complexes of streptavidin-conjugated quantum dots (QDs) with biotinylated EGF are biochemically competent ligands for erbB1, the EGF receptor (Lidke *et al.*, 2004). The application of multicolor EGF-QDs allowed tracking endocytosis of the receptor-ligand complex to follow subsequent steps in time. Figure 1.6 (A,B) shows two different colors of ligand-QDs delivered sequentially to identify early and late endosomes (Lidke *et al.*, 2007). In addition, a previously unreported retrograde transport of activated erbB1 receptors on cellular filopodia was detected at the single molecule level (Lidke *et al.*, 2005). QDs allowed the visualization of the displacement of EGF-EGFR complexes on filopodia towards the surface and the interior of living A431 cells (Figure 1.6 (C,D).

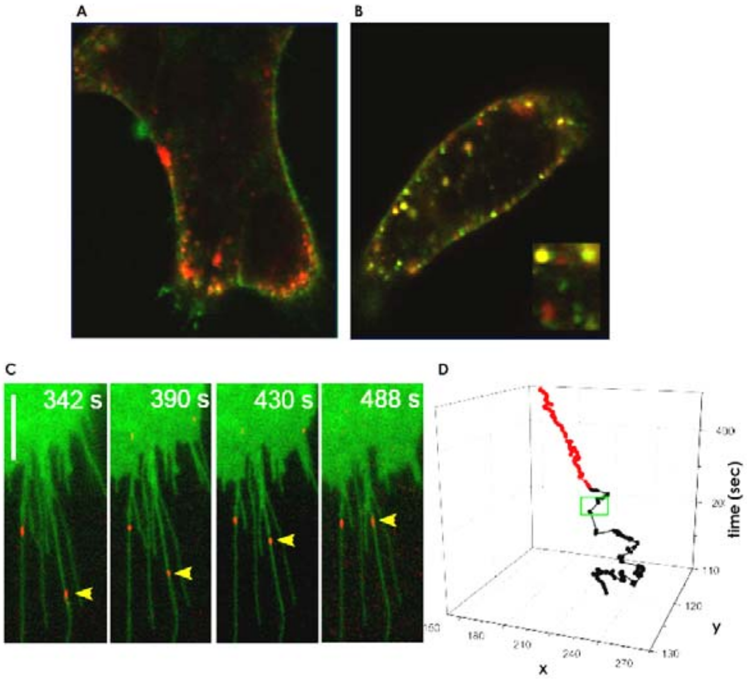

Figure 1.6: Tracking of endosomes with two different color QD-EGF complexes. A: QD605-EGF added to A431 cells, incubated RT for 3 min, washed and incubated for 5 min at 37° C, then QD525-EGF were added and images acquired for 8 min at 37° C. Early endosomes: red only whereas QD525-EGF is predominantly external. **B:** QD525-EGF washed and observed 20 min later at 37° C. Several classes of endosomes containing red only, green only or both QD colors (see inset). Early, sorting and late endosomes are loaded (Lidke *et al.*, 2007). **Retrograde transport visualized with single EGF tagged QD. C:** Selected frames of an A431-erbB1-GFP cell (green) from a time series after binding 5 pM EGF-QD (red) followed by addition of free EGF (50 ng/ml) at 300 s. Wide field image, scale bar is 5 µm. Images arecontrast enhanced. **D:** Trajectory of the indicated monomer erbB1-EGF-QD complex (yellow arrow) on a filopodium that exhibits random diffusional movement (black) until the addition of unlabeled EGF (green box), after which the complex exhibits active retrograde transport (red). Adapted from (Lidke *et al.*, 2005).

The recent advances in the chemistry of QD coating permit the simultaneous conjugation of two or more different molecules, and thus, the simultaneous stimulation of several receptors, further broadening the potential applications of these fluorescent probes for dynamic studies of cellular processes (Xiaohu Gao, 2004). However, the existence of multiple groups on the surface of QDs can be considered a disadvantage in comparison to single attachment sites or reactive entities. In fact, a high number of molecules contributing with multiples sites of conjugation leads to a distribution of QDs subpopulations differing in particle-label stoichiometries and undesirable cross-linking. Procedures for achieving precise control of the number of sites have been developed (Sperling, 2006; Lidke *et al.*, 2007).

Multiple sites can be advantageous for multifunctionality, for instance, the combination of targeted QDs and lipid carriers in a single nanoparticle can serve to elucidate the internalization route, fate of carriers and processing of therapeutic drugs. The attractiveness of such hybrid nanoparticles are:

- Lipid carrier and QDs can be surface functionalized with a ligand for specific targeting
- Complexes of drug-QDs can be encapsulated in the lipid carriers improving QDs biocompatibility and providing a therapeutic effect
- The fluorescent lipid vehicle can be tracked continuously
- Combining two colors QDs on the surface and inside the lipid vesicle, the fate of the carrier and the loaded drug could be followed independently

1.6. Aims and organization of the thesis

A new emerging field in targeted delivery is the multi-modality carrier, in which a therapeutic molecule, an imaging agent or a fluorescent probe and a targeting entity are assembled in a single nanometer-scaled scaffold for simultaneous imaging and therapy.

The aim of this thesis was to develop a QD labeled and EGFR targeted delivery system mediated by Biotinylated Lipid Particles (BLP).

The human epidermoid carcinoma cell line A431 was chosen because of its large overexpression of EGFR, approximately 10^6 receptors per cell.

The original approach proposed here was not only the specific targeting but the novel encapsulation of QDs in these lipid particles by a detergent dialysis technique. A dual-color labeling strategy with loaded and surface bound QDs was introduced to follow the intracellular localization of the cargo and carrier by confocal microscopy.

EGFR targeted and QD labeled BLP were loaded with plasmid DNA and cell specificity and transfection efficiency of the delivery system were evaluated according to the expression of the GFP reporter gene.

Finally, a DNA labeling strategy was conceived to achieve sequence specific and non-covalent labeling of DNA using a single QD and *bis*-peptide nucleic acids (*bis*-PNA). The objective was to obtain a transfection competent and labeled DNA cargo for the developed BLP.

The specific objectives were:

- Create a functional ligand-QDs labeled BLP
- Demonstrate enhanced receptor-mediated uptake of the complex and gene expression

- Develop the imaging methodology to follow intracellular localization of lipid particles and cargo by confocal microscopy
- Design a QD-PNA-DNA complex for cellular imaging of DNA in delivery systems

The results obtained in this study are divided in three sections. The first one describes the preparation of biotinylated liposomes (BLP) with encapsulated DNA or Quantum Dots, and the physicochemical characterization of the particles according to size, biotinylation and DNA or QDs encapsulation efficiency.

The second section presents the EGF-based targeting strategy of the BLP either loaded with DNA or QDs and then focuses on the cell binding experiments. A two-color BLP labeling strategy usign QDs was designed, where colocalization of green emitting QD_{525} and red emitting QD_{655}, allowed the immediate recognition of targeted BLP during live cell imaging by confocal microscopy.

The specificity for the EGF receptor was examined in a competitive binding assay in the presence of excess ligand EGF and after incubation of BLP with cell lines devoid of the receptor.

Transfection competencies of EGFR-targeted and DNA loaded BLP particles were evaluated as the percentage of cells expressing GFP compared to cells incubated with non-targeted particles.

The third section presents the non-covalent DNA labeling strategy using *bis*-PNA and a single QD per plasmid and describes the characterization of the labeled complexes by gel electrophoresis and Atomic Force Microscopy. The data, although preliminary, are complementary to the main results of this thesis and represent the first steps towards a QD-labeled plasmid that could be monitored along the pathway to the nucleus. Such a labeled plasmid appears as an attractive cargo for the BLP.

2. Materials and methods

2.1. Reagents

2.1.1. Lipids

Lipids were purchased from Avanti Polar Lipids (Alabaster, USA) and from Northern Lipids (Vancouver, Canada) as lyophilized powders or dissolved in chloroform. Chemical structure and nomenclature are depicted in Table 2.1. Lipids were stored under argon in a desiccator at -20 °C.

Description	Nomenclature	Chemical structure
Phospholipid	**DOPE** 1,2-Dioleoyl-*sn*-Glycero-3-Phosphoethanolamine	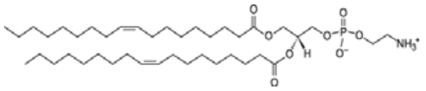
Cationic lipid	**DOTAP** 1,2-Dioleoyloxy-3-trimethylammoniumpropane chloride	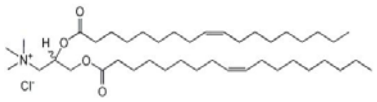
Biotinylated lipid	**Biotin-PEG-DSPE** 1,2-Distearoyl-*sn*-Glycero-3-Phosphoethanolamine-N-[Biotinyl (Polyethylene Glycol) 2000] (Ammonium Salt)	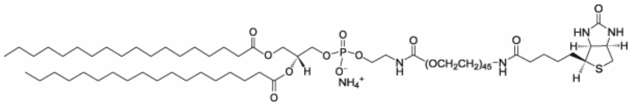
PEG-modified ceramide	**PEG-Cer-C20** N-Arachidoyl-Sphingosine-1-[Succinyl (Methoxy (Polyethylene Glycol) 2000)]	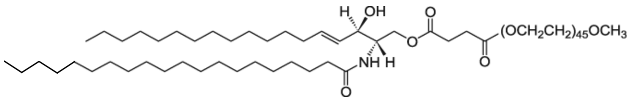
PEG-modified ceramide	**PEG-Cer-C8** N-Octanoyl-Sphingosine-1-[Succinyl (Methoxy (Polyethylene Glycol) 750)]	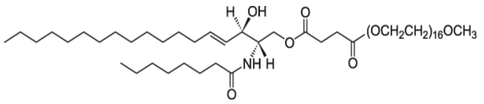
pH-sensitive lipid	**PEG-DSGS** 3-O-[2'-(omega-monomethoxy (Polyethylene Glycol) 2000) succinoyl]-1,2-Distearoyl-*sn*-Glycerol	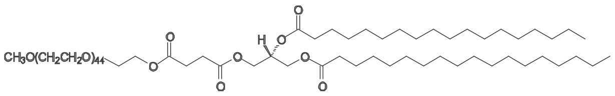

Table 2.1: Synthetic lipids used in the formulation of lipid particles.

Chloroform, Ethanol, Methanol, Isopropanol and Water HPLC quality were purchased from Merck.

Buffers were prepared with analytical grade chemicals. Detergent, Triton X-100 was purchased from Fluka, detergent 1-o-n-octyl-β-D-glucopyranoside (OGP), sucrose, HABA 4-Hydroxyazobenzene-2-carboxylic acid) and kanamycin from Sigma and nonpolar polystyrene adsorbents Bio-Beads SM-2 from BioRad.

UltraPure™ Agarose was purchased from Invitrogen.

Luria Bertani (LB) medium in powder form was obtained from Difco.

2.1.2. Biotin and biotin-related reagents

Biotin and Biocytin were purchased from Sigma, *Ez link Sulfo NHS-LC-LC-Biotin* and *EZ-Link PEO-Biotin Dimer (+)-Biotinyl-hexaethyleneglycol dimmer* from Pierce.

Biotin-EGF and EGF (human recombinant) were obtained from Molecular Probes.

2.1.3. Buffers

Hepes buffered saline (HBS): 10 mM HEPES (2-hydroxyethyl)-1-piperazine ethanesulphonic acid, 150 mM NaCl (sodium chloride), pH 7.4.

Hepes-Mg buffer: 10 mM HEPES (2-hydroxyethyl)-1-piperazine ethanesulphonic acid, 5 mM $MgAc_2$ (Magnesium Acetate), 10 mM KCl pH 7.4 prepared with Ultrapure Water HPLC quality and filtered through 0.02 µm pore size.

Phosphate buffered saline (PBS): 137 mM NaCl, 2.7 mM KCl, 7.9 mM Na_2HPO_4,1.5 mM KH_2PO_4, pH 7.3.

Tyrode's buffer: 135 mM NaCl, 10 mM KCl, 0.4 mM $MgCl_2$, 1 mM, $CaCl_2$, 10 mM HEPES, pH 7.2.

20 mM Glucose and 0.1% BSA were added before use.

10 mM Sodium Acetate buffer pH 5.2: 1g/l Sodium acetate tri-hydrate and 0.16 g/l acetic acid (glacial).

50X TAE: 242 g Tris base, 57.1 g glacial acetic acid, 100 ml of 0.5 M EDTA, pH 8.0.

2.1.4. Quantum Dots

Streptavidin-coated QDs (StAv-QDs) with maximum fluorescence emission peaks at 525 nm (StAv-QD_{525}), 605 nm (StAv-QD_{605}) and 655 nm (StAv-QD_{655}) and ITK-carboxyl QD_{655} were purchased from Invitrogen.

2.1.5. Labeled proteins and organic fluorophores

Streptavidin Alexa $Fluor_{488}$ (ex. 488 nm/em. 519 nm), Transferrin Alexa $Fluor_{488}$, Sybr Green (ex. 495 nm/em. 521 nm), Cy5 NHS ester (ex. 650 nm/ em. 670 nm) and Hoechst 33342 (exc. 365 nm/ em. 455 nm) were purchased from Molecular Probes.

2.1.6. Plasmid DNA

Plasmid pEGFP-C1, 4.7 Kb encoding the Enhanced Green Fluorescent Protein (EGFP: ex. 488 nm/em. 507 nm), was bought from Clontech Laboratories (Heidelberg, Germany). This encodes a red-shifted variant of the wild-type green fluorescence protein.

2.1.7. *bis*-PNA (*bis* Peptide Nucleic Acid)

bis-PNA (*bis*- Peptide Nucleic Acid) MW: 5655 ($\varepsilon_{260\ nm}$= 107840 $M^{-1}cm^{-1}$) was acquired from Oswel, Southampton, UK.

bis-PNA sequence: NH_2-LL-**TCCCCCTTT**-LLL-**TTTCCCCCT**-LL, where L represents *8-amino-3,6-dioxaoctanoic acid.*

bis-PNA anchoring sequence in p-EGFP C1 plasmid: **AGGGGGAAA** at base pair position 4515-4523.

2.1.8. Restriction endonucleases and DNA standards

Restriction endonucleases Apa LI, Ava II and Ase I and the corresponding buffers were obtained from New England Biolabs. DNA markers of 100 bp and 1 Kb were from Invitrogen.

2.2. Cell lines, media and labware

Human epidermoid carcinoma cell line A431 and CHO (Chinese hamster ovary) cell line were obtained from the American Tissue Culture Collection, while the melanoma cell line WM983A, was kindly provided by Prof. Meenhard Herlyn (Wistar Institute, Philadelphia, PA).

Dulbecco's Minimal Essential Medium was obtained from Gibco. Leibovitz's L15 medium was from Mediatech, Inc. FBS was bought from PAN. Penicillin and Streptomycin and Trypsin were purchased from Gibco. EDTA, BSA and glucose were from Sigma.

Paraformaldehyde (PFA) of analytical grade was freshly prepared as a 4% solution in PBS for cell fixation.

Glass coverslips 12 mm were acid washed and sterilized. LabTek 8-well or 2-well glass chambers, plastic cell culture dishes and flasks were purchased from Nunc or Sarstedt.

2.3. Miscellaneous

- Ultraconcentrators 3 kDa and 10 kDa cut-off, Amicon (Millipore), Vivaspin (Viva Science Sartorius, Göttingen)
- Gel filtration columns Sephacryl-HR 200 and HR-400 and Superdex™ 75 /Superdex™ 200 (GE Healthcare)
- Native 3-8 % Polyacrylamide precasted gels (Invitrogen)
- Dialysis Cassettes, Slide-A-Lyzer, 10 kDa cut-off for 0.5-3 ml sample, (Pierce)
- Streptavidin-coated magnetic beads Dynabeads M-280, (Dynal Biotech)
- Thin-wall polypropylene centrifuge tubes 2.5 ml (Beckman)

- Filters set for fluorescence microscopy (Chroma and Omega)
- Silicon Nitride ultrasharp cantilevers for AFM (Veeco and Mikromarsch)

2.4. Equipments and softwares

Bench top centrifuge	Mini spin plus (Eppendorf)
Centrifuge	Beckman Avanti J-25
Ultracentrifuge/rotor with swinging buckets	TL-100/TLS 55 Beckman
Chromatographic system	SMART, Pharmacia Biotech, GE Healthcare Life Sciences
Laser-based scanning system for fluorescence detection	Typhoon, Amersham Biosciences
UV-Vis spectrophotometer	Cary 100 Scan
Fluorescence spectrophotometer	Varian Cary Eclipse
Particle analyzer	Zeta Sizer Nano (Malvern Instruments)
Atomic Force Microscope	Nanoscope IIIa Multimode AFM (Veeco)
Electron microscope	Philips CM 12
Optical microscopes	Axiovert 100 (Zeiss, Göttingen, Germany) Olympus IX71
iXon CCD camera for microscopy	Andor technology
Laser Scan Confocal Microscope	LSM 510 Meta (Zeiss, Göttingen, Germany)
Flow cytometer	Coulter Epics
Software for Image analysis and data handling:	
AFM analysis: Vision 700	Nanoscope v. 7.00. (Veeco)
Image analysis:	
Image J free software for microscopy	(http://rsb.info.nih.gov)
DIPImage toolbox in Matlab 7.01	(http://www.ph.tn.tudelft.nl/DIPlib/index.html)
Flow cytometry analysis: Reflex software	(http:// www.freewebs.com/cytoflex)

2.5. Preparation of Biotinylated Lipid Particles (BLP)

As depicted in the diagram below (Figure 2.1), to prepare 1 ml of BLP formulation, 8.4 µmols DOPE (neutral lipid), 0.6 µmols DOTAP (cationic lipid) and 0.024 µmols Biotin-DSPE were initially mixed in 2 ml glass vials. In individual vials containing this lipid mixture, different micromolar amounts of PEG-lipids (Table 2.1) were added to obtain 1.4, 2.7 and 10 (mol%) PEG content and a final lipid concentration of ~10 mg/ml in the BLP formulation. These solutions were dried with a stream of argon and residual chloroform was removed under vacuum overnight.

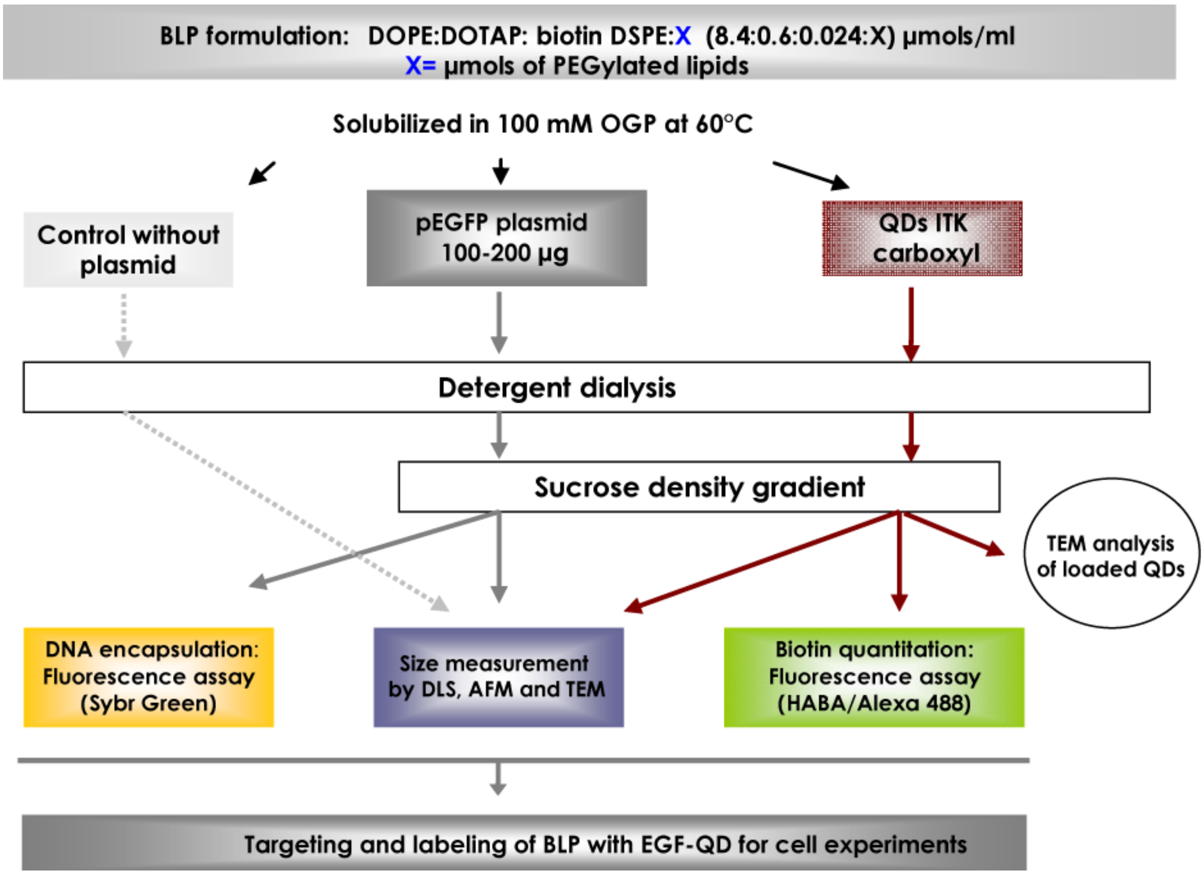
BLP formulation: DOPE:DOTAP: biotin DSPE:X (8.4:0.6:0.024:X) µmols/ml
X= µmols of PEGylated lipids
Solubilized in 100 mM OGP at 60°C
Control without plasmid
pEGFP plasmid 100-200 µg
QDs ITK carboxyl
Detergent dialysis
Sucrose density gradient
TEM analysis of loaded QDs
DNA encapsulation: Fluorescence assay (Sybr Green)
Size measurement by DLS, AFM and TEM
Biotin quantitation: Fluorescence assay (HABA/Alexa 488)
Targeting and labeling of BLP with EGF-QD for cell experiments

Figure 2.1: Flow diagram of BLP preparation with encapsulated plasmid DNA or QDs.

2.5.1. Detergent dialysis technique

The resulting lipid film was hydrated in 0.5 ml of HBS containing 100 µl of 1M OGP detergent with continuous magnetic stirring at 60 °C to favour complete dissolution. For the preparation of BLP with encapsulated DNA (BLP-DNA), the detergent dialysis technique described by (Hofland *et al.*, 1996) was applied with modifications. In this approach, 100 µg or 200 µg peGFP-C1 plasmid (purified as described in 2.10.1) were diluted in 0.5 ml HBS and added with stirring to the solubilized lipids-detergent solution (0.5 ml). The mixture was kept at

RT for 30 min and followed by a dialysis at RT against HBS using a 10 kDa MWCO membrane for 2-3 h or until turbidity was noticeable. Then, the dialysis was continued in a cold room (~4 °C) overnight and after two buffer changes of 1 l HBS, residual detergent OGP was removed by adding polyestyrene SM2 Biobeads (adsorbent capacity ~117 mg OGP/g beads). Control BLP samples without plasmid were prepared in parallel.

In order to prepare BLP with encapsulated QDs (BLP-QDs), ITK-carboxyl QD_{655} were added to the corresponding lipid-detergent mixture in HBS (50 nM final QDs concentration). Samples were immediately dialysed as described for BLP-DNA particles.

2.5.2. Ultracentrifugation in sucrose density gradient

In order to separate and recover DNA and QDs loaded BLP from less dense empty BLP and non encapsulated material, the samples obtained after the detergent dialysis were loaded on top of a discontinuous sucrose density gradient.

The sucrose gradient was prepared in 2.5 ml Beckman ultraclear thin-wall centrifuge tubes by carefully applying with a tip or syringe, layers of 0.6 ml 2.5 %, 10%, and 20% (w/v) sucrose in HBS (Mok *et al.*, 1999). The BLP samples recovered from the detergent dialysis were adjusted to 1% (w/v) sucrose density and were added on top of the gradient. Ultracentrifugation was carried out for 5 h at 160,000 *g* at 10 °C in a TLS-55 rotor with swinging buckets.

The resolved turbid bands from BLP-DNA samples were carefully recovered and, together with aliquots of the gradient, were analyzed for particle size, biotin content and DNA encapsulation efficiency.

Centrifuge tubes containing BLP-QDs samples were briefly illuminated with UV light to detect QD_{655} fluorescence, and consequently the location of QDs containing bands. Fluorescent bands were analyzed by TEM at the Electron Microscopy Department of the institute.

2.5.3. Particle size analysis by Dynamic Light Scattering

The mean hydrodynamic diameter of the obtained BLP was measured by Dynamic light scattering (DLS) which involves the determination of how the intensity of the light scattered by a solution of moving particles varies with time. This variation is correlated with the speed at which particles move, which can be characterized by their diffusion coefficients (Pecora and Aragon, 1974). The hydrodynamic diameter **d** of particles is obtained from the diffusion coefficients **D**, according to:

$$\mathbf{d} = \frac{\mathbf{kT}}{\mathbf{3\pi\, \eta\, D}}$$

where, **k** is the Boltzman constant, **T** is the temperature and **η** is the solvent viscosity.

DLS measurements were performed with a NanoZetasizer from Malvern Instruments, detecting the back scattered light from a 633 nm laser at a fixed angle of 173°.

Samples were diluted in PBS and the measurements performed at RT. The PBS used to dilute the samples was previously filtered through 0.02 µm pore size to eliminate potential interfering impurities.

The operating protocol was chosen for spherical particles, applying 12 to15 runs per measurement, which were automatically selected according to the concentration of particles in the sample, and three measurements were performed on each sample. The autocorrelation function for size distribution was calculated using the CONTIN mathematical approach for heterodisperse, polydisperse and multimodal systems (Provencher, 1982).

The mean hydrodynamic diameter obtained represents only an intensity-based average value and does not give any information on the prevailing size distribution. For this reason, the polydispersity index (pdi) is also stated to give information about the actual distortion of a monomodal distribution. The pdi can have values between 0-1 and is equivalent to the variance σ2 of the size distribution. Samples with pdi <0.25 are considered as monodisperse solutions.

2.5.4. DNA quantitation

The amount of plasmid recovered and encapsulated after dialysis and ultracentrifugation in sucrose density gradient was quantitated using the Sybr Green fluorescence assay (Zhang *et al.*, 1999). In the presence of DNA, the dye binds specifically to double-stranded DNA and emits at 522 nm. Briefly, 25 µl aliquots of standard solutions varying from 0-5 µg/ml plasmid DNA or dilutions of BLP were mixed with 25 µl of HBS buffer containing 0.5 µg/µl Sybr Green solution. Sybr Green fluorescence was excited at 495 nm and emission spectra were collected from 505 to 700 nm with a slits width of 10 nm for both excitation and emission.

The plasmid DNA content in BLP formulations was calculated from the linear curve fitting obtained after plotting the maximum fluorescence intensity (a.u.) of Sybr Green at 522 nm as a function of DNA concentration in µg/ml plasmid (Figure 2.2).

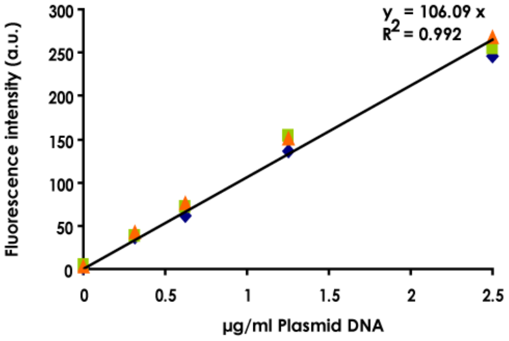

Figure 2.2: Representative DNA calibration curve using Sybr Green dye. Sybr Green excited at 495 nm and emission recorded from 505-700 nm. Maximum fluorescence intensity (a.u.) at 522 nm was plotted as a function of plasmid DNA concentration. Data correspond to three curves obtained in

independent experiments. Each point is an average of duplicates. Free Sybr Green is non-fluorescent in HBS (0 µg/ml plasmid DNA). The presence of 0.1% Triton-X100 did not change the maximum fluorescence intensity at 522 nm of Sybr Green upon DNA binding (not shown).

Free or exposed plasmid DNA was quantitated directly in BLP solutions. Then, lipid particles were solubilized with 0.1% Triton X-100 and total DNA content was measured. The obtained value was related to the initial amount added to compute DNA encapsulation efficiency.

2.5.5. Biotin quantitation

The biotin content of BLP was determined on samples recovered after detergent dialysis and ultracentrifugation in sucrose gradient.

The fluorometric assay used is based on Foster resonance energy transfer (FRET) (Batchelor *et al.*, 2007), providing high sensitivity to detect nanomolar concentrations of biotin linked to proteins or nucleic acids. In this assay (Figure 2.3A), the Alexa Fluor$_{488}$-streptavidin conjugate (StAv-Alexa$_{488}$) acts as FRET donor and the dye HABA as a quencher, occupying the biotin binding sites of the dye-labeled streptavidin. In the absence of biotin, HABA quenches the fluorescence emission of the Alexa Fluor$_{488}$ dye via FRET. When biotin or a biotinylated molecule is added, HABA is displaced from the biotin binding sites resulting in an increase in the donor fluorescence intensity proportional to the amount of biotin present in the sample.

The standard curve of biocytin, a water-soluble biotin analogue, was obtained by titrating a solution containing 25 nM StAv-Alexa$_{488}$ and 125 µM HABA in HBS. Biocytin was added from an aqueous stock solution to give final concentrations of 0–200 nM in 50 µl samples. Fluorescence of standards and samples was measured in a spectrofluorometer, Alexa Fluor$_{488}$ dye was excited at 485 nm and emission spectra were collected between 500-700 nm.

The fluorescence intensity at the emission maximum (519) nm was plotted as a function of biocytin concentration (nM) and the data were fitted to a sigmoid curve to obtain the corresponding values for the unknown samples (Figure 2.3B). In the conditions assayed a ~6-fold increase in fluorescence signal upon complete displacement of HABA was observed with a detection limit of approximately 3 nM biocytin (Figure 2.3C).

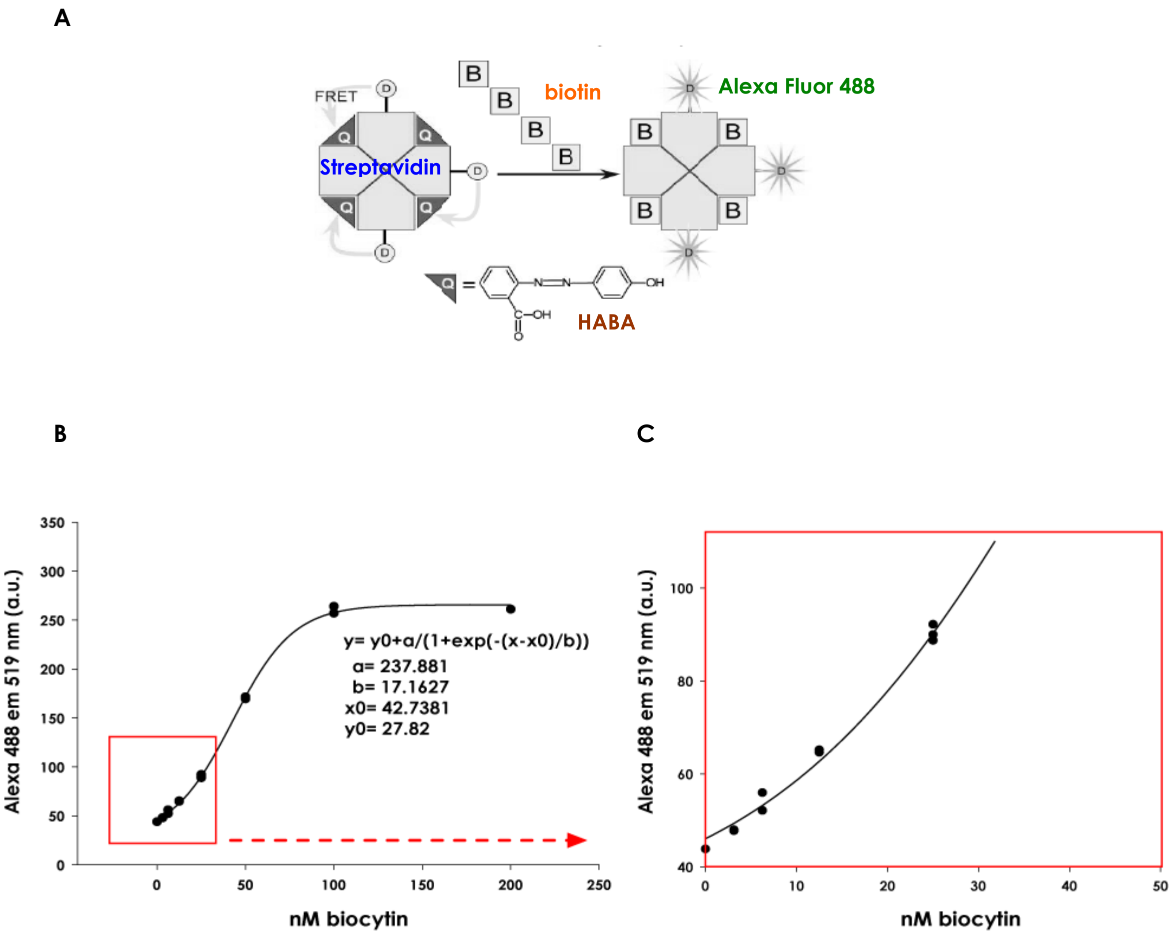

Figure 2.3: Fluorometric assay for biotin quantitation. A: General scheme of the assay adapted from (Batchelor *et al.*, 2007). HABA acts as acceptor of Alexa Fluor$_{488}$ fluorescence while bound to biotin binding sites. When biotin or biocytin is added, HABA is displaced and the fluorescence signal of Alexa Fluor$_{488}$ increases. **B:** Biocytin standard curve obtained by titrating a solution containing 25 nM StAv-Alexa$_{488}$ and 125 µM HABA in HBS. At least 8 values were obtained to plot the data within a biocytin range of 0-200 nM. Excitation of Alexa$_{488}$ at 485 nm and emission collected from 500 to 700 nm. The data illustrate a ~6-fold increase in fluorescence signal upon complete displacement of HABA. According to manufacturers, three biotin-binding sites are available per streptavidin molecule corresponding to 75 nM biotin binding sites **C:** The detection limit achieved was approximately 3 nM biocytin.

2.5.6. Transmission Electron Microscopy

The size and morphology of BLP and encapsulated QDs were analyzed by TEM by Dr. Dietmar Riedel in the Electron Microscopy department at the MPIbpc.

2.6. Labeling and targeting of BLP

2.6.1. EGF-QDs preformed complexes

The formulation of the streptavidin conjugated QDs includes a polyethylene glycol 2000 (PEG) outer layer to which 6-8 streptavidin molecules per QDs are covalently linked. This allows variations in the stoichiometry of the ligand-QD complexes. Procedures for binding biotinylated ligands to commercial streptavidin conjugated quantum dots were optimized in our lab and detailed protocols are described in (Lidke *et al.*, 2007).

Biotin-EGF were coupled to StAv-QD_{525} (or QD_{605}) at ratio 2:1 or 4:1 in HBS with 0.2% BSA at 50 nM QDs final concentration. Solutions were incubated at 15 °C for at least 30 min with gentle agitation before coupling to BLP.

2.6.2. EGF-QDs coupling to BLP

BLP loaded with QD_{655} or plasmid DNA were incubated with preformed complexes of EGF-QD_{525} (1:1 v/v) in HBS suplemented with 0.2% BSA. Final concentration of QD_{525} was 25 nM whereas final biotin concentrations on BLP varied from 0.2-10 µM biotin. This mixture was incubated for at least 2 h at 15 °C with continuous shaking.

Separation of EGF-QDs-BLP from EGF-QDs could not be achieved by size exclusion chromatography or sucrose gradient (data not shown) and resulted in considerable sample loss. Therefore, upon incubation with cells, residual free preformed complexes (EGF-QDs) were expected to bind to EGF receptors (Lidke *et al.*, 2004) being indistinguishable from the targeted particles (EGF-QD–BLP). In order to solve this problem, two-color BLP labeling strategies were designed for BLP either loaded with QDs (Figure 2.4A) or plasmid DNA (Figure 2.4B).

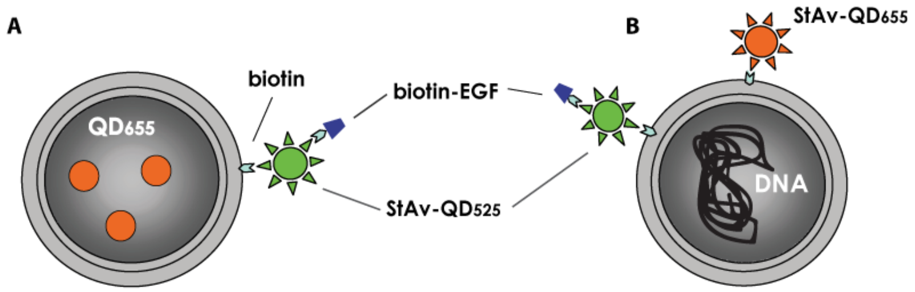

Figure 2.4: EGF tagged and two-color labeled BLP. A: with encapsulated carboxyl-QD_{655}. **B:** with encapsulated plasmid DNA.

In the case of BLP-DNA (Figure 2.4B), particles were incubated first with EGF-QD_{525} in HBS supplemented with 0.2% BSA for 30 min at 10 °C. Then, the non-targeted StAv-QD_{655} were added to the EGF-QD_{525}-BLP particles, and incubation proceeded for at least 2 h at 10 °C before *in vitro* cells experiments. The final concentration of both StAv-QDs was 25 nM whereas the final concentration of encapsulated DNA varied among preparations and is stated in each experiment.

In both approaches, the green emitting StAv-QD_{525} are the ones targeted to the EGFR in A431 cells, whereas the red emitting QD_{655} without the ligand, serve to track the BLP themselves.

2.7. Live-cell experiments

2.7.1. Cell culture

A431 and CHO cell lines were cultured in Dulbecco's Minimal Essential Medium (D-MEM) supplemented with 10% fetal calf serum (FCS), 50 U/ml of penicillin and 50 U/ml of streptomycin. WM983A cells were grown in three parts DMEM and one part Leibovitz's L15 medium supplemented with 10% heat inactivated (56 °C for 20 min) FCS and Pen-Strep. All cells were grown as a monolayer at 37 °C in a humidified atmosphere containing 5% CO_2. For microscopy experiments, cells were seeded one or two days in advance onto 12-mm-diameter glass coverslips and employed at a 40-50% confluence. For binding experiments, cells were starved in serum free DMEM for 4 h prior to the incubation with BLP to reduce signaling induced by growth factors present in the serum.

2.7.2. Experimental conditions for the incubation of A431 cells with BLP

Two-color QDs labeled, EGFR-targeted and non-targeted BLP-DNA or BLP-QDs were diluted in 200 or 500 µl Tyrode buffer with 0.5% BSA, to obtain 0.5 nM QD_{525} and 2 nM EGF final concentration. Preincubation of targeted and non-targeted BLP with starved A431 cells was carried out first at 15 °C, a temperature non-permissive for endocytosis. This preincubation time was varied from 5 to 30 min, then cells were warmed at 37 °C and were incubated from 10 min to 2 h. Finally, unbound BLP were removed and cells washed with Tyrode's buffer.

Confocal fluorescence microscopy was performed on live cells immediately after removing the complexes and after 30 min and 1, 2, 4, 12, 24 and 48 h incubation at 37 °C. When incubation was extended for more than 1h after removing the BLP, Tyrode's buffer was replaced by complete DMEM.

2.7.3. Incubation of EGF-QDs and Transferrin-$Alexa_{488}$ complexes with A431 cells

A431 cells were grown on glass coverslips at a density 40-50 % and serum-starved before experiments. Transferrin-Alexa $Fluor_{488}$ (60 nM) and EGF-QD_{605} complexes (2 nM) were added to the cells to allow simultaneous internalization. Incubation with the complexes at 37 °C proceeded for 10 and 30 min.

In a second experiment, EGF-QDs complexes were added first to the cells and after 2 h incubation at 37 °C, Transferrin-Alexa $Fluor_{488}$ complexes were added for 5 min. Then, complexes were removed and the cells rinsed and fixed in 4% paraformaldehyde for 15 min on ice to prevent redistribution of the QDs. After fixation, coverslips were mounted in PBS for confocal microscopy.

QD_{605} and Alexa $Fluor_{488}$ were excited with the 488 nm laser line and the emission collected with 565-615 nm and 520-30 nm BP filters, respectively. When QD_{655} were employed, they were excited with the 532 nm line and the emission was collected through a 650 nm LP filter.

2.7.4. Competitive binding assay

Free ligand EGF (recombinant human) was added to starved A431 cells at 200 ng/ml (33 nM) final concentration and cells were incubated for 10 min at 10 °C to prevent internalization. Then, the EGFR targeted BLP (EGF-QD_{605}-BLP-QD_{655}) were added to the cells at a final concentration of 2 nM EGF at 10 °C and incubation proceeded at 37 °C for 10 min. Cells were rinsed with Tyrode's buffer and confocal microscopy images were acquired immediately in live cells during 60 min at RT.

The same protocol for applied for binding experiments with excess ligand was carried out to test for unspecific binding of EGFR targeted BLP in CHO cell line and WM983A melanoma cell line, both devoid of EGF receptor.

2.7.5. Experimental conditions for targeted gene delivery by BLP

Cells were seeded in 6-well plates at a density of 0.8-1 x 10^5 cells per well 24 h prior to incubation with BLP-DNA. Starved and non-starved A431 cells were incubated with EGFR-targeted and non-targeted BLP-DNA. Since lipid particles with multiple biotins can cause aggregation of EGF-QDs, the following two-step protocol was applied to decrease the possible cross-linking of BLP and maximize the binding of BLP-DNA to A431 cells:

1. Preformed complexes of EGF-QD_{655} (molar ratio 1:4) were added to A431 cells at final concentration 0.5 and 2 nM QDs and incubated on ice for 5 min.
2. Cold BLP-DNA solution containing 1µg plasmid DNA was added for 15-30 min at 15 °C to allow binding but not endocytosis.

Control of non-targeted delivery was carried out by adding cold BLP-DNA (1µg plasmid) for 15-30 min at 15 °C to A431 cells without the preincubation with EGF-QD_{655} complexes.

After incubation at 37 °C for 10, 30 or 60 min, complexes were removed and the cells were washed with Tyrode's buffer. Incubation proceeded for up to 48 h at 37 °C in complete DMEM before analyzing GFP expression by fluorescence microscopy or flow cytometry (see section 2.9).

2.8. Confocal fluorescence microscopy

2.8.1. Simultaneous detection of two different colors of QDs

Scanning confocal fluorescence microscopy is a powerful technique for studying dynamic processes in specific intracellular compartments. It is particularly suitable to report whether two different probes of interest are physically located in the same compartment. Colocalization of labeled molecules can be analyzed by scanning single focal planes along the z-axis inside a cell without interference of the out of focus light from other focal planes (Chen *et al.*, 2004). Multiple x-y focal planes can be stacked to reconstruct a 3D- image of the subcellular region under study.

Confocal fluorescence microscopy was performed with a Zeiss 510 Confocal Laser Scanning microscope using a water immersion objective C-Apochromat 63x/1.2 NA (numerical aperture).

In order to localize the two-color QDs labeled BLP, the simultaneous excitation of QD_{525} and QD_{655} was achieved with the 488 nm laser line, or in some experiments with the 458 nm line to increase the fluorescence intensity. QDs signals were simultaneously detected and collected in separated channels with appropriate filters, in this case, 520/20 BP for QD_{525} and 585 LP for QD_{655}. When QD_{525} was replaced by QD_{605} in preformed complexes with biotin EGF, the QD_{605} and QD_{655} were detected using 585-615 BP and a 650 LP filters, respectively. To eliminate possible cross-talk when using the same excitation wavelength, single color EGF-QDs controls were tested for optimization of the gain settings. Time series with single and multiple focal planes were acquired with a pinhole set to 1 Airy disc. With the given settings, channel cross-talk was negligible as determined using single-labeled samples. For qualitative analysis, images were background-corrected before performing brightness and contrast enhancement. The same modifications were applied to all samples and controls. Digital image analysis was carried out with the free software Image J (http://rsb.info.nih.gov) and orthogonal sections were reconstructed using the software provided with the microscope.

2.8.2. Colocalization analysis

For quantitative colocalization analysis of QDs in targeted and labeled BLP during binding experiments, background was substracted from both QDs channels. The degree of colocalization was evaluated by the Pearson's correlation coefficients estimated according to specialized algorithms applied to the images (Costes *et al.*, 2004; Kreft *et al.*, 2004).

Pearson's correlation coefficient

Pearson's correlation coefficient R_r, is one of the standard measures in pattern recognition. In the equation displayed below, $S1$ represents signal intensity of pixels in the channel 1 and $S2$ represents signal intensity of pixels in the channel 2; $S1_{aver}$ and $S2_{aver}$ reflect the average intensities of these respective channels.

$$R_r = \frac{\sum_i (S1_i - S1_{aver})(S2_i - S2_{aver})}{\sqrt{\sum_i (S1_i - S1_{aver})^2 (S2_i - S2_{aver})^2}}$$

Rr is used for describing the correlation of the intensity distributions between channels. It takes into consideration only similarity between shapes, while ignoring the intensities of signals. Its values range between −1.0 and 1.0, where 1.0 indicates significant correlation, 0 indicates no correlation and −1.0 indicates negative correlation. Negative values of Rr, however, should be interpreted very cautiously.

Colocalization of QD_{525} and QD_{655} in dual-labeled BLP was demonstrated by presenting a plate of three images, two corresponding to the red (QD_{655}) and green (QD_{525}) channels, and a third image where the channels are merged and the overlapping pixels displayed in yellow. The distribution of pixels according to channels can be visualized in a two-dimensional scattergram or correlation plots where the degree of colocalization is described by Rr.

2.9. Quantitative GFP expression analysis

2.9.1. Epi-fluorescence microscopy

Conventional epifluorescence microscopy was performed with an Olympus IX71 microscope equipped with a Plan-Fluor 10X objective and a CCD camera (Andor). The following filter sets were applied:

i. For Hoechst H33342 (ex. 350/50 BP, 400 DM, em. 460/50 BP)
ii. For GFP (ex. 480/30 BP, 505 DM, em. 535/40 BP)
iii. For QD_{655} (ex. 560/55 BP, 595 DM, em. 655/40 BP)

Quantitative GFP expression analysis was performed with the DIPimage toolbox for Matlab 7.01 (http://www.ph.tn.tudelft.nl/DIPlib/index.html). The percentage of cells expressing GFP was calculated relative to the total number of cells analized in 20 random microscopic fields. These were detected by staining the nuclei with the fluorescent dye bisbenzimidazole Hoechst H33342 (1 mM) for 20 min at RT in PBS-BSA buffer.

The number of cells per field was determined automatically based on the number of Hoechst stained cell nuclei (blue). This was carried out by measuring the total blue area (in pixels), corresponding to nuclear staining divided by the average nucleus area calculated independently for each field. The number of GFP expressing cells was calculated by counting the number of blue nuclei colocalized with green cytoplasm and visually inspected for control.

The input to the algorithm is two images: one with Hoechst-stained cell nuclei and one with GFP protein fluorescence. The images were processed as follows:

In images with Hoescht stained nuclei:

1. Correction of uneven illumination
2. Thresholding the blue Hoechst image
3. Labeling of all spots using connected component analysis
4. Filtering out spots with an area less than 100 pixels and not round
5. Finding the mean area of the spots: this will serve as the average area of a single nucleus
6. Division of the total amount of pixels above the threshold (step 2) by the average nucleus area to get the total number of cells in the image

In images with GFP expressing green fluorescent cells:

1. Suppression of spot-like negatives using elliptic gray-value erosion of width 4
2. Thresholding the image, marking 10% as passed pixels
3. Binary erosion of width 4 to suppress poisson noise
4. Labeling of all spots using connected component analysis
5. Filtering out of spots with area smaller than twice the average area of the nucleus

In combined images:

1. Finding pixels that are both part of a nucleus (blue) and labeled with GFP (green).
2. Division of the number of pixels obtained in step 1 by the average area of a single nucleus to obtain the number of GFP-expressing cells
3. Division of the number of GFP-expressing cells by the total number of cells in each field analyzed to get the percentage of GFP-expressing cells.

2.9.2. Flow cytometry

A431 cells incubated with BLP-DNA (following protocol in 2.7.5) were resuspended with Trypsin-EDTA in PBS, fixed in 4% PFA/PBS and the percentage of cells expressing GFP was analyzed in a Coulter Epics Elite flow cytometer equipped with a 488 nm argon ion laser.

GFP fluorescence was excited at 488 nm and emission detected using a 525/40 nm BP filter. To discriminate between viable and dead cells and to exclude doublets, cells were appropiately gated by forward/side scatter and 10.000 events per sample were collected. Further data analysis, subpopulation gating and statistic calculations were performed using the software Reflex.

2.10. *bis*-PNA:DNA Hybrids

2.10.1. Plasmid DNA amplification and purification

Competent bacterial strain *E. coli* DH5α was transformed with the pEGFP-C1 plasmid. The transformation mix was plated onto a selection agar containing kanamycin 30 µg/ml and incubated at 37 °C overnight. A single bacterial colony was picked and inoculated in 2 ml LB/kanamycin medium then, incubation proceeded at 37 °C with vigorous shaking for 8 h. This culture was afterwards, inoculated into 500 ml of LB/kanamycin and incubated overnight at 37 °C with shaking. The bacterial culture was harvested by centrifugation and plasmid DNA purified by ion excahnge chromatography using the QiaFilter Plasmid Maxi Kit, according to the manufacturer´s instructions.

2.10.2. Biotinylation of *bis*-PNA

bis-PNA sequence, NH_2-LL-TCCCCCTTT-LLL-TTTCCCCCT-LL L=*8-amino-3,6-dioxaoctanoic acid*, was biotinylated at the terminal amino group by adding a 20 molar excess of Sulfo NHS-LC-LC-Biotin reagent in PBS and incubating for 90 min at RT without removing the excess of reagent. Biotin incorporation was 80-90% for three independent preparations measured indirectly as the amount of free non-modified amino groups. This was calculated upon reacting the free amino groups with the fluorophore fluorescamine (Udenfriend *et al.*, 1972), the fluorescence obtained was proportional to the percentage of available amino groups.

2.10.3. Cy5 labeling of *bis*-PNA

Labeling reaction with Cy5 was performed by mixing 5 µM *bis*-PNA and 50 µM NHS-Cy5 in Carbonate buffer 0.1 M pH 8.3, the reaction mix was incubated for 2 h at RT followed by 2 h at 4 °C.

Purification of labeled PNA was performed in a chromatographic system (Smart) using a gel filtration column with matrix of dextran Superdex 75 and eluted in 10 mM Acetate buffer pH 5. The concentration of the recovered Cy5-*bis*-PNA was calculated using the extinction coefficient of Cy5 at 650 nm, $\varepsilon_{650\ nm} = 250{,}000\ M^{-1}cm^{-1}$.

2.10.4. Hybridization of *bis*-PNA to pEGFP-C1 plasmid

Biotin-*bis*-PNA or Cy5-*bis*-PNA were hybridized to the anchoring site in pEGFP-C1 plasmid at position 4515-4523 (sequence AGGGGGAAA). Biotin-*bis*-PNA or Cy5-*bis*-PNA were added to 2 µg plasmid in 10 mM Sodium Acetate buffer pH 5 at molar ratios of *bis*-PNA to plasmid, 2:1, 4:1, 8:1, 20:1 and 40:1. The mixtures were incubated for 3 h at 37 °C and hybrids were purified from excess labeled or biotinylated *bis*-PNA using Sephacryl HR-400 spin columns pre-equilibrated with 10 mM Sodium Acetate buffer pH 5. After sample addition, a centrifugation step was carried out for 2 min at 800 g to recover the purified hybrids. Biotin-*bis*-PNA-plasmid

DNA will be referred as biotinylated Hybrids. Purity and quality of the recovered plasmid were determined by enzymatic digestion with restriction endonucleases.

2.10.5. QD labeling of Hybrids

QD labeled Hybrids were obtained by reacting biotinylated Hybrids (2 nM biotin) with StAv-QD_{655} (2 nM streptavidin) in 50 mM Sodium Borate buffer pH 8.5 for 4h at 4 °C under agitation. These complexes will be referred as QD-Hybrids.

2.10.6. Restriction fragment analysis by gel electrophoresis

Hybrids were analyzed by digestion of pEGFP-C1 plasmid with the following endonucleases:

Apa LI: Restriction site at position 4360
Ava II: Restriction sites at positions 1270, 3272, 3717
Ase I: Restriction site at position 4731
PNA target site in plasmid: 4515-4523 bp

Plasmid digestion with Apa LI and Ava II generates restriction fragments of 445 bp, 643 bp, 1641 bp and 2002 bp. The PNA target site is located in the 1641bp fragment.

Digestion with Apa LI and Ase I produces two fragments of 379 bp and 4352 bp. The PNA target site is located in the 379 bp fragment.

Reaction mix for plasmid digestion

Plasmid DNA (0.5-1 µg) was incubated with 2 µl 10X buffer NB4**, 1-2 U (Units*) restriction enzyme and 1 µg/µl BSA. Milli Q water was added to a final volume of 20 µl and the reaction mixture incubated at 37 °C for 1 h. Restriction fragments were analyzed in 1% agarose gels.

*One unit of restriction enzyme is the amount of enzyme required to completely digest 1 µg substrate DNA in 1 hr.

**NEB 4: 20 mM Tris-acetate (pH 7.9), 10 mM Magnesium acetate, 1 mM DTT, 50 mM Potassium acetate

Agarose gel electrophoresis

Biotinylated, Cy5 labeled and QDs labeled Hybrids, and restriction fragments were electrophoresed in 0.8 or 2% agarose gels in 1X TAE buffer. Electrophoresis was carried out at RT under constant voltage (60 V) and gels were protected from direct light exposure. After electrophoresis, gels were stained with 0.5 µg/µl Sybr Green solution in 1X TAE to visualize total DNA content. Sybr Green, Cy5 and QDs fluorescence were detected in gels with a laser-based scanner (Typhoon instrument). The laser lines were selected according to the corresponding excitation wavelengths of the dyes and fluorescence emission detected using a 520/30 nm BP filter for Sybr Green, and a 670 nm LP filter for Cy5 and QD_{655}.

Band shift assay in polyacrylamide gels

DNA restriction fragments containing the hybridized biotin-*bis*-PNA were analyzed in a band shift assay in native polyacrylamide gels with a concentration gradient varying from 3-8% polyacrylamide in 1X TAE buffer. Gels were stained with 0.5 µg/µl Sybr Green solution after electrophoresis.

2.10.7. Conjugation of QD-Hybrids to biotin coated magnetic beads

QDs-Hybrids were vizualized in biotin coated magnetic beads prepared as follows:

i. Biotin-coated magnetic beads were obtained by conjugating a biotin dimer, EZ link PEO-Biotin dimer (200 µM) to streptavidin coated magnetic beads (76 nM streptavidin) in 50 mM Borate buffer pH 8.0 for 2 h at 4 °C
ii. Biotinylated Hybrids (20 mM biotin) were conjugated to StAv-QD_{655} (2 nM QDs and 6-8 StAv per QD) in 50 mM Sodium Borate buffer pH 8.5 and incubated ON at 4°C
iii. QD_{655}-Hybrid complexes were incubated with biotinylated beads for 2 h at RT with shaking and protected from light
iv. Samples were placed in a magnetic stand and beads washed with 50 mM Sodium Borate pH 8.5 and incubated with 0.5 µg/µl Sybr Green solution for 5 min
v. Control samples of biotinylated Hybrids, free QD and free plasmid were incubated with streptavidin or biotin coated magnetic beads and then stained with Sybr Green
vi. Treated beads were washed and resuspended in 50 mM Sodium Borate buffer pH 8.5 and were deposited on glass coverslips for fluorescence microscopy analysis

The coupling of Hybrids on magnetic beads was visualized in an inverted microscope Zeiss Axiovert 100 equipped with a CCD camera. Sybr Green fluorescence was detected with excitation filter 480/30 BP, 505 DM (dichroic mirror) and emission filter 535/40 BP, QD_{655} detection: excitation filter 560/55 BP, 595 DM and an emission filter 655/40 BP. The acquired images were processed using the DipImage Toolbox from Matlab 7.01.

2.11. Atomic Force Microscopy analysis

The Atomic Force Microscope, also called scanned-proximity probe microscopy works by measuring a local property of a sample, such as height, with a probe or "tip" placed very close to the sample. This results in a three-dimensional profile of the surface that can reach atomic resolution on hard flat surfaces.

Unlike traditional microscopes, scanned-probe systems do not use lenses. Therefore, the size of the probe rather than the diffraction effects, generally limits their resolution. Lateral resolution of 5 nm and a <0.1 nm resolution in height can be achieved.

The 'Tapping mode' of scanning overcomes problems associated with friction, adhesion and electrostatic forces by shortly placing the tip in contact with the surface to provide high resolution and then lifting the tip off the surface to avoid dragging the tip across the sample surface. This mode inherently prevents the tip from sticking to the surface and causing damage during scanning. The AFM can scan the sample under air, vacuum or in a variety of fluids where the sample must be previously deposited on a flat substrate, such as mica or glass.

Images of BLP or DNA were obtained with a NanoScope III MultiMode AFM (Veeco Instruments Inc., Santa Barbara, CA) operating in tapping mode in air using silicon cantilevers. Height and amplitude images were recorded simultaneously and section analysis performed using the software available with the instrument.

2.11.1. Sample preparation for scanning

For the analysis of BLP morphology, a droplet of lipid particles solution purified from sucrose density gradient was deposited on a mica surface and was air-dried before scanning. For the QD-Hybrids analysis, samples containing 2 µg/ml plasmid were applied on the mica surface pretreated with 2.5 mM $MgCl_2$. After 30 seconds, the mica surface was rinsed with water and was gently dried with a flow of nitrogen before AFM scanning.

3. Results: "Characterization of Biotinylated Lipid Particles"

The spontaneous formation of DNA-lipid particles in the neutral detergent octyl-β-D-glucopiranoside (OGP) was initially described by (Zhang *et al.*, 1997). This method was optimized to encapsulate single plasmid molecules with a 50-70% efficiency in particles of ~70 nm size (Wheeler *et al.*, 1999). The physical characteristics of these particles known as SPLP (Stable Plasmid Lipid Particles) appear ideal for *in vivo* application. However, the transfection potency of SPLP is quite limited due to the PEG coating which decrease the cell association of SPLP and subsequent uptake. The length of the carbon chain in the PEG-lipid directly affects the rate of DNA released from SPLP. For, instance, short acyl chain (C8) in PEG-lipids have transfer rates from SPLP in the order of minutes and are referred as to exchangeable lipids, whereas PEG-lipids with acyl carbon chain longer than C20 have transfer rates of hours or days and are referred as to non-exchangeable lipids (Mok *et al.*, 1999).

The approach explored in this thesis involved the addition of a biotinylated lipid (biotin-PEG-DSPE) to enhance cell targeting ability by subsequently coupling the EGF ligand via streptavidin-biotin interaction. These new liposomes were named BLP (Biotinylated Lipid Particles).

This chapter focuses on the preparation of three different BLP formulations containing exchangeable and non-exchangeable PEG-lipids and a pH-sensitive PEG-lipid followed by the characterization of the particles according to size, biotin content and DNA/QDs encapsulation efficiency.

3.1. Encapsulation of plasmid DNA and QDs in BLP

3.1.1. BLP formulations

Various BLP batches were prepared by mixing DOPE (8.4 mM), DOTAP (0.6 mM) with different amounts of the PEGylated lipids. In Table 3.1 are shown the main differences between BLP and the original SPLP formulations such as the inclusion of a biotinylated lipid (Biotin-PEG-DSGS), a PEGylated pH-sensitive lipid (PEG-DSGS) and ≤10% PEG-lipid content.

PEG-lipid	**PEG content (mol %)**	
	BLP	**SPLP**
PEG-Cer-C_{20}	10	10
PEG-Cer-C_8	1.4 ; 2.7 ; 10	10-20
PEG-DSGS	1.4 ; 2.7	-
Biotin-PEG-DSPE	0.24	-

Table 3.1: PEG-lipids composition of BLP compared to SPLP. PEG-Cer-C20 (non-exchangeable PEG-lipid); PEG-Cer-C8 (exchangeable PEG-lipid); PEG-DSGS (pH sensitive PEG-lipid) and Biotin-PEG-DSGS (biotinylated lipid). The final lipid concentration was ~10 mM.

Lipid recovery was estimated from the amount of incorporated biotin-PEG-DSGS after detergent dialysis. Biotin content was quantified using a fluorometric assay with nanomolar sensitivity. The estimated values of lipid recovery obtained from three independent BLP preparations were, 58 ±14 % for BLP loaded with DNA and 65 ±7 % for BLP loaded with QDs.

3.1.2. Time course formation of BLP during detergent dialysis

Lipids-detergent solutions prepared with plasmid DNA and control samples without plasmid were dialyzed. In the presence of DNA, visible turbidity was detected within the first hour of dialysis, suggesting the formation of self-assembled lipid-DNA particles (Zhang *et al.*, 1997).

The hydrodynamic diameter of such particles during the course of detergent dialysis was measured by DLS. As shown in Figure 3.1A, after 45 min regardless of the presence of DNA, particles with a mean hydrodynamic diameter of ~30 nm were detected. This value was consistent with the size of mixed micelles of lipids and detergent (Zumbuehl and Weder, 1981). At this time point, the polydispersity index (pdi) was greater than 0.25, indicating that more than one lipid particles population contributed to the intensity of scattered light (see below). After 180 min, control BLP without plasmid achieved their final size with a mean diameter of ~50 nm and appeared homogeneous in size (pdi<0.25). On the other hand, in the presence of DNA, particles continuosly grew in size up to ~300 nm during the initial 3 h followed by a slight size increase upon vesiculation.

As stated by pdi values greater than 0.25, the heterogeneity of the samples was examined from the size distribution profiles for empty BLP (Figure 3.1B) and DNA loaded BLP (Figure 3.1C). In the absence of DNA, the two peaks in the size distribution profile observed after 45 min were attributed to mixed micelles and empty BLP. After 360 min, the mixture was enriched in particles of homogeneous size of ~50 nm (Figure 3.1B).

In the case of lipid-DNA mixtures (Figure 3.1C), the two peaks in the initial bimodal size distribution observed after 45 min, probably represent mixed micelles and lipid-DNA particles (>1µm). After 360 min dialysis, the bimodal size distribution still persisted but the two peaks were centered on ~60 nm and ~400 nm, indicating the formation of empy BLP and DNA loaded particles (BLP-DNA) respectively.

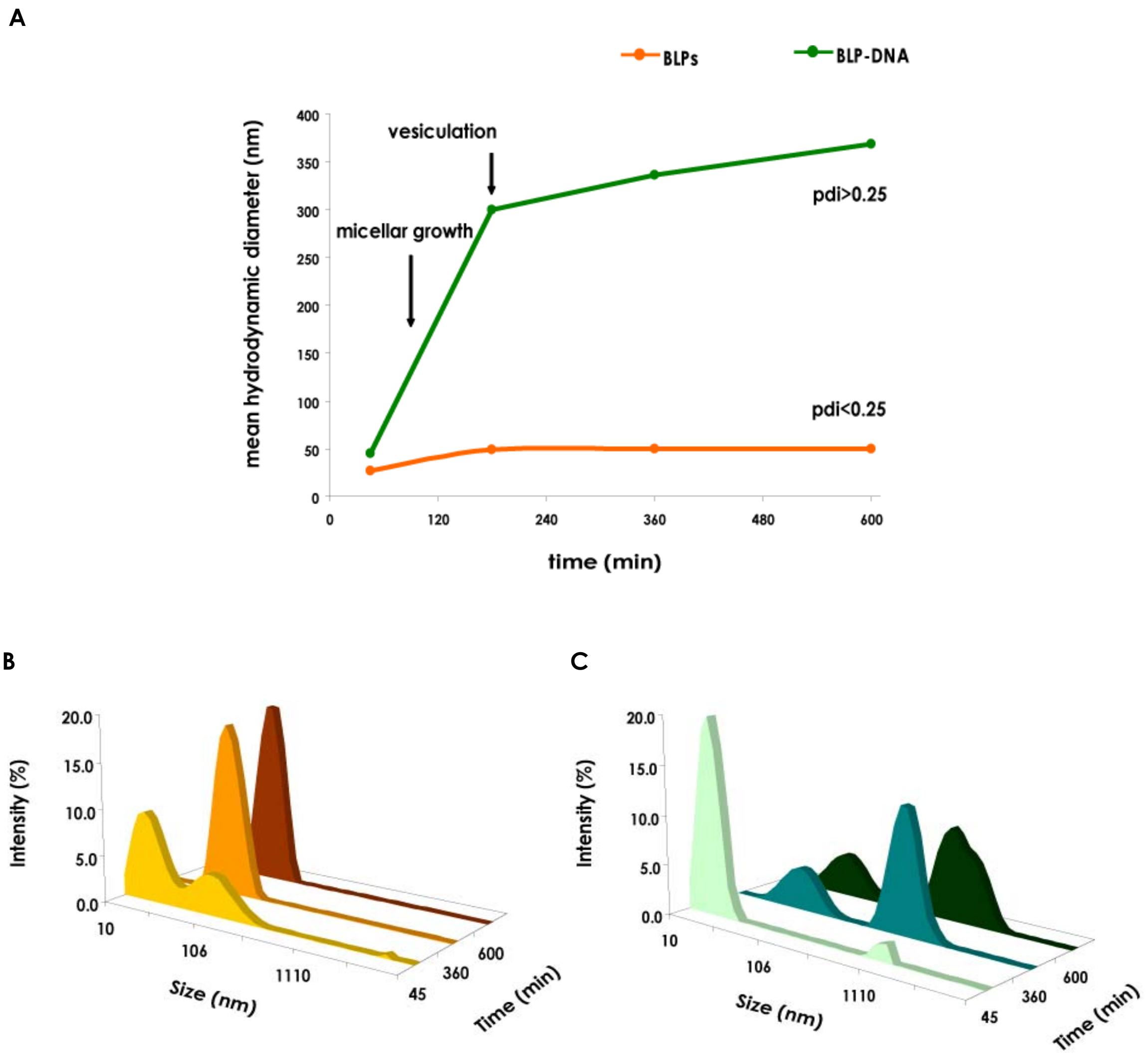

Figure 3.1: BLP formation during detergent dialysis. A: Mean hydrodynamic diameter measured by DLS after 45, 180, 360 and 600 min of detergent removal. Mixed micelles of detergent and lipids coexisted after 45 min dialysis for BLP prepared without plasmid DNA (—) and with 200 µg plasmid DNA (—), respectively. Empty BLP achieved their final size after 3 h whereas vesiculation and growth of lipid-DNA particles continued for up to 6 h. **B:** Intensity based size distribution of control BLP showing the evolution of the initial bimodal distribution into an homogeneous in size BLP population. **C:** Intensity based size distribution of lipid-DNA particles showing the likely coexistence of mixed micelles and lipids-DNA aggregates after 45 min dialysis. After vesiculation and growth (360 min), the bimodal distribution likely represents empty and DNA loaded BLP. Formulation containing 10% PEG-Cer-C20.

3.1.3. BLP-DNA purification from non-encapsulated DNA

The detergent dialysis procedure resulted in the formation of a turbid suspension due to vesicle formation. However, it was likely that empty vesicles (as shown in Figure 3.1) as well as non-encapsulated plasmid were also present. A first attempt to separate BLP-DNA particles from free plasmid using anionic exchange chromatography resulted in a significant sample loss due to the interaction of BLP with the column matrix (data not shown). As empty vesicles were expected to be less dense than BLP-DNA particles, an alternative method of purification employing a discontinuous sucrose gradient was adopted (Mok *et al.*, 1999). Samples recovered after dialysis were loaded in a gradient of 2.5, 10 and 20% sucrose and centrifuged at 160.000 g for 5 h at 10 °C in swinging buckets. A control sample of 50 µg plasmid was centrifuged in identical conditions as used for BLP. The distribution of empty and DNA loaded BLP, as well as free DNA along the gradient was determined by DNA quantitation using the Sybr Green assay and size analysis by DLS.

Figure 3.2 shows the relative amount of DNA recovered in each sucrose fraction, for free plasmid (panel A), and for three different lipid formulations of BLP-DNA (panels B-D). The free plasmid in control sample without BLP, concentrated in the 20% sucrose fraction. In the case of samples containing BLP-DNA, nearly 90% of the plasmid loaded on the gradient was recovered in the 10% sucrose fraction whereas less than 2% of the total DNA loaded was located in the 20% sucrose fraction.

In order to correlate the presence of DNA with the presence of lipid particles, size measurements were carried out on each sucrose fraction by DLS (Left panel). The 2.5% sucrose fraction was enriched in particles with a mean size of ~60 nm, correlating with the size of empty BLP, whereas the 10% sucrose fraction contained particles larger than 200 nm, most likely corresponding to DNA loaded BLP.

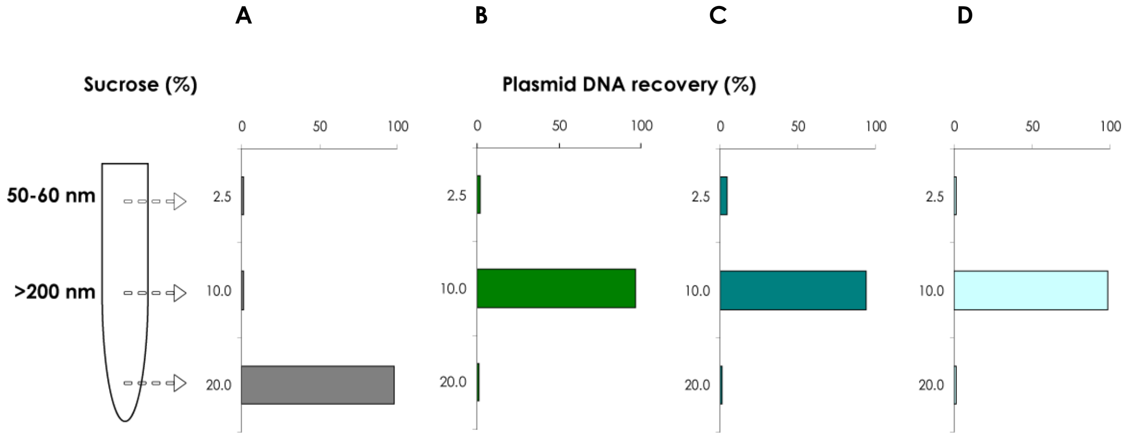

Figure 3.2: DNA distribution across the sucrose density gradient. A: control of free plasmid recovered in the 20% sucrose fraction. **B:** BLP-DNA formulated with 2.7% PEG-Cer-C8. **C:** BLP-DNA formulated with 10% PEG-Cer-C8. **D:** BLP-DNA formulated with 2.7% PEG-DSGS. The left panel shows the size analysis by DLS. The 2.5% sucrose fractions containing less than the 5% of loaded DNA concentrated vesicles of 50-60 nm in size, whereas the 10% sucrose fraction with 90% of the loaded DNA contained particles bigger than 200 nm. Total DNA was quantitated by Sybr Green assay after dissolution of BLP with 0.1% Triton X-100 to release encapsulated DNA. Free plasmid amount in samples without BLP was also calculated in the presence of 0.1% Triton X-100.

These results demonstrated that ultracentrifugation in a sucrose densitiy gradient constitutes a useful and convenient technique for BLP-DNA purification.

3.1.4. Effect of PEG content in DNA encapsulation efficiency and particle size

One objective of the characterization of BLP was to determine whether the PEG content in the formulation had a direct effect on BLP size, plasmid DNA encapsulation efficiency and plasmid DNA protection.

DNA was considered to be encapsulated in BLP, if it was able to interact with Sybr Green only after solubilization of the lipid particles with 0.1% Triton X-100. Therefore, the DNA encapsulation efficiency in BLP samples recovered after detergent dialysis was estimated by measuring Sybr Green fluorescence before and after addition of 0.1% Triton X-100 and was defined as:

$$\textbf{DNA encapsulation efficiency (\%)} = \frac{\mu\textbf{g of DNA (+) Triton X100 - }\mu\textbf{g of DNA (-) Triton X100}}{\mu\textbf{g of DNA added}} \textbf{ x 100}$$

For successful gene delivery and expression, the encapsulated plasmid DNA has to be protected from the extracellular environment. Therefore, DNA protection was measured in samples purified from sucrose density gradient by measuring Sybr Green fluorescence before and after addition of 0.1% Triton X-100 but, in this case, related to the total DNA recovered in the purified fraction:

$$\textbf{DNA protection (\%)} = \frac{\mu\textbf{g of DNA (+) Triton X100 - }\mu\textbf{g of DNA (-) Triton X100}}{\mu\textbf{g of DNA (+) Triton X100}} \textbf{ x 100}$$

Encapsulation efficiency after the detergent dialysis and DNA protection after the sucrose gradient were compared among four formulations with differences in PEG content and PEG-lipids composition and were related to the BLP size as determined by DLS.

As shown in Table 3.2, neither the efficiency of encapsulation (40-70%) nor DNA protection (65-70%) were sensibly affected by the PEG percentage, PEG-lipids or initial plasmid concentration.

The effect of different PEG content demonstrated a deeper impact in the final size than in the encapsulation efficiency of DNA in BLP. Only BLP formulated with 10% PEG-Cer-C20, formed particles of discrete sizes between 50 nm and 350 after detergent dialysis in line with previous observations on SPLP (Wheeler *et al.*, 1999).

After sucrose density gradient, BLP populations with discrete sizes between 70 nm and 340 nm were resolved for all formulations except for BLP with 2.7% PEG-Cer-C8 that tended to form aggregates. This observation was expected and it could be attributed to the effect of both, low PEG content and short acyl chain ceramide (C8) generating less sterically stabilized BLP than those containing 10% PEG-Cer-C20.

	After detergent dialysis		After sucrose density gradient	
% PEGylated lipid	**Size (nm)**	**DNA encapsulation efficiency (%)**	**Size (nm)**	**DNA protection (%)**
10% PEG-Cer-C20	50-350	10, 66	70, 90, 160, 110, 340	72
10% PEG-Cer-C8	50-1000	57 ± 4	80, 140, 160, 190, 220	64
2.7% PEG-Cer-C8	50-1000	42 ± 10	> 500 nm	68
2.7% PEG-DSGS	50-1000	62 ± 12	90, 150, 150, 220	66

Table 3.2: Plasmid DNA encapsulation efficiency and protection in BLP. DNA encapsulation and protection were measured in samples recovered after dialysis and purified from sucrose density gradient, respectively. DNA was quantified using Sybr Green in the presence and absence of 0.1% Triton X-100. The differences in PEG content in the BLP formulations showed more impact in the final size of the particle than in the DNA encapsulation efficiency or protection in BLP. Data obtained from 3-5 independent BLP preparations for each formulation. DNA encapsulation efficiency was expressed as average ± SD whereas DNA protection was expressed as median values.

3.1.5. BLP size analysis by AFM

The morphology of the BLP-DNA was explored by Atomic Force Microscopy (Ruozi *et al.*, 2005). Droplets of constant volume of BLP were deposited on a mica surface and scanning was carried out in air using tapping mode. This operation mode was selected because the contact between the tip and the sample is minimized and therefore, is more suitable for the study of soft and deformable samples, such as liposomes. Sample tilt was removed by flattening the AFM image using second-order fitting.

In Figure 3.3A, a 3-D topographical image of BLP-DNA formulated with 10% PEG-Cer-C20 shows a population of spherical particles as expected for liposome based delivery systems (Lasic and Papahadjopoulos, 1995). Three lipid particles were selected from the top view of the image in Fig.3.3A and their diameter estimated along the line profiles shown in Figure 3.3C, i.e. as the vertical distance between the mica surface and the top of the particles. Size values between 180-350 nm were obtained, in agreement with the mean hydrodynamic diameters calculated by DLS for this formulation (Table 3.2). The major drawback of this technique is the possible deformation of the soft liposomal sample due to solvent evaporation and the vertical force applied with the tip.

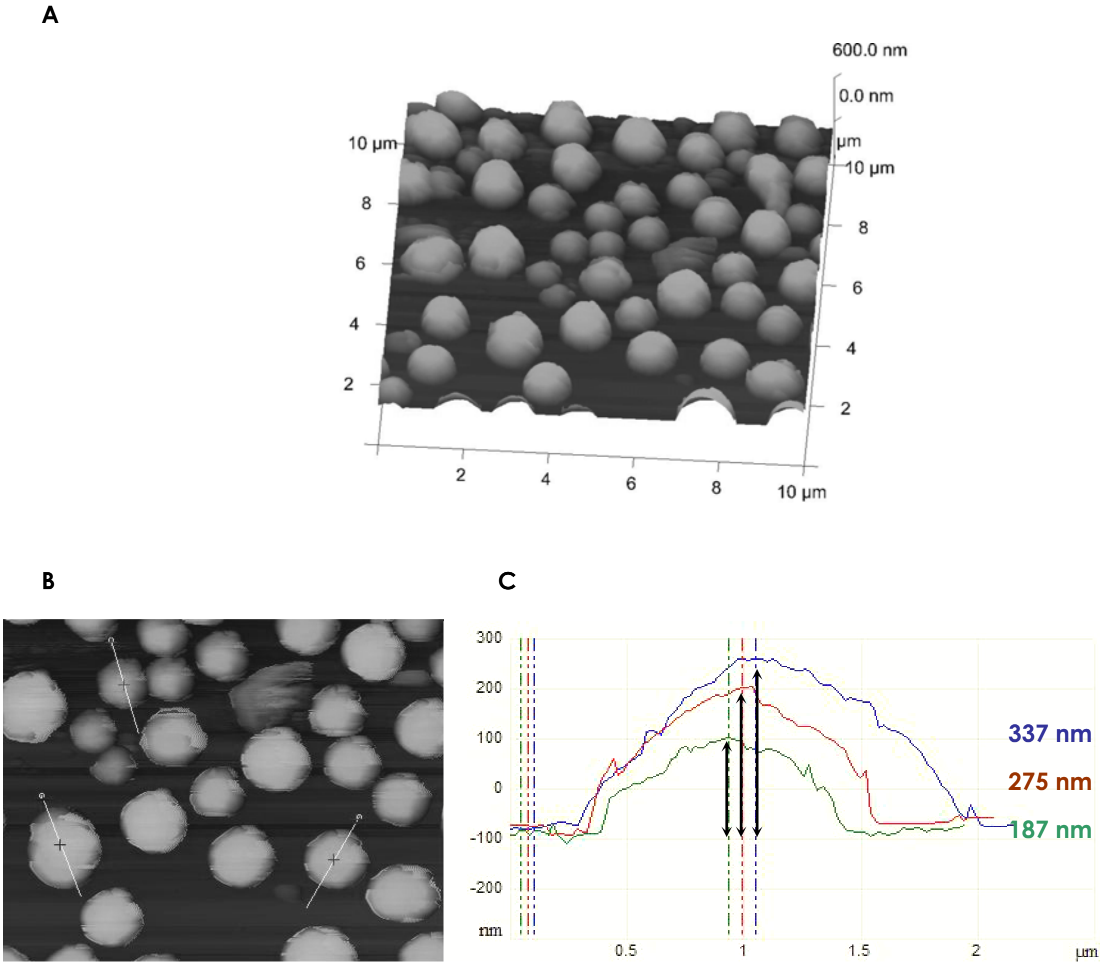

Figure 3.3: Representative AFM images of BLP-DNA on mica surface performed on tapping mode in air. A: 3-D topographical view from the height image. **B:** 2-D height image, top view from A. **C:** Height profiles along the lines shown in B. BLP-DNA with 10% PEG-Cer-C20 recovered from sucrose density gradient.

3.1.6. Encapsulation of QDs in BLP by the detergent dialysis method

BLP particles prepared by the detergent dialysis method were initially conceived for DNA encapsulation. However, to address the specificity of BLP binding to cells after tagging the particles with the EGF ligand, a fluorescent BLP was required. Therefore, the detergent dialysis technique was explored for the encapsulation of red emitting QD_{655} with a mean core size of 10 nm in formulations containing 1.4 and 2.7% PEG-Cer-C8 and 1.4 % PEG-DSGS.

During detergent dialysis of lipids-QD_{655} mixtures, the typical turbidity observed during BLP-DNA formation was not noticeable. In order to determine whether QDs were indeed encapsulated in lipid particles, samples were loaded directly in the sucrose density gradient using the same conditions as those employed for BLP-DNA and QDs fluorescence intensity distribution was examined under UV light excitation.

3.1.7. Characterization of fluorescent BLP-QDs

After ultracentrifugation in the sucrose gradient, three well-defined fluorescent fractions were observed (Figure 3.4A): a less dense bright fluorescent band on top (fraction I), a broader and less intense fluorescent band underneath (fraction II) and a fluorescent pellet (fraction III). The different densities of the particles concentrated in the two upper bands (fractions I and II) could be the result of a variable number of QDs encapsulated per particle. On the other hand, the pellet was enriched in free QDs and no biotin was detected in this fraction indicating the absence of lipid particles. As the brightest band may also contain free lipids and empty vesicles, this fraction was not further characterized.

Electron dense QD cores allow their detection by electron microscopy. TEM performed on particles recovered from fraction II (Figure 3.4B), revealed BLP containing on average of 2 to 5 encapsulated QDs. The diameter of the BLP varied from 100 to 130 nm, depending on the number of loaded QDs. Empty BLP or those containing only one QD were generally smaller than 100 nm. These values were in agreement with those obtained by DLS measurements for BLP-QD (Figure 3.4 C). The mean hydrodynamic diameter for BLP in fraction II, determined for two independent preparations and three different formulations was 109 ±16 nm (pdi <0.25). This fraction was recovered for coupling the EGF ligand to target the BLP to A431 cells.

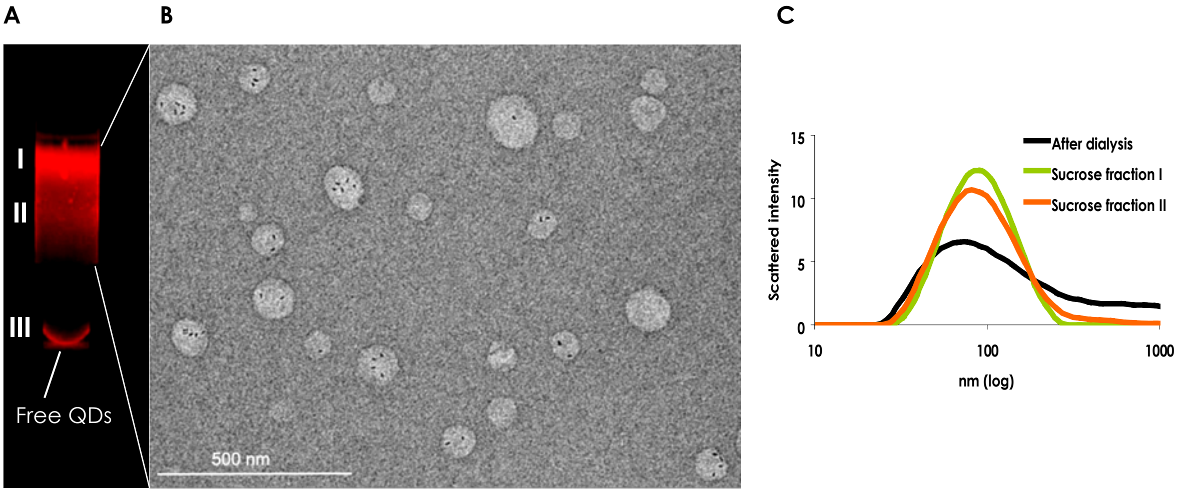

Figure 3.4: Purification and size characterization of BLP-QD. **A:** Fluorescent fractions corresponding to particles associated with QDs were found on the top layers of the gradient (fractions I and II) whereas free QDs were found mainly in the pellet (fraction III). **B:** TEM image of BLP showing particles of 100-180 nm in diameter containing 2-5 encapsulated QDs. Empty liposomes smaller than 100 nm. Scale bar 500 nm. **C:** Representative size distribution of BLP formulations with encapsulated QDs measured by DLS after dialysis and after purification in sucrose density gradient.

In summary, the size analysis of BLP-DNA particles by DLS indicated that their final size could be modulated by varying the percentage of PEG content. For BLP-DNA, formulations containing 10% PEG-Cer-C20, 10% PEG-Cer-C8 or 2.7% PEG-DSGS showed that particles with a size ranging from 150 to 350 nm could be recovered from sucrose density gradients.

In a novel application of the detergent dialysis technique, QDs were successfully encapsulated in BLP, showing a monomodal size distribution within a range of 100-130 nm. In contrast to BLP-DNA, BLP-QDs remained stabilized and did not aggregate even when PEG-lipid content was < 2.7%. In addition, ultracentrifugation in sucrose density gradient allowed the purification of BLP-DNA and BLP-QDs particles from non-encapsulated material and empty vesicles.

4. Results: “Cell uptake of EGFR targeted and QDs-labeled BLP”

The epidermal growth factor receptor (EGFR, erbB1, HER1) is overexpressed in a broad spectrum of malignant tumors and, as discussed in the introduction, represents an interesting target for delivery of therapeutic liposomes (Kullberg *et al.*, 2005; Mamot *et al.*, 2005). Biotinylated EGF ligand conjugated to streptavidin-coated QDs binds to EGFR leading to the receptor activation and internalization (Lidke *et al.*, 2004; Lidke *et al.*, 2005). The attachment of the fluorescent nanoparticle did not impair the binding capacity and biological functions of this growth factor (Lidke *et al.*, 2007).

The aim of the work presented in this chapter was to target the purified BLP carrying either DNA or QDs to A431 cells overexpressing the EGFR by tagging the particles with the EGF ligand. The first concern to be addressed, was whether the internalization of EGF tagged BLP could be impaired, as the large size of the lipid carrier may interfere with the dimerization of the EGFR necessary for the subsequent activation and internalization by endocytosis.

The targeted delivery system was evaluated regarding:

- binding ability
- intracellular fate of targeted BLP
- delivery of encapsulated QDs
- transfection efficiency of the encapsulated DNA

The effect of PEG content and the presence of a pH sensitive lipid or PEG-ceramides with variable carbon-chain lengths in the efficiency of cargo delivery were investigated.

The specificity for the EGFR was examined in a competitive binding assay in the presence of free EGF ligand. In addition, EGFR targeted BLP were incubated with two different cell lines that do not express the EGF receptor.

Labeling and targeting of BLP were achieved by coupling preformed EGF-QD complexes providing a monitoring tool for the specificity of BLP uptake and cargo release in live cells by confocal laser scan microscopy (CLSM).

4.1. Targeting and labeling of BLP

In order to target the BLP to the EGFR, particles loaded with QD_{655} (red) were coupled via biotin-streptavidin linkage to preformed complexes of EGF-QD_{525} (green) as depicted in Figure 4.1. These particles were detected by CLSM in live cells, using a single excitation wavelength for both QDs colors. With this approach, colocalized red-green dots would be indicative of specific uptake, whereas red fluorescence would reveal unspecific binding of non-targeted BLP-QD_{655}. Free unconjugated EGF-QD_{525} can be clearly distinguished as single green dots.

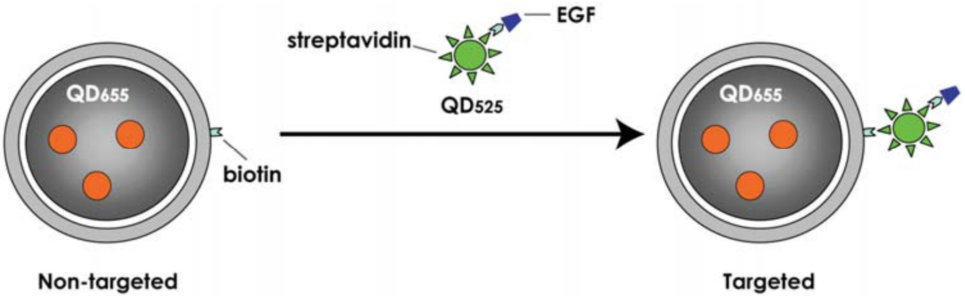

Figure 4.1: Scheme depicting the targeting and labeling strategy of BLP with encapsulated QD_{655}. Preformed complexes of EGF-QD_{525}, (molar ratio 4:1) were conjugated to biotin molecules on the BLP surface. Specific uptake would be evidenced as colocalized dots by confocal fluorescence microscopy. Red fluorescence would indicate unspecific binding of non-targeted BLP-QD_{655}. Free unconjugated EGF-QD_{525}, when present, would be detected as green dots.

The strategy of adding the EGF ligand as a preformed complex with QDs instead of direct binding to BLP was adopted in order to take advantage of the multiple streptavidins coating the nanoparticle. The QDs used in this study carried 6-8 streptavidins (according to the manufacturer). Therefore, the amount of biotinylated EGF ligands per QD particle was selected to enhance binding while still leaving unoccupied streptavidins for coupling to BLP.

The two-color BLP labeling strategy was designed to evaluate whether specific uptake of BLP and the cytoplasmic delivery of the cargo took place. Intracellular colocalization of both nanoparticles would indicate not only the specific uptake but the presence of QD_{655} still trapped inside the lipid particle and poor release. If the BLP were able to fuse with endosomal membranes and release the QDs, colocalization was expected be lost and the characteristic blinking of individual QDs be observed.

4.1.1. Cell uptake of targeted BLP-QDs

The interaction of BLP with A431 cells was evaluated by fluorescence confocal microscopy with EGF-tagged and dual-labeled BLP containing 1.4% and 2.7% PEG-Cer-C8 and 1.4% PEG-DSGS upon incubation for 1 h at 37 °C. As shown in Figure 4.2, both QDs extensively colocalized after 1 h, indicating that targeted EGF-QD_{525}-BLP-QD_{655} particles were internalized. Non-targeted BLP-QD_{655} were not taken up by cells or were observed as a faint fluorescence for all lipid formulations examined (Figure 4.2 panels A, B, C). The cell uptake of BLP was associated with a dot-pattern distribution, which could be attributed to the clustering of the lipid particles in endosomal compartments.

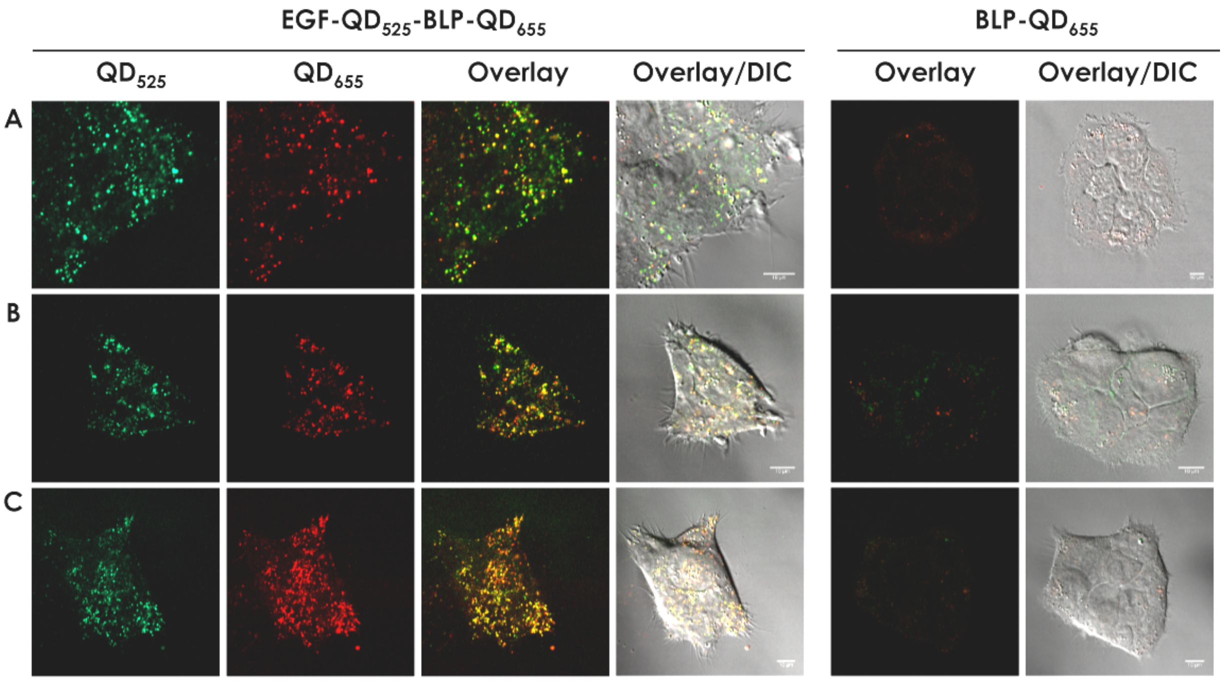

Figure 4.2: Intracellular localization of targeted EGF-QD$_{525}$-BLP-QD$_{655}$ and non-targeted BLP-QD$_{655}$. A431 cells were incubated with EGFR targeted and non-targeted BLP for 1 h at 37 °C. Unbound complexes were removed and live imaging performed by confocal fluorescence microscopy at RT in Tyrode’s buffer. **A:** BLP-QDs 1.4% PEG-Cer-C8. **B:** BLP-QDs 2.7% PEG-Cer-C8. **C:** BLP-QDs 1.4% PEG-DSGS. Colocalization of QD$_{525}$ and QD$_{655}$ showing BLP distributed in presumably endosomal compartments. Scale bar: 10 µm.

4.1.2. Intracellular distribution of internalized BLP

Figure 4.3 (Panels A-C) shows a reconstructed three-dimensional image of two A431 cells that had internalized many targeted BLP-QDs during a 10 min pulse followed by 1h incubation (chase) at 37 °C. Interestingly, most of the internalized EGF-QD$_{525}$-BLP-QD$_{655}$ complexes accumulated in the perinuclear region of the cell (Panel A), although a large fraction was still visible in small structures underneath the cell membrane (Panel B). Close observation of single vesicles inside the cells (Panel D) showed that colocalized QDs had variable intensities for each QD color as evidenced by the heterogenous yellow-orange pseudocolor. This could be explained as a distribution in the number of encapsulated QDs in BLP (1-5 QDs) as showed by TEM (Fig. 3.4), and presumably the presence of a variable number of EGF-QD$_{525}$ bound per lipid particle. In addition, and possibly most important, fusion of vesicles ocurring during endosomal sorting (Maxfield and Yamashiro, 1987) could have brought several particles together.

Single green dots (Figure 4.3D and E) indicating free EGF-QD$_{525}$, were expected, as they were not eliminated from the initial incubation mixture with BLP.

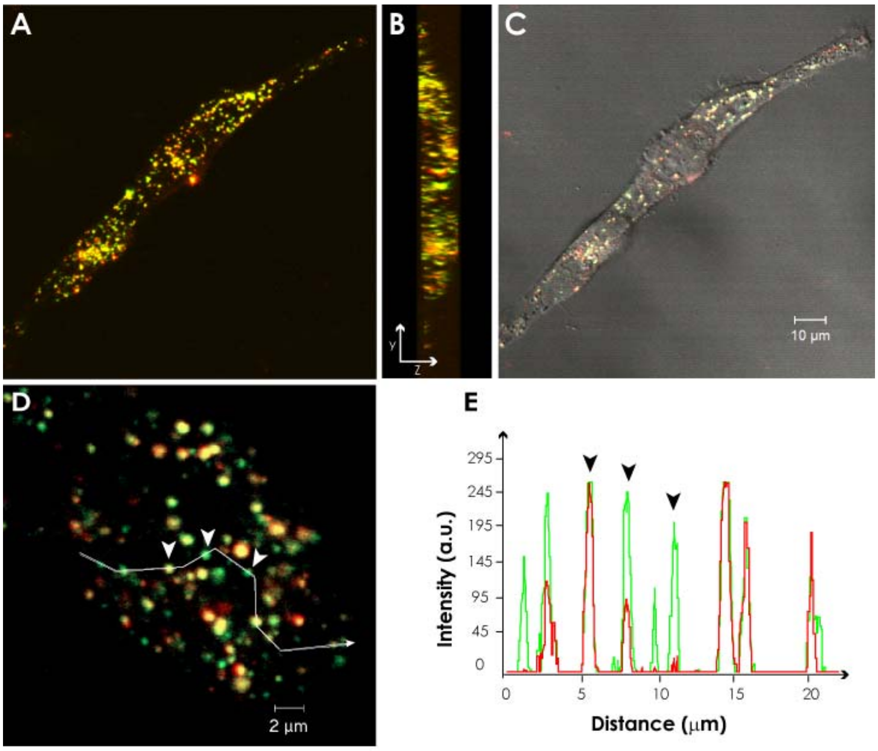

Figure 4.3: **Intracellular fate of EGFR targeted and QDs labeled BLP. A:** 3-D reconstruction of two A431 cells with internalized BLP after 10 min pulse incubation and 1 h chase at 37 °C. **B**: y-z plane showing colocalized QDs inside cells and underneath the cell membrane. **C:** Overlay of image A with DIC image. **D:** Line-profile across endosomal vesicles. **E:** Fluorescence intensity along the line-profile in D revealing different intensity levels for colocalized QDs as well as size variations among vesicles. Internalized two-color QDs labeled and targeted BLP were distinguished from independently internalized green EGF-QD_{525} complexes (arrowheads in panels D and E). Scale bar 2 µm.

4.1.3. Time course of BLP internalization

Quantitative binding and endocytosis analysis of preformed complexes of EGF-QDs in A431 cells has shown that ~50% of the QD ligands accumulated intracellularly in approximately 20 min (Lidke *et al.*, 2004). To get insight into the time course of binding and endocytosis of BLP tagged with preformed EGF-QD_{525} complexes, confocal microscopy was performed on live A431 cells for 1 h in the presence of the targeted particles. Figure 4.4 shows that visible accumulation of dual-labeled and targeted BLP on the cell membrane occurred during the first 10 min of incubation. After 20 min, targeted BLP were identified as colocalized yellow dots internalized and close to the cell membrane in a pattern similar to that described for single EGF-QDs.

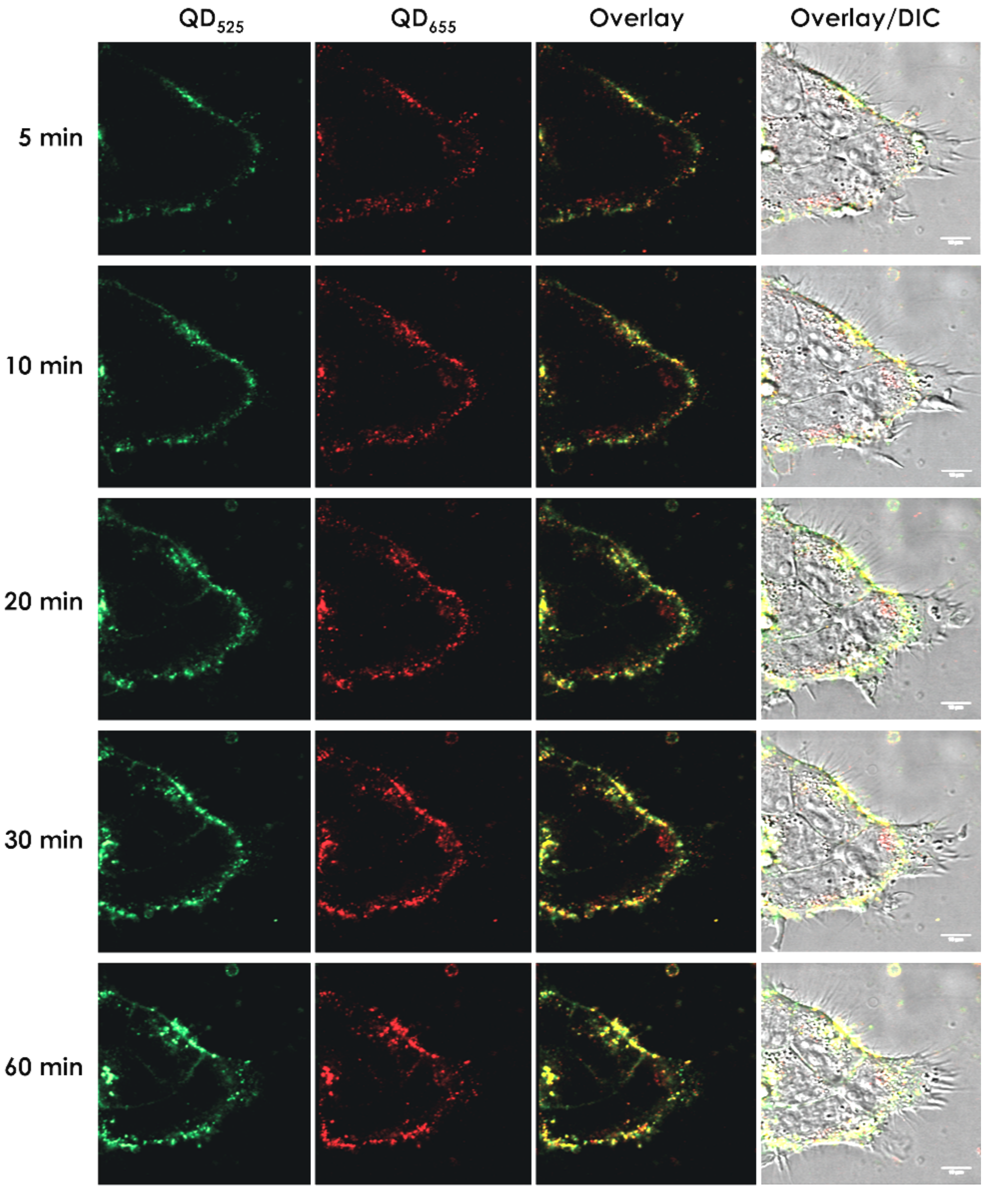

Figure 4.4: Real time uptake of targeted BLP in A431 cells. Targeted BLP were present during the acquisition of confocal images. After 10 min BLP were already bound to the cell membrane and small dots were distinguished. After 20 min, an increase in fluorescence intensity indicated a clustering of the particles. The size of vesicles increased during the process, probably as the result of vesicles fusion. After 1 h, particles were still binding to the cell membrane. Final concentrations in the binding reaction: 4 nM EGF, 1 nM QD_{525}. Scale bar 10 µm.

This result suggests that the size of the BLP did not delay the uptake mediated by EGF. After 60 min a shift of the colocalized dots toward the perinuclear region was accompanied with a clustering of fused endosomal vesicles as evidenced by the increasing fluorescent intensity. These observations are in agreement with those reported for ligand induced activation of the EGFR by preformed complexes of EGF-QDs (Lidke *et al.*, 2004).

4.1.4. EGFR targeted BLP follow the route of EGF-QDs complexes

In order to determine whether the targeted BLP followed the same route as EGF-QDs complexes and indeed were sorted from early endosomes, the uptake of EGF tagged BLP was compared to that of free EGF-QDs complexes and labeled ligand Transferrin. Although the endocytosis of EGFR and Transferrin receptor share the same clathrin-dependent pathway in A431 cells, they are differentially sorted from early endosomes (Hanover *et al.*, 1984; Lamaze *et al.*, 1993). Whereas Transferrin receptor is constitutively recycled back to the cell membrane, EGFR internalization is ligand-induced and EGF-EGFR complexes are mainly sorted to mature lysosomes as a general downregulation mechanism for growth factors receptors (Hanover *et al.*, 1984) (Hopkins *et al.*, 1985). Therefore, binding and uptake of targeted BLP were examined in the presence of Transferrin-Alexa$_{488}$ (TA) after 10, 30 and 120 min incubation with A431 cells (Figure 4.5).

EGF-QD$_{605}$-BLP-QD$_{655}$ and TA were added simultaneously to cells and incubated for 15 min at 4 °C to allow binding while avoiding endocytosis, followed by 10 min or 30 min incubation at 37 °C. Cells were rinsed to remove the unbound complexes and were fixed immediately for confocal microscopy analysis. In a second experiment, cells were incubated with EGF-QD$_{605}$-BLP-QD$_{655}$ for 120 min at 37 °C and TA was added for 10 min before removing the unbound complexes.

As shown in Figure 4.5A, after 10 min of incubation EGF-QD$_{605}$-BLP-QD$_{655}$ extensively colocalized with TA at the cell membrane [r= 0.59]. After 30 min, targeted BLP partially colocalized with Transferrin [r= 0.37] and colocalization completely disappeared after 120 min [r= 0.14]. At this time, targeted BLP clustered around the perinuclear zone were likely sorted from early endosomes.

Control samples of EGF-QD$_{605}$ and TA simultaneously incubated with A431 cells for 30 min at 37 °C (Figure 4.5B), still showed partial colocalization of both ligands [r= 0.5] but barely colocalized after 2 h [r= 0.3].

Figure 4.5 A: Sorting pathway of EGF-QD605-BLP-QD655 in A431 cells: Targeted BLP and TA added simultaneously extensively colocalized at the cell membrane after 10 min (r=0.59) and partially colocalized after 30 min (r=0.37). After 120 min targeted BLP appeared in clusters around the perinuclear region and no colocalization with TA was observed (r=0.14). Triple-color colocalization of QD$_{605}$, QD$_{655}$ and TA is highlighted in white.

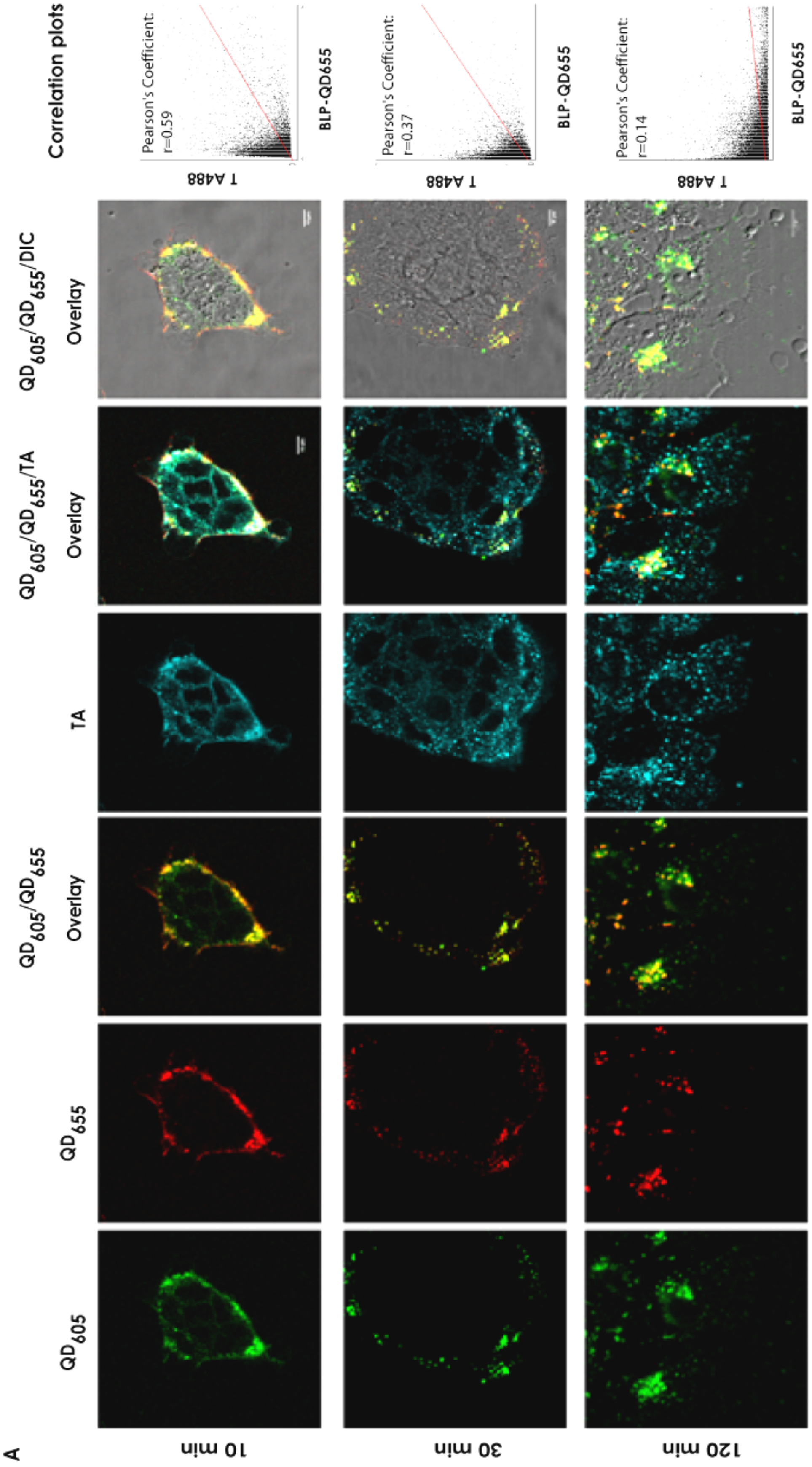
A
QD605
QD655
QD605/QD655 Overlay
TA
QD605/QD655/TA Overlay
QD605/QD655/DIC Overlay
Correlation plots
10 min
30 min
120 min
Pearson's Coefficient: r=0.59
Pearson's Coefficient: r=0.37
Pearson's Coefficient: r=0.14
T A488
BLP-QD655

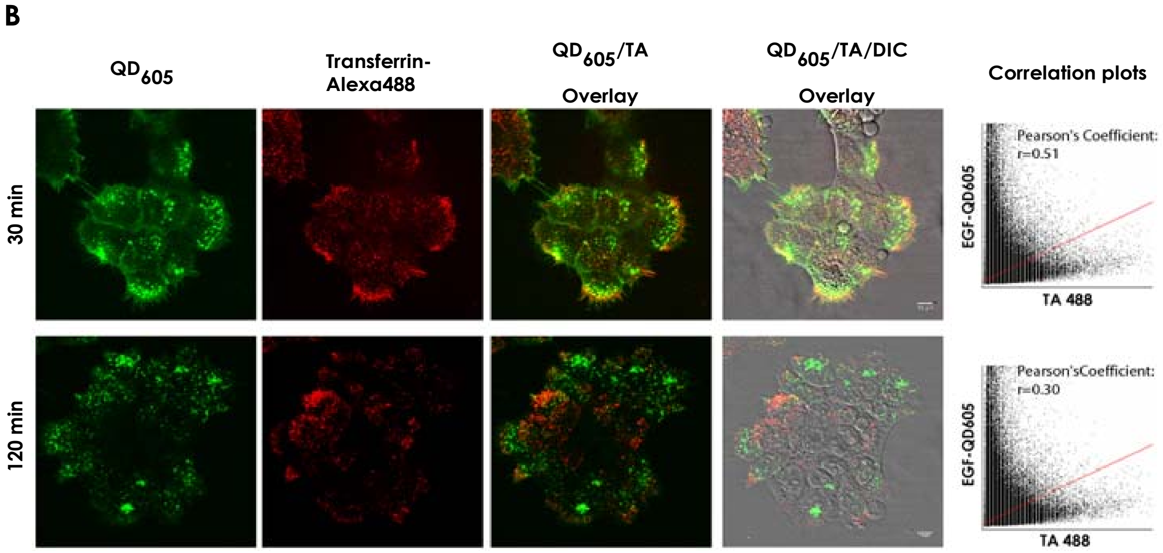
B
QD605
Transferrin-Alexa488
QD605/TA Overlay
QD605/TA/DIC Overlay
Correlation plots
30 min
120 min
Pearson's Coefficient: r=0.51
EGF-QD605
TA 488
Pearson'sCoefficient: r=0.30
EGF-QD605
TA 488

Figure 4.5 B: Control experiments without BLP. EGF-QD$_{605}$ and TA added simultaneously and incubated for 30 min showed partial colocalization (r= 0.51) and after 2 h, they were partially colocalized (r= 0.3). Correlation plots on the right show the corresponding Pearson's coefficients (r). Confocal images were acquired in fixed cells. BLP formulations: 2.7% PEG-Cer-C8, 1.4 % PEG-DSGS and 0.5 nM EGF, 2 nM QD$_{605}$. Scale bars 10 µm.

These observations support the idea that EGF tagged BLP followed the route of free EGF mediated endocytosis, sorting out from early endosomes after 20-30 min diverging from Transferrin ligand in the internalization pathway.

4.1.5. Intracellular fate of QDs encapsulated in targeted BLP

It is well described that trafficking from early to late endosomes in clathrin mediated endocytosis takes place within 20 min (Vonderheit and Helenius, 2005). According to the results observed with Transferrin, if targeted BLP were sorted from early endosomes after 30 min, BLP bearing pH sensitive or exchangeable lipids would be in principle able to fuse more readily with the endosomal membranes, thereby releasing the QDs. Therefore, for the dual-labeled EGF-QD$_{525}$-BLP-QD$_{655}$ complexes, the initial colocalization observed within 30 min was expected to decrease with time.

Targeted and non-targeted BLP-QD$_{655}$ were incubated with cells for 10 min (pulse) at 37 °C, unbound complexes were washed and the QD labels chased for 4 h (Figure 4.6A) and 12 h (Figure 4.6B). Even after after 12 h, dissociation of the two QD signals was not apparent, indicating that the encapsulated QDs were not able to escape from the endosomes.

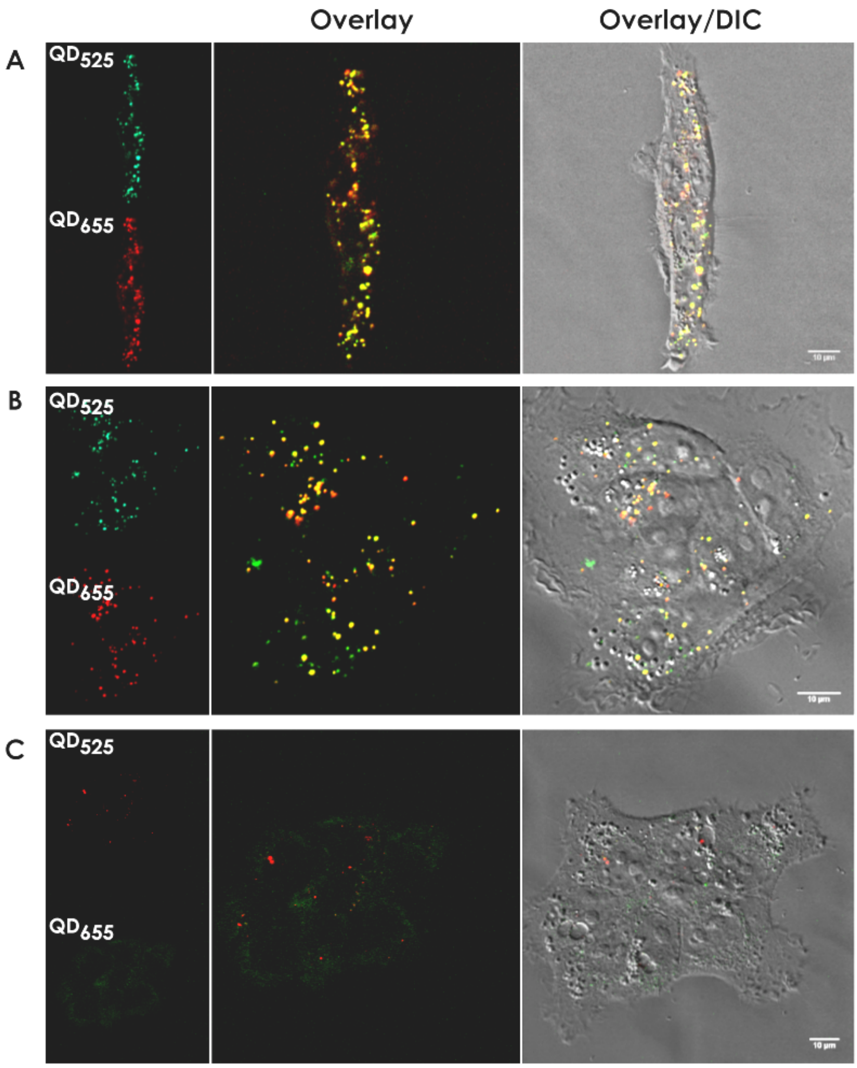

Figure 4.6: Fate of encapsulated QD$_{655}$ delivered by EGF-QD$_{525}$-BLP-QD$_{655}$. After 10 min of incubation at 37 °C with A431 cells, unbound EGF-QD$_{525}$-BLPQD$_{655}$ were removed and cells imaged for up to 12 h. Colocalization of EGF-QD$_{525}$ tagged BLP with encapsulated QD$_{655}$ was visualized on live cells by confocal microscopy. Both QDs remained extensively colocalized after 4 h (**A**) and after 12 h (**B**), showing no evidence of QDs release in the cytoplasm. **C:** Non-targeted BLP-QD$_{655}$. Scale bar 10 µm.

4.2. Receptor specificity of targeted BLP

4.2.1. Competitive assay

To evaluate whether the EGFR was involved in the endocytic uptake of targeted BLP, a competition assay was carried out by adding the EGF-QD$_{525}$-BLP-QD$_{655}$ complexes to A431 cells in the presence of a 66-fold molar excess of free ligand EGF. Under these conditions, the binding of the targeted BLP was substantially diminished (Figure 4.7B), as compared to the positive controls in absence of free ligand (Figure 4.7A).

4.2.2. Interaction of BLP with EGFR-negative cells

In order to confirm that the EGFR was essential for the improved uptake, additional experiments with EGFR-negative cells were performed. Neither CHO cells nor WM983A cells internalized the EGFR targeted BLP as observed in Figure 4.7C and D.

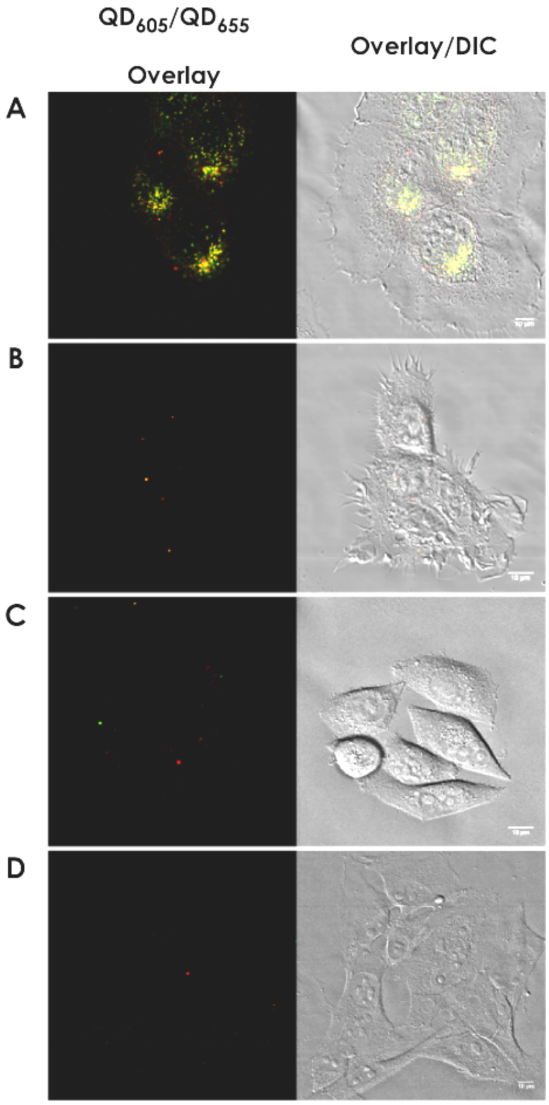

Figure 4.7: Binding specificity of targeted BLP for EGFR. A: A431 cells incubated with EGF-QD_{605}-BLP-QD_{655}. **B:** Cells coincubated with EGF-QD_{605}-BLP-QD_{655} and a 66-fold molar excess of free competing ligand EGF. **C:** CHO cells devoid of EGFR incubated with targeted BLP. **D:** WM983A cells devoid of EGFR incubated with targeted BLP. Scale bar 10 µm.

Taken together, these results indicated that the enhanced uptake of targeted BLP was due to the specific interaction with EGFR.

4.3. Delivery and transfection abilities of targeted and QDs labeled BLP-DNA

The results obtained with BLP loaded with QDs indicated that although receptor-mediated uptake was taking place, the release of QDs from endosomal compartments was not Demonstrated. Additionally, because encapsulated QDs are coated with carboxyl groups could be speculated that they are neutralized in the acidic environment of endosomes forming aggregates before being released. Therefore, the delivery ability was further explored with EGFR targeted BLP carrying encapsulated DNA containing the GFP as reporter gene. The efficiency of the targeted gene delivery was estimated as the percentage of GFP positive cells, compared to that obtained with the non-targeted BLP.

4.3.1. Intracellular fate of dual-labeled and targeted BLP-DNA

In order to monitor the initial binding and uptake of BLP with encapsulated DNA, these particles were also labeled with two colors of QDs with a modified strategy as depicted in Figure 4.8. In order to assess the specificity of binding and track the particles, BLP-DNA were first coupled to preformed EGF-QD_{525} complexes, followed by a second color labeling using QD_{655} without EGF.

Targeted particles are denoted as (EGF-QD_{525}/QD_{655})-BLP-DNA. As free QD_{655} does not internalize in the absence of ligand, the uptake of QD_{655} is dependent on previous binding to targeted EGF-QD_{525}-BLP-DNA. Similar to the BLP-QDs labeling strategy, colocalized QD_{525} and QD_{655} in this case would be indicative of the presence of EGF targeted particles. The monocolor non-targeted particles labeled with QD_{655} are denoted as (QD_{655})-BLP-DNA.

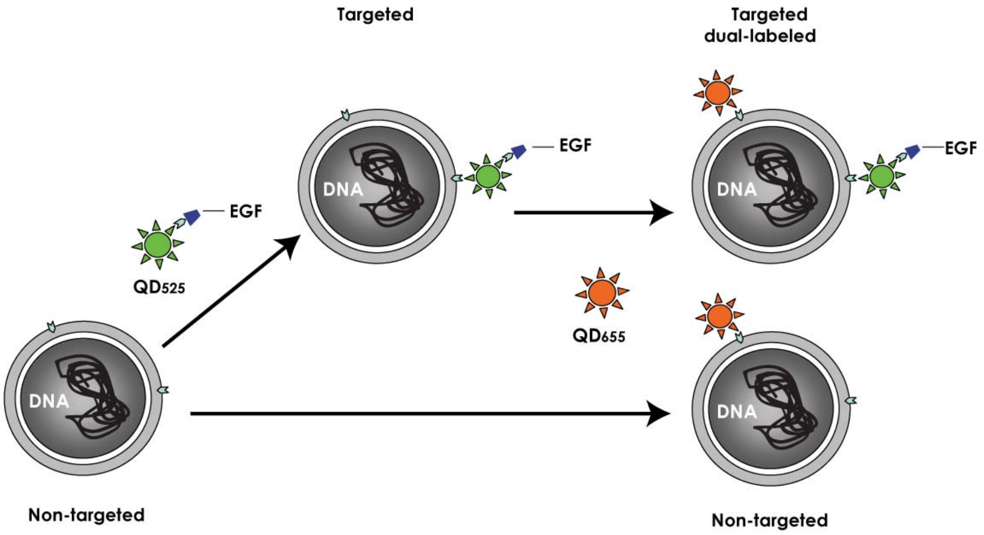

Figure 4.8: Diagram depicting the targeting and labeling strategy of BLP with encapsulated DNA. Preformed complexes of EGF-QD_{525}, containing 2-4 EGF molecules per QD particle, were conjugated to biotins on BLP. In a subsequent step, the second color QD_{655} was added at equimolar amounts as QD_{525}. Specific uptake would be evidenced as colocalized dots, while unspecific uptake as red

fluorescence of non-targeted BLP-DNA labeled only with QD_{655}. BLP formulations employed: 10% PEG-Cer-C20, 10 % PEG-Cer-C8 and 2.7 % PEG-DSGS.

The binding was performed as already described for BLP-QDs. For BLP-DNA formulations, PEG content was increased to 10% of PEG-Cer-C8 and C20.

First, ($EGF-QD_{525}/QD_{655}$)-BLP-DNA were prepared with 10% PEG-Cer-C20. This formulation showed an average size of 70 nm, DNA encapsulation efficiency of <50% and was the targeted analogue of described SPLP (Wheeler *et al.*, 1999). Due to their homegeneous and small size compared to the other formulations tested, they were examined for binding and targeting ability in A431 cells. Upon incubation with cells for 3 h at 37 °C unbound complexes were removed and uptake was analyzed in live cells by confocal fluorescence microscopy.

As shown in Figure 4.9A, targeted ($EGF-QD_{525}/QD_{655}$)-BLP-DNA were identified as colocalized QD_{525} and QD_{655}, (yellow pseudocolor in the overlay). The distribution in a dot pattern was consistent with endosomal localization, as previously observed for QDs loaded BLP. No uptake was detected for the non-targeted BLP for the same incubation conditions (Figure 4.9B). Control experiments with $EGF-QD_{525}$ and free QD_{655} showed that non-targeted QD_{655} were not internalized (Figure 4.9B).

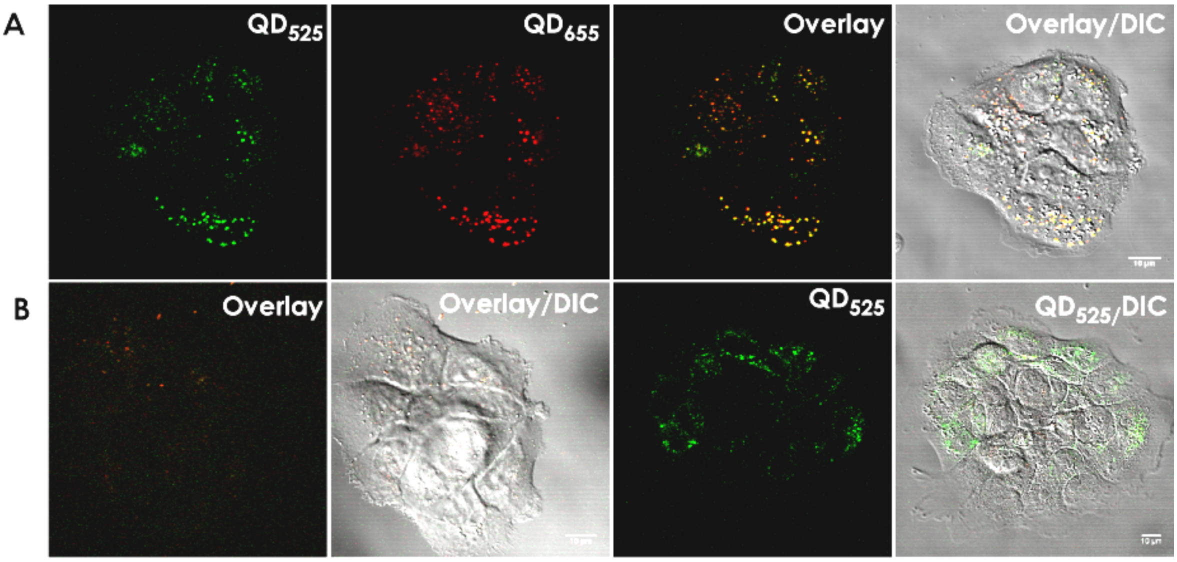

Figure 4.9: Binding and uptake of $EGF-QD_{525}-QD_{655}$ BLP-DNA. A: A431 cells were incubated with targeted particles for 3 h at 37 °C. Live imaging performed in Tyrode's buffer with 1% glucose. The dot pattern suggested endosomal localization. **B:** Control experiments with QD_{655} (left panels) and EGF-QD_{525}, showing that non-targeted particles were not internalized. BLP formulation: 10% PEG-Cer-C20. Scale bar 10 µm.

These results indicated that binding was not impaired for targeted BLP-DNA despite the high PEG content (10%PEG-Cer-C20).

4.3.2. Transfection competency of dual-labeled and targeted BLP-DNA

The transfection activity of dual-labeled and targeted BLP-DNA was explored in formulations containing lower PEG content (2.7%) and pH sensitive lipids. Starved A431 cells were incubated with (EGF-QD_{605}/QD_{655})-BLP-DNA for 10 min at 37 °C cells, then unbound complexes were removed and BLP distribution and GFP expression in A431 cells were analyzed after 48 h.

Figure 4.10 (A,B), demonstrates that EGFR-targeted BLP loaded with DNA behaved similarly to BLP-QDs regarding the binding and cellular distribution upon internalization of the particles. The presence of colocalized dots in non-transfected cells (Figure 4.10A), may reflect a difficulty of BLP to destabilize the endosomes or, alternatively, may indicate the presence of targeted but empty particles, as expected for the 70% DNA encapsulation efficiency obtained. In Figure 4.10C a 3D-reconstruction of confocal planes shows the perinuclear localization of targeted BLP in cells expressing GFP.

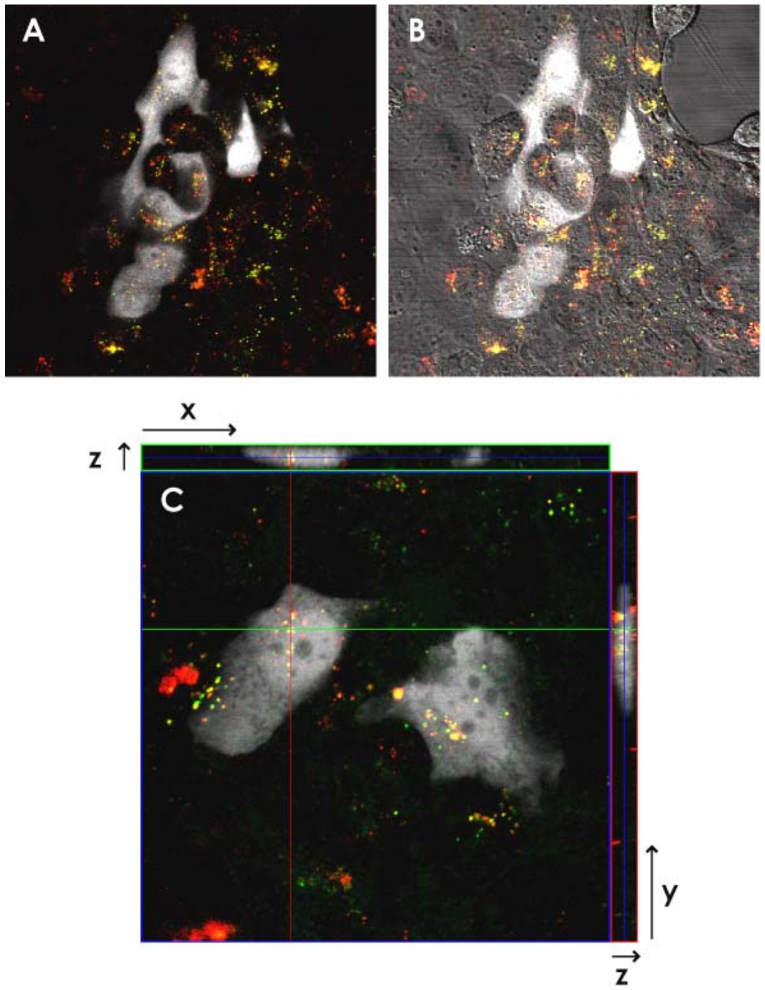

Figure 4.10: GFP expression upon plasmid delivery with dual-labeled and EGFR targeted BLP-DNA. (EGF-QD_{525}/QD_{655})-BLP-DNA were incubated for 10 min at 37 °C in Tyrode’s buffer ph 7.4, then unbound complexes were removed and cells were incubated in complete DMEM for 48 h before imaging. **A:** Merged images corresponding to colocalized QDs (overlay of $QD_{605/655}$ channels) with the green

channel corresponding to GFP fluorescence (pseudo color, white). **B:** Image on A merged with the DIC image. **C:** Three-dimensional reconstruction. The x-y section, as indicated by the blue lines in the x-z and y-z projections, showed the internalized BLP. BLP formulation: 2.7% PEG DSGS, 1μg plasmid /well, BLP-DNA particle size ~200 nm. Scale bar 10 μm.

The two-color BLP labeling strategy allowed to associate the presence of internalized targeted particles with their transfection ability as indicated by the expression of GFP.

4.3.3. BLP targeting in a two-step procedure

In order to improve the access of EGF to the cell surface and decrease the formation of possible crosslinked species, the coupling of preformed complexes of EGF-QDs to BLP was performed in two steps. The advantage of using this procedure has been also described by (Lidke *et al.*, 2007).

In a first step, to accomplish the targeted delivery, preformed complexes of EGF-QDs were added to target A431 cells at 4 °C to prevent early internalization. In a second step, BLP-DNA samples recovered after detergent dialysis (non-purified fractions) or purified in sucrose gradient (purified fractions) were added to the cells at 10 °C for 15 min and then incubated at 37 °C during 30 or 60 min before removing the BLP. A431 cells incubated directly with non-purified and purified fractions BLP-DNA (only Step 2) were employed as control of non-targeted delivery.

The percentage of transfected cells were quantified after 48 h by FACS or fluorescence microscopy. Although a smaller number of cells were evaluated by microscopy as compared to flow cytometry, the sensitivity for fluorescence detection was improved using a CCD camera to allow the detection of the onset of GFP expression at later times (Figure 4.11A,B, red arrows).

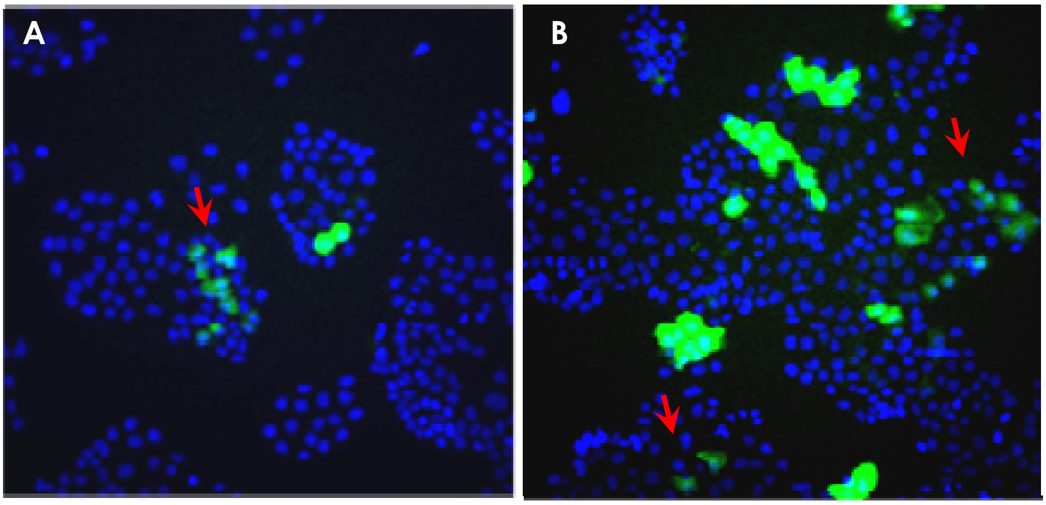

Figure 4.11: GFP expression analysis in A431cells by a two-step targeting procedure. A: Control cells incubated with unmodified BLP-DNA (non-targeted delivery). **B:** Cells preincubated with EGF-QD_{655} complexes followed by the addition of BLP-DNA (targeted delivery). After 48 h A431 cells with late onset of GFP expression, indicated by low levels of GFP were also detected. Green fluorescence: GFP positive cells. Blue fluorescence: Nuclear staining with Hoechst.

As described in the previous chapter, fractions recovered after detergent dialysis and after sucrose densitiy gradient differ in the size homegeneity of the BLP particles, which can affect directly the binding, internalization efficiency and consequently the transfection ability of the targeted BLP. Therefore, it was of interest to evaluate the effect of non-purified and purified BLP-DNA fractions in the transfection efficiency of targeted particles containing 1 and 2 µg plasmid DNA in each well. The percentage of cells expressing GFP following the two-step incubation procedure was determined by fluorescence microscopy and flow cytometry (Table 4.1).

BLP	**Fraction and size range**	**GFP expressing cells (%) by flow cytometry**		**GFP expressing cells (%) by microscopy**	
		(-) EGF	**(+) EGF**	**(-) EGF**	**(+) EGF**
10% PEG-Cer-C8	**Non-purified 50-1000 nm**	3	3.9		
	Purified 80-220 nm	1.4	4.8	0	2.4
2.7% PEG PEG-DSGS	**Non-purified 50-1000 nm**	2.9	3.2		
	Purified 90-220 nm	1.4	3.9	0.8	1.9

Table 4.1: GFP expression levels obtained with purified and non-purified BLP-DNA. Samples recovered after detergent dialysis (Non-purified) and after sucrose density gradient (Purified) for two BLP formulations. Preformed complexes of EGF-QDs (2-4 nM EGF) were added to starved A431 cells at 10 °C. Then, cells were incubated with BLP-DNA (1 or 2 µg plasmid) for 30 min at 37 °C (for flow cytometry measurements) or 60 min at 37 °C (for quantitative fluorescence microscopy). Non-purified fractions: Fractions of BLP recovered after detergent dialysis composed of non encapsulated plasmid (~40%), empty BLP and aggregates. Purified fractions: Fractions of BLP recovered after sucrose density gradient composed of BLP with encapsulated DNA. Values are median of 3-5 measurements with each method performed in three independent experiments.

As shown in Table 4.1 treatment with non-purified fractions (containing free plasmid and aggregates) produced similar number of GFP expressing cells for targeted and non-targeted delivery of BLP-DNA (3-4 %), indicating that non-targeted particles were equally efficient for transfection as targeted particles. Since equal amounts of free plasmid added did not show any transfection activity, the GFP expression observed for non-purified fractions was attributed to DNA-loaded BLP and aggregates of lipid-DNA, the later presumably entering through a non-receptor mediated route.

When purified fractions were tested, targeted BLP-DNA showed 2-3-fold increase in GFP expression as compared to the non-targeted particles for both formulations analysed. Despite the very low total transfection efficiency of the BLP, this finding suggested that after removing the aggregates the transfection levels observed were presumably accomplished by smaller and targeted BLP-DNA (< 250 nm).

5. Results: ”Single Quantum Dot labeling of plasmid DNA”

In the previous chapter, BLP tagged with QDs were used to monitor the specificity of the binding and receptor-mediated uptake of the carriers by fluorescence microscopy. The transfection efficiency of the targeted BLP-DNA was assessed by measuring the number of GFP expressing cells. However, the intracellular localization of the plasmid at any time during the delivery process could not be determined and related to the fate of the BLP. At this point, the use of a fluorescently labeled plasmid is critical to shed light on the mechanism by which DNA is released from the lipid carrier. Coupling multiple fluorescent tags may involve covalent modifications of the plasmid DNA, which may interfere with the expression of the reporter gene. In this regard, the present chapter deals with the labeling of plasmids mediated by peptide nucleic acids (PNA) for non-covalent and sequence specific binding of a single QD to plasmid DNA.

5.1. *bis*-PNA strand invasion of supercoiled plasmids

The ability of *bis*-PNAs to form (*PNA*)2–DNA triplexes has been used for effective strand invasion of linear DNA duplexes, where the two *bis*-PNA strands are designed as a single molecule connected by flexible linkers (Cherny *et al.*, 1998). Figure 5.1 depicts such a strategy, where *bis*-PNA, in this work modified with a single biotin, binds by Hoogsteen interactions to a unique target site in the pEGFP-C1 plasmid. The binding site in the plasmid is located far away from the transcription initiation site, in order to avoid any interference with the expression of the GFP reporter gene. One disadvantage of this strategy is that *bis*-PNAs are restricted to bind purine sequences due to steric hindrance of the Hoogsteen binding with target sites containing pyrimidine bases (Demidov *et al.*, 2001). Therefore, hybridization takes place only under acidic conditions (~pH 5) to maintain the citosines protonated for Hydrogen-bond formation.

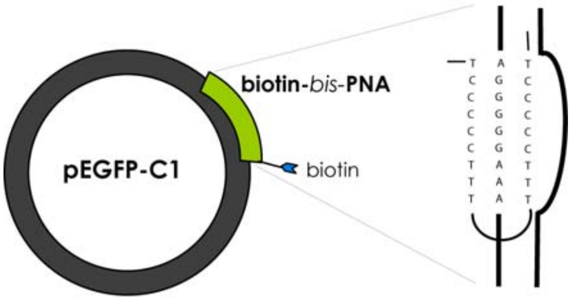

Figure 5.1: Schememematic representation of hybridization of *biotin-bis-PNA* to a specific sequence in plasmid pEGFP-C1.

In the strategy applied a biotynilated *bis*-PNA was employed for subsequent conjugation to streptavidin coated QDs (StAv-QDs).

Hybrids were prepared at 2:1, 4:1, 8:1, 20:1 and 40:1 biotin-*bis*-PNA to plasmid molar ratios and digested with the restriction enzymes Apa LI and Ase I to generate a short 379 bp DNA fragment containing the *bis*-PNA binding site and an additional 4352 bp fragment. Fragments were electrophoresed in a 3-8% gradient native polyacrylamide gel. The binding of biotin-*bis*-PNA is expected to retard the migration of the 379 bp fragment. As shown in Figure 5.2A, the Sybr Green stained gel revealed a retarded DNA band running behind the fragment containing the target sequence for biotin-*bis*-PNA. The amount of the retarded fragment notably increased at higher biotin-*bis*-PNA to plasmid molar ratio (20:1). In spite of the excess of biotin-*bis*-PNAs, less than 50 % Hybrid yield was estimated from the Sybr Green intensity of the retarded band. As the remaining larger restriction fragment (4352 bp) did not migrate in the gel due to the high percentage of polyacrylamide, a non-specific interaction between biotin-*bis*-PNA and this fragment could not be assessed. To address this problem, additional hybridization experiments were performed using a fluorescently labeled *Cy5-bis*-PNA that could be detected independently of the size of the fragments. Similarly as before, hybrids were formed at Cy5-*bis*-PNA to plasmid molar ratios of 2:1, 4:1, 8:1, 20:1 and 40:1. In this case, the pEGFP-C1 plasmid was digested with Apa LI and Ava II to obtain DNA fragments of 2002 bp, 1641 bp (containing the target site), 445 bp and 643 bp. Hybrids were analyzed in a 2% agarose gel in 1X TAE and Cy5 fluorescence was detected before staining with Sybr Green. The left panel in Figure 5.2B shows a single band Cy5-labeled corresponding to the fragment of 1641 bp bearing the *bis-PNA* binding site. Cy5 fluorescence was not detected in the remaining restriction fragments, shown in the right panel of Figure 5.2B, representing the total DNA, as determined by Sybr Green stainning. These results indicated that unspecific hybridization is not taking place in the presence of 40-fold excess of *bis*-PNA to plamid DNA.

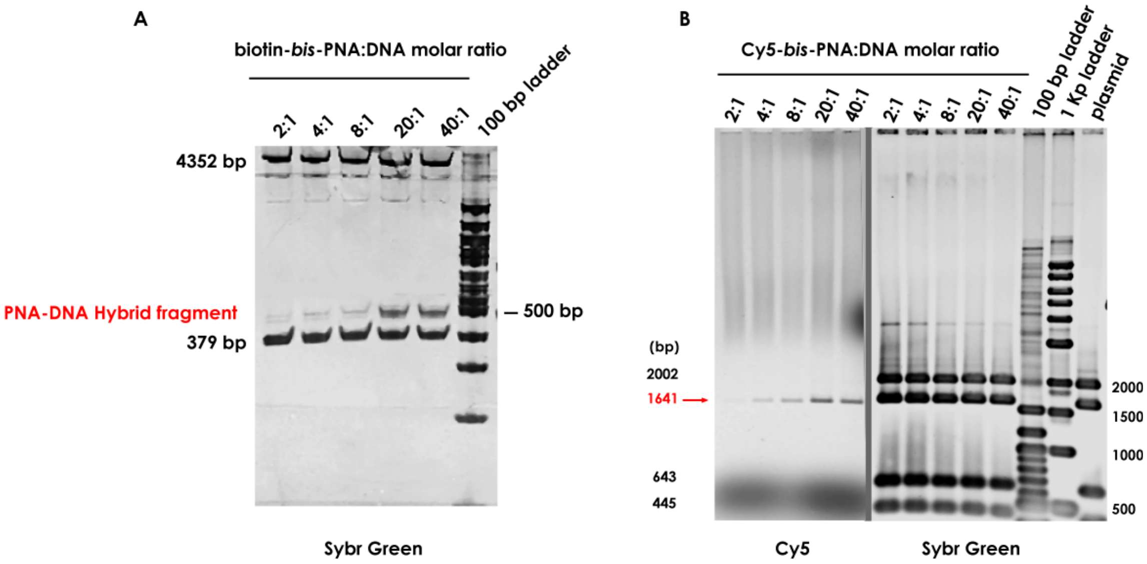
A
biotin-bis-PNA:DNA molar ratio
2:1
4:1
8:1
20:1
40:1
100 bp ladder
4352 bp
PNA-DNA Hybrid fragment
379 bp
500 bp
Sybr Green
B
Cy5-bis-PNA:DNA molar ratio
2:1
4:1
8:1
20:1
40:1
2:1
4:1
8:1
20:1
40:1
100 bp ladder
1 Kp ladder
plasmid
(bp)
2002
1641
643
445
2000
1500
1000
500
Cy5
Sybr Green

Figure 5.2: Hybrid formation between *bis*-PNA and pEGFP-C1 plasmid by restriction fragment analysis in gel electrophoresis. A: Retarded band migration in polyacrylamide gel 3-8 % in 1X TAE. Sybr Green stained gel showing digested fragments obtained with Apa LI and Ase I. The 379 bp fragment contains the target sequence **B:** Restriction fragments obtained with Apa LI and Ava II and analyzed in 2% agarose gel in 1X TAE. Left panel, Cy5 labeling; right panel, Sybr Green stainning. The 1641 bp fragment contains the PNA target sequence. Biotin-*bis*-PNA (or Cy5-*bis*-PNA):plasmid molar ratios were 2:1, 4:1, 8:1, 20:1, and 40:1.

5.2. Quantum Dot labeling of biotin-*bis*-PNA: plasmid DNA Hybrids

QD-Hybrid complexes (Figure 5.3) were formed by adding streptavidin coated QD_{655} to biotinylated Hybrids at 1:1 molar ratio.

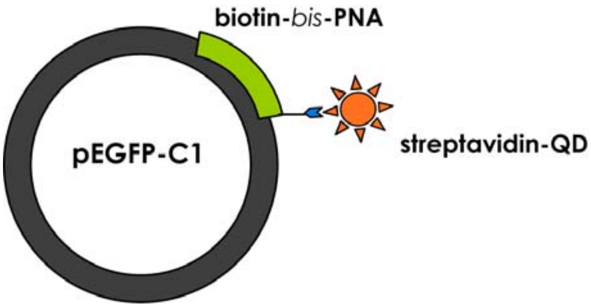

Figure 5.3: Diagram of a single StAv-QD-labeled plasmid mediated by biotin-*bis*-PNA hybridization

The resulting mixture was analyzed by agarose gel electrophoresis along with control samples consisting of QDs alone or in the presence of plasmid. QD-Hybrids were scanned under UV light and the emission of QD_{655} was collected using a LP 580 filter. In addition, the gel was stained with Sybr Green to visualize total DNA (Figure 5.4). The band shift observed was the result of binding StAv-QDs to biotinylated Hybrids. This retarded migration was expected considering that QDs are slightly negative as compared to plasmid DNA and ran behind the plasmid when loaded alone (third lane). Furthermore, the $StAvQD_{655}$ retarded the migration of both, supercoiled and the open-relaxed circular conformations of the plasmid, as evidenced by comparing QD labeled bands with Sybr Green stained bands (right panel). This also implied that Hybrids were stable in both conformations. The presence of faint retarded bands (red arrows) could be due to the binding of multiple biotin-*bis*-PNA:plasmid to a single QD, since the nanoparticles are coated by 6-8 streptavidins. This observation may also explain the presence of free StAv-QDs, although the reaction was carried out at equimolar amounts of QD particles and Hybrids. Controls of unbound QDs and plasmid DNA ran as the corresponding free molecules confirming the absence of non-specific interaction. As expected, DNA staining showed that hybridization was not complete, in good agreement with previous results obtained with restriction enzymes (Figure 5.2).

Attemps to purify the QD-labeled Hybrids by electroelution resulted in a very low sample recovery.

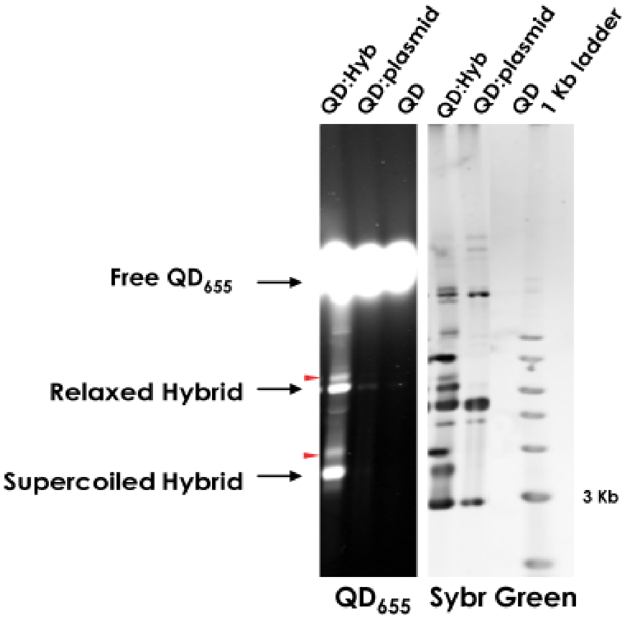

Figure 5.4: Visualization of QD-labeled Hybrids. Gel electrophoresis performed in 0.8% agarose gel in 1X TAE. Left panel, QD_{655} fluorescence. Right panel, Sybr green staining. StAv-QD_{655} to biotinylated Hybrids molar ratio was 1:1.

5.2.1. Specificity of single QD labeling revealed by AFM

Taking advantage of the rough and size of QD particles, direct visualization of the degree of labeling, as well as the specificity of *bis*-PNA for its target sequence was accomplished by AFM measurements.

QD-Hybrids and the corresponding control plasmids were deposited on a mica surface in 5 mM Mg^{+2} and imaged in tapping mode in air. Figure 5.5A displays representative amplitude images of supercoiled (top) and linear Hybrids (bottom). It is clearly visible from these images that a single QD was attached per DNA molecule, for both supercoiled and linear conformation of the plasmid.

As a direct control for the specificity of the biotin-*bis*-PNA recognition, the position of the QDs was estimated in linearized Hybrids (Figure 5.5B, top panels). The length of the short protruding fragment measured from the center of the QD particle (segment between blue crosses) was estimated in ~63 nm (5.5B, bottom panel). Considering that the length of one base pair in the B-form of DNA is 0.34 nm, the protruding fragment would be ~185 bp. This was considered a good approximation to the 208 bp-distance measured from the end of the target site (position 4523 bp) to the end of the fragment at position 4731 bp in pEGFP-C1. Thus, the experimentally determined binding location correlated well with the expected binding domain of *bis*-PNA.

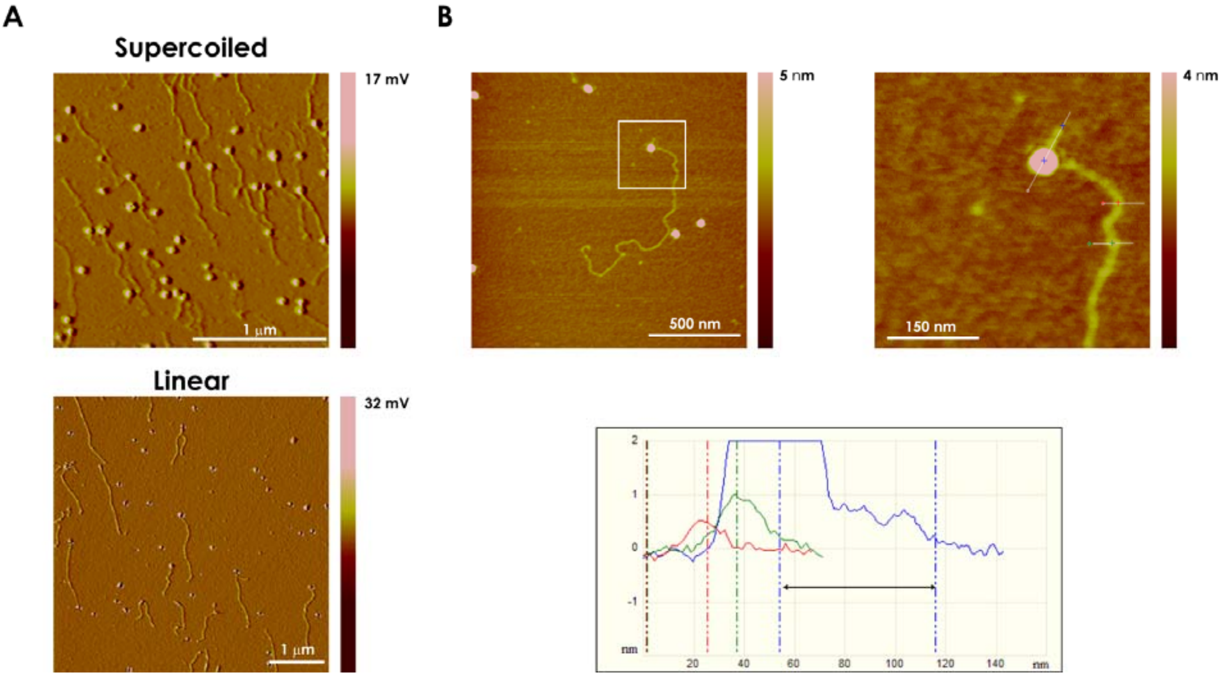

Figure 5.5: Site specific QD labeling of Hybrids as revealed by AFM. **A:** Amplitud images of QD:Hybrid complexes showing a single QD attached per DNA molecule. **B:** Procedure applied to estimate the location of the *bis*-PNA binding site from the height images. The right image is a zoomed view of the box selected in the left image. The distance measured from the center of the QD particle to the end of the restriction fragment (double-headed arrow in the bottom panel) suggested that QD is positioned at the expected PNA binding site.

In summary, AFM images clearly showed that a single QD was located at the target position in the Hybrid. This fact highlights the specificity of *bis*-PNA for its target sequence, as already demonstrated by gel electrophoresis.

5.2.2. Visualization of Hybrids and QD:Hybrids complexes on magnetic beads

In order to explore whether QD labeling was suitable for tracking plasmids by fluorescence microscopy, QD:Hybrid complexes were coupled to magnetic beads. This approach was intended to imitate the conditions required for live cell imaging.

Biotinylated Hybrids and QD-Hybrids were coupled to streptavidin or biotin coated magnetic beads, respectively. After incubation, beads were washed to remove unbound material and were stained with Sybr Green to reveal attached plasmid DNA. The samples were deposited on glass coverslips and Sybr Green and QD_{655} fluorescence were then visualized in a wide field inverted microscope equipped with a CCD camera. The results are summarized in Figure 5.6. In a first set of experiments, biotinylated Hybrids were incubated with streptavidin-coated magnetic beads. This preparation showed positive DNA staining revealing the presence of Hybrids (Figure 5.6A). Neither Syber Green nor StAv-QD_{655} signal were detected in control experiments performed with unmodified plasmid (Figure 5.6B).

In a second set of experiments, the QD-Hybrid complexes were incubated with biotin-coated magnetic beads and then DNA was stained with Sybr Green. In this case, colocalization of Sybr Green and QD_{655} fluorescence was observed only when the StAv-QDs were preincubated with the biotinylated Hybrid before the addition to the beads (Figure 5.6C). As expected, StAv-QDs were also bound to biotinylated magnetic beads (Figure 5.6D).

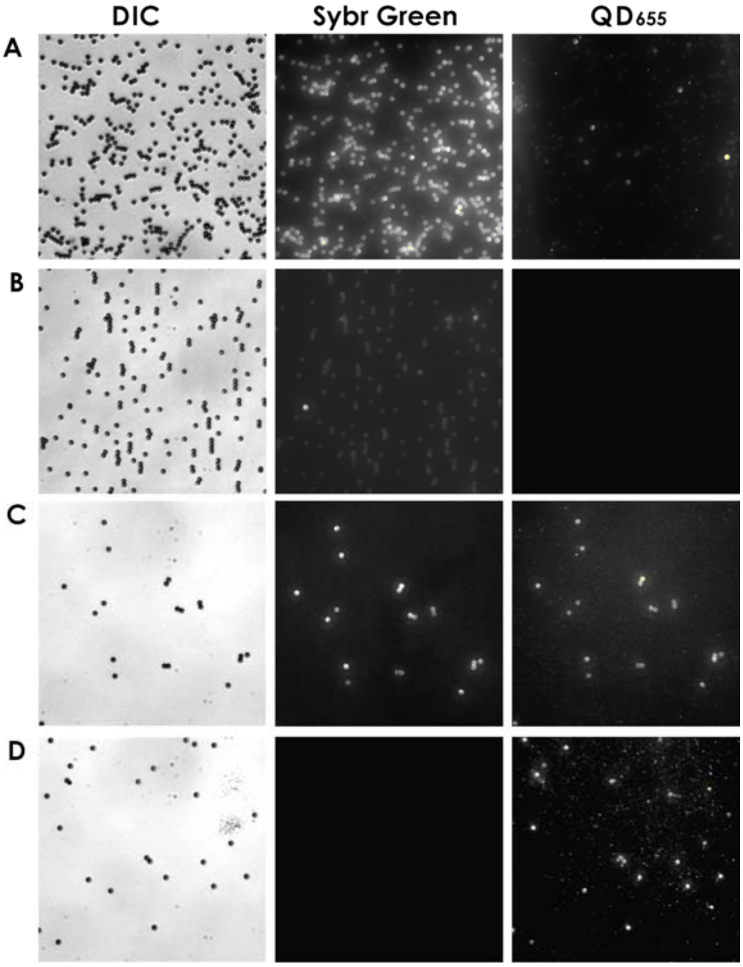

Figure 5.6: Visualization of QD labeled Hybrids coupled to magnetic beads by fluorescence microscopy. A: Biotinylated Hybrids incubated with streptavidin-coated magnetic beads. **B:** Control of unmodified pEGFP-C1 plasmid incubated with streptavidin-coated magnetic beads. **C:** QD-Hybrids incubated with biotin-coated magnetic beads. 20 nM biotinylated Hybrids were preincubated with StAv QD_{655} (2 nM QDs) in Sodium Borate buffer pH 8.5 before addition to the magnetic beads. **D:** StAv-QD_{655} incubated with biotin-coated magnetic beads. Ex/Em filters: for Sybr Green: ex. 480/30 BP, 505 DM (dichroic mirror), em. 535/40 BP, QD_{655} ex. 560/55 BP, 595 DM , em. 655/40 BP.

In summary, although Hybrids yield and purification of labeled complexes need further optimization, the results presented in this chapter point out the potential of peptide nucleic acids as useful tools for the site specific non-covalent labeling of plasmids. In addition, the sensitivity provided by the highly fluorescent and photostable QDs would allow single molecule tracking of the Hybrids in live cells by fluorescence microscopy.

6. Discussion

The new era of PEGylated liposomes has greatly improved the systemic delivery of therapeutic agents into tumor or disease-affected tissues in distal locations of the body (Woodle and Lasic, 1992; Harris and Chess, 2003). To introduce cell specificity receptor-mediated endocytic pathways are being exploited for nonviral gene/drug delivery. For this purpose, targeting molecules have been incorporated into liposomal carriers. For instance, coupling of suitable ligands and antibodies to these synthetic vehicles, particularly to target cell receptors overexpressed in certain tumors, has enhanced enormously the specificity of delivery, reducing toxic side effects in normal surrounding tissues (Hofland *et al.*, 2002; Wei *et al.*, 2003).

Stabilized Plasmid Lipid Particles (SPLP) are a new generation of liposomes, stabilized by PEG-Ceramide lipids. SPLP are able to encapsulate plasmid DNA with high efficiency (50-70%) in particles smaller than 100 nm (Fenske *et al.*, 2002). An unwanted side effect of PEG-Ceramide coating on SPLP, necessary to engender the long circulation lifetimes, is the putative inhibition of liposome-cell association and uptake required for an efficient transfection. Therefore, the dissociation rate of PEG-Ceramides from SPLP has been modulated by varying the acyl chain length of the ceramide anchor. The transfection efficiency of these particles have proven superior after replacing PEG-Cer-C20 by a shorter acyl chain PEG-Cer-C8 (Mok *et al.*, 1999).

An essential improvement can be expected from the inclusion of cell-specific targeting ligands on SPLP. However, this possibility had not been explored prior to this thesis. A single application was recently reported for lactoferrin tagged SPLP aimed to specifically transfect hepatocytes *in vivo* (Weeke-Klimp *et al.*, 2007). This approach, despite showing efficient cell targeting and transfection capacity *in vitro*, was unable to accomplish the expression of the reporter gene *in vivo.*

The epidermal growth factor receptor (EGFR, erbB1, HER1) is an attractive target for drug and gene delivery since it is overexpressed in a wide variety of human tumors, including lung, liver and breast cancer (Yarden, 2001). Deep knowledge into the dynamics of EGF-EGFR interactions has been achieved with the application of targeted Quantum Dots (QDs). Fluorescent QDs conjugated with EGF ligand have enabled the recognition of multiple targets and elucidation of cellular dynamic processes such as activation and signal transduction mediated by the receptor tyrosin kinase erbB1 (Lidke *et al.*, 2004) as well as a mechanism of retrograde transport in filopodia (Lidke *et al.*, 2005). Their exceptional photostability is the essential feature for long-term fluorescence imaging (Smith *et al.*, 2004).

Prior to this thesis, the application of EGF tagged QD for targeting and labeling of SPLP-like carriers had not been explored. Therefore, a combined strategy of EGFR targeting and QD labeling was developed for modified SPLP. Biotinylated and stabilized lipid particles (BLP) were loaded with plasmid DNA or QDs and modified with preformed complexes of EGF-QDs in order to accomplish targeted delivery into A431cells overexpressing the EGF receptor (EGFR).

6.1. PEGylated and Biotinylated Lipid Particles

Biotinylated liposomes stabilized with PEG were prepared using a detergent dialysis technique described for the preparation of SPLP (Wheeler *et al.*, 1999). This method was adapted for the encapsulation of small QD_{655} (~10 nm) in a novel approach for delivering this fluorescent nanoparticles into cells.

Three different BLP formulations were investigated for their receptor-mediated uptake, these including PEG-Ceramides (carbon chains lengths C20 and C8) and a pH sensitive lipid PEG-DSGS at percentages ranging from 1.4 to 10 mol% PEG.

Two main lipid particles populations were recovered after detergent dialysis, consisting of empty BLP and particles loaded with DNA (BLP-DNA) or QDs (BLP-QDs). As determined by DLS, BLP-DNA particles were far more heterogeneous in size than BLP-QDs for the same BLP formulation. This heterogeneity was evidenced by the presence of sedimenting particles when the PEG-lipid content in the formulation decreased from 10 to 2.7 mol% or when Ceramide C20 was replaced by Ceramide C8. These findings were not surprising and indicated that the amount of PEG-lipid was insufficient to effect steric stabilization of DNA loaded particles. The observed aggregates were probably the result of strong electrostatic interactions between negatively charged DNA with the cationic lipid DOTAP present at 6 mol% in all formulations, after the detergent monomers were removed from the initial DNA-lipid-detergent mixture during the dialysis process (Zuidam and Barenholz, 1999). Furthermore, only BLP-DNA formulated with 10% PEG-Cer-C20 showed particles of discrete sizes after detergent dialysis (Figure 3.1 and Table 3.2). These findings are in line with the reported behavior of SPLP stabilized with 10% PEG-Cer-C20 (Wheeler *et al.*, 1999; Zhang *et al.*, 1999). Interestingly, although the variations in PEG content directly affected the particle size and homogeneity of plasmid DNA loaded BLP, no differences were observed regarding plasmid DNA encapsulation efficiency or protection (Table 3.2).

On the other hand, BLP with encapsulated QDs showed discrete sizes (100-130 nm) even for the BLP formulations containing the lowest PEG-lipid content (1.4% mol% PEG-DSGS and PEG-Cer-C8)(Fig 3.4). This supports the idea that electrostatic interactions between DNA and DOTAP are stronger than between carboxyl groups in QDs and amino groups in DOTAP, driving the aggregation of the DNA loaded particles.

Non-encapsulated DNA or QDs, as well as empty BLP likely present after dialysis, were removed by ultracentrifugation in a sucrose density gradient. This technique has proven suitable for purification of DNA loaded (Fig. 3.2) and QD loaded particles (Fig. 3.4). An additional advantage was that BLP-DNA particles smaller than 350 nm were clearly separated from aggregates also containig DNA and lipids (Table 3.2). For BLP-QDs, the sucrose density gradient allowed the purification of QD-loaded particles from free QDs (Fig. 3.4A).

Sucrose fractions analyzed by TEM revealed an average of 2 to 5 QDs successfully encapsulated in BLP ranging from 100 to 130 nm in size (Fig. 3.4B). Particle dimensions estimated from TEM were in excellent agreement with the mean hydrodynamic diameter of ~110 nm as determined by DLS for BLP-QDs (Fig. 3.4C). The encapsulation of QDs in stabilized lipid particles by the detergent dialysis method was presented as a novel approach, without deleterious effect in the fluorescence of QDs. Additionally, the spherical morphology of BLP shown by TEM was confirmed by Atomic Force Microscopy.

6.2. Single step conjugation for targeting and labeling of BLP

The characterized BLP were surface modified with preformed complexes of EGF-QDs to target the delivery system to cells overexpresssing the EGFR. As monocolor complexes of EGF-QD_{525}-BLP would not be distinguishable from free EGF-QD_{525} upon incubation with cells, two-color tagging approaches were designed to clearly identify the EGFR targeted particles (Fig. 4.1 and 4.8).

In the approach presented in Fig. 4.1, QDs play a dual rol acting as surface tag on the BLP carrier (QD_{525}) and as encapsulated cargo (QD_{655}). The rationale behind this two-color labeling strategy was that only QD_{525} and QD_{655} that are colocalized would indicate the intracellular distribution of the targeted BLP and the fate of loaded QDs. In a continuous monitoring of the delivery process by confocal microscopy, colocalization of both QDs can be interpreted as the persistence of the cargo in the delivery carrier, whereas a gradual loss of colocalization would indicate that QDs are being released.

The first observation was, that targeted EGF-QD_{525}-BLP-QD_{655} were internalized by the A431 cells, whereas non-targeted BLP-QD_{655} were not even bound to the membrane, suggesting that uptake of the particles was mediated by the EGFR (Fig. 4.2).

The labeled and targeted BLP were continuously monitored using confocal microscopy during cell binding and uptake for periods longer than 1h without significant photobleaching (Fig. 4.4), highlighting the convenience of QDs as labeling probes for long-term imaging of dynamic processes.

Upon internalization of EGF-QD_{525}-BLP-QD_{655}, the variations in the relative levels of colocalized intensities found for both QDs (Fig. 4.3 D-E) could have been due to an uneven distribution in the number of encapsulated QD_{655} and EGF-QD_{525} associated with individual BLP. Additionally, QDs intensity variation could be the result of endosomes fusion bringing several BLP together (Gruenberg *et al.*, 1989).

The colocalization of both QDs allowed a clear distinction between the targeted and QD_{655} loaded BLP (yellow-orange pseudocolors) and the independently internalized green

EGF-QD_{525} complexes (Fig. 4.3), avoiding the tedious purification of targeted BLP from free EGF-QDs.

When internalization was continuously monitored during 60 min, colocalized dots clustered around the perinuclear region of the cell (Fig. 4.4) indicating that they were sorted from early endosomes (Hopkins *et al.*, 1990). This observation was supported by cell uptake experiments and colocalization analysis in the presence of labeled Transferrin used as an early-endosome marker (Hanover *et al.*, 1984; Lamaze *et al.*, 1993). After 30 min only partial colocalization was observed and after 2 h no colocalization at all was evident between EGF and Transferrin (Fig. 4.5), indicating that EGF tagged BLP as well as EGF-QDs preformed complexes were likely sorted from early endosomes (Hanover *et al.*, 1984).

The specificity of EGF-QD_{525}-BLP-QD_{655} for the EGF receptor was supported by a competitive binding assay performed in the presence of 66-fold molar excess of free ligand EGF. Under these conditions, binding of EGF-QD_{525}-BLP-QD_{655} to A431 cells was completely abolished (Fig. 4.7A and B). In line with these observations, CHO cells and WM983A melanoma cells that do not express the EGFR showed no binding of the targeted particles (Fig. 4.7C and D).

As mentioned above the observed colocalization of both QDs after 2 h was interpreted as the persistence of the cargo in the delivery carrier. Therefore, the delivery ability of targeted BLP was examined after 4 and 12 h. Formulations of BLP-QDs containing a pH sensitive PEG-lipid were expected to promote BLP-endosome bilayers contact and destabilization by protonation during the acidification experienced in the endocytic process (Li *et al.*, 2005), whereas PEG-ceramides with short acyl carbon chains (Shi *et al.*, 2002) were expected to promote destabilization of BLP by lipid exchange. However, even for the lowest PEG content (1.4%) in BLP formulations, the presence of colocalizated QDs at 12 h after EGFR targeted delivery indicated that QDs remained encapsulated and presumably trapped in endo-lysosomal compartments (Fig.4.6). This finding could be explained by the shielding effect of PEG, which does not hinder the accesibilitiy of EGF, but presumably prevents the contact between BLP-endosome bilayers required for cargo release. These results obtained with QDs loaded particles suggested that DNA release could also be hampered assuming that encapsulated DNA would follow a similar route as the encapsulated QDs with identical formulation and similar size. Therefore, the following aim was to study the behavior of targeted and labeled BLP with encapsulated DNA by colocalization analysis employing the two-color labeling approach presented in Fig. 4.8. In this case, both QDs were surface-coupled to the BLP, while the encapsulated DNA was unlabeled. One of the QDs was carrying the ligand (EGF-QD_{525}) whereas the second color QD_{655} remained untargeted. As free QDs do not internalize into cells in the absence of ligand, the rationale behind this strategy was that only QD_{655} particles bound to EGF-QD_{525}-BLP-DNA would be endocytosed. Therefore, the intracellular fate of BLP-DNA was monitored by colocalization of both QDs and the ability to release the plasmid was examined quantifying the GFP expression from the reporter gene encapsulated in these targeted BLP. A remarkable observation was that only 10 min incubation with A431 cells was sufficient to promote receptor-mediated uptake of the targeted particles (Fig. 4.10) showing a similar time response as observed for BLP-QDs. After 48 h treated cells showed improved GFP expression demonstrating that, although at a very low efficiency, endosomal escape of plasmid was indeed taking place. The presence of targeted BLP (colocalized QDs) in cells that do not express GFP suggested that the low transfection levels reflect more a difficulty to achieve endosomal escape rather than a hindered binding or internalization. Consequently, the two-color labeling strategy proposed for BLP-DNA particles provided information about the efficiency of the gene delivery system as well as the potential barriers that BLP may encounter during the uptake process.

It was demonstrated by different approaches that the size of the carrier determines the internalization pathway as well as the processing of the gene carrier thus, directly affecting the transfection efficiency (Rejman *et al.*, 2004). In this connection, it was of interest to compare the targeting effect between non-purified BLP after detergent dialysis, still containing aggregates (>1 µm), and purified particles of discrete sizes <350 nm recovered from sucrose density gradient.

Due to the low levels of GFP expression obtained with the dual-labeled and targeted particles, a two-step targeting procedure was employed in order to decrease possible crosslinked aggregates between BLP and EGF-QDs and to improve the initial binding of BLP-DNA to cell receptors. First, A431cells were incubated with preformed complexes of EGF-QDs and, in a second step, incubated with BLP containing the same total amount of plasmid DNA. In the case of non-purified fractions, the total amount of DNA added included a 40% of free non-encapsulated plasmid, DNA loaded BLP and DNA containing aggregates and for purified fractions the total DNA plasmid added was considered to be encapsulated.

For non-purified fractions, a similar percentage of GFP expressing cells were determined for targeted and non-targeted delivery of BLP-DNA, evidencing that non-targeted particles were equally efficient to transfect cells as targeted particles. Since free plasmid added at equal amounts as the encapsulated DNA did not lead to GFP expression in cells, the transfection activity observed for non-purified fractions could have been generated by DNA-loaded BLP and aggregates of lipid-DNA, the later probably entering through another non-receptor mediated route.

Not surprisingly, targeted BLP showed a 3-fold increase in GFP expression after purification as compared to the purified but non-targeted particles (Table 4.1), indicating that after removing aggregates the contribution to the transfection activity by unspecific uptake was minimized.

The low (5%) overall efficiency of the targeted system was expected, considering that targeted BLP are formed by multivalent components. On one hand, the biotinylated particles contain, at least, two available biotins as has been demonstrated by colocalized dots upon surface tagging BLP with QD_{525} and QD_{655} (Fig. 4.10). The second multivalent component is the streptavidin-coated QD, which acts as a bridge to couple BLP and EGF in a single particle. Although the stoichiometry of EGF:QD ratio has been carefully controlled in cell binding experiments previously described in our lab (Lidke *et al.*, 2007), it was not evident that the addition of BLP, variable in size, to the remaining free streptavidins in EGF-QDs preformed complexes could have been equally controlled. Furthermore, due to this size variation within BLP, the number of biotin molecules per BLP could not be determined. Although increasing the number of EGF ligands per particle should in principle improve the binding to cells and increase the number of internalized particles, the larger size of the carrier would probably interfere with the receptor-mediated endocytosis. After ligand-induced receptor dimerization, autophosphorylation of the cytoplasmic domain of the tyrosine kinase receptor erbB1 (EGFR) is known to be essential for internalization through the rapid clathrin dependent route (Marmor *et al.*, 2004). The EGF induced stimulation and activation of the signalling cascade by targeted BLP is part of the ongoing work, relevant since EGFR activity controls a wide variety of biological responses (Bublil and Yarden, 2007).

6.3. Non-covalent Quantum Dot labeling of plasmid DNA

Elucidating the intracellular transport mechanisms of delivered genes has been a challenging task because of the difficulties in labeling DNA without affecting its biological activity. Labeling strategies to attach QDs to plasmids while maintaining a functional DNA are still required. A more recently approach is to bind non-covalently any label or biological entitiy to DNA by employing molecular beacons such as *bis*-PNA (Svahn *et al.*, 2004). PNA specifically hybridizes by strand invasion into a target sequence in supercoiled plasmid DNA providing a controlled and sequence specific tagging of DNA (Nielsen and Egholm, 1999).
Therefore, as a final aim, the idea of obtaining a QD labeled DNA as a potential cargo for the targeted BLP was appealing, since a labeled plasmid would provide information about the physical barriers encountered by the encapsulated plasmid and the efficiency of nuclear translocation upon DNA release.

In principle, a single QD per plasmid can provide enough signal for the detection at the single molecule level (Crut *et al.*, 2005). This is relevant since a single QD can be 2 to 10 fold larger than conventional organic fluorophores (Michalet *et al.*, 2005) and multiple QDs may affect the biological activity or nuclear translocation of the labeled plasmid. Consequently, the first task was to achieve the specific hybridization of a single biotin-*bis*-PNA entity synthetized to recognize a 12 bp target sequence in the plasmid pEGFP-C1. Once, the biotin-bis-PNA sequence specificity was demonstrated by band shift assay in gel electrophoresis (Fig. 5.2), the biotinylated Hybrids were labeled with StAv-QDs. Scanning by AFM indeed confirmed the presence of a single QD attached to the biotin-*bis*-PNA binding site in the plasmid (Fig. 5.5) and the labeled QD-Hybrids were clearly detected by fluorescence microscopy (Fig. 5.6). Although preliminary and still limited by the low yield of biotinylated Hybrids obtained, these QD-DNA particles appear as an attractive cargo for targeted BLP.

6.4. Rational liposome design

The increasing requirements of lipid-based delivery systems to accomplish their therapeutic activity have propelled multiple designs in which liposomes are viewed as a 'ready to use' toolbox able to open the route into the cells, increasing the efficacy while reducing the side effects (Torchilin, 2005; Dos Santos ***et al.***, 2007). In the schema of Fig. 6.1 a new-generation liposome is presented that can be modified either on its surface or by loading molecular entities in order to modulate stability, specificity, labeling and function. Among the chemical modifications that account for this versatility are:

a. surface coating with a protective polymer to favor long-term circulation and prevent unspecific interactions before reaching the target tissue.
b. inclusion of a positively charged lipid or polymer to condense and complex the loaded DNA.
c. addition of stimuli-sensitive lipids to promote the endosomal escape.
d. conjugation of a ligand to target a specific cell receptor.
e. coating with cell penetrating peptides to favour membrane translocation.
f. inclusion of a lipophilic drug to act as a therapeutic agent.

According to the results obtained during this thesis, the contribution proposed to the rational design involves:

g. labeling with two colors of QDs on the surface and in the internal space of the carrier for the real-time monitoring of cell binding, uptake and cargo release processes.
h. incorporation of plasmid labeled with a single StAv-QD that can be further modified, for instance with a biotinylated nuclear localization signal to drive the plasmid vector into the nucleus.

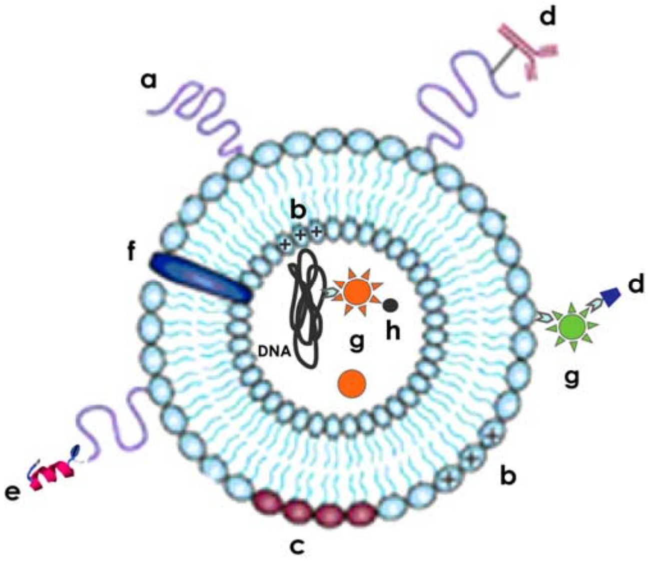

Figure 6.1: Schematic representation of a new-generation of BLP. See text for details. Adapted from (Torchilin, 2005).

In this thesis, I contributed by developing a multifunctional delivery system with sensitive detection. The addition of Quantum Dots into liposomal carriers with a dual rol, as cargo and as a surface tag will provide a flexible system for targeting and monitoring lipid-mediated delivery processes. The system will also contribute to a better understanding of the uptake mechanisms of liposomes by cells as well as the physical barriers to the effective gene or drug release and therapeutics.

7. Conclusions

The major outcome of this thesis was the design of a versatile lipid-based carrier, able to encapsulate small nanoparticles such as the fluorescent QDs for live-cell imaging and macromolecules with a potential therapeutic application such as plasmid DNA.

The targeting strategies applied combine the flexibility of the biotin-streptavidin linkage for ligand coupling, the photostability and bright fluorescence of QDs and the pharmacokinetic and drug delivery capabilities of sterically stabilized liposomes.

The optimization of the BLP formulation with other available pH-sensitive lipids and exchangeable lipids with high rate transfer to promote endosomal escape within minutes may certainly improve the gene delivery efficiency of the developed BLP system.

The knowledge of the average number of biotins per BLP will allow controlling the stoichiometry of ligand-QD preformed complexes that can be added to rationally improve cell binding conditions, particularly necessary in the case of certain tumor cells with overexpressed receptors that are rapidly cleared from the cell surface by ligand-induced endocytosis.

The bicolor QD labeling strategy for the BLP was designed for monitoring the specificity of BLP binding and uptake in live cells by fluorescence confocal microscopy. Despite the multivalency of the BLP and QDs, that prevents controlled stoichiometry of ligand-carrier, the overall specificity of the BLP system was not affected. The colocalization of green emitting QD_{525} and red emitting QD_{655}, allowed the immediate recognition of the targeted particles from the untargeted counterparts, as well as the presence of free EGF-QD_{525} complexes during live-cell imaging. A purification procedure, otherwise unavoidable in monocolor labeling, is by-passed.

The targeted and labeled BLP can serve as gene or QD delivery platform for targeting different tumor cells, providing a long-term probe for imaging and diagnosis. Any biotinylated ligand can be in principle conjugated to streptavidin-coated QDs whenever the size of the final complex does not interfere with its receptor recognition, internalization and intracellular function. This approach can be used to elucidate the fate of lipid particles in real time, providing more refined information on the still poorly understood trafficking process and subcellular barriers encountered by lipid-based carriers.

The non-covalent labeling of plasmid DNA using a single QD and a *bis*-PNA anchor directed to a specific target sequence is being conducted to further characterize the process involved in EGFR-targeted and non-targeted gene delivery. The preliminary results obtained open an interesting possibility for loading labeled DNA in BLP that can be tracked in real time to follow the route into the nucleus.

References

AL-JAMAL, W.T., and KOSTARELOS, K. (2007). Liposome-nanoparticle hybrids for multimodal diagnostic and therapeutic applications. In *Nanomed. pp.* 85-98.

ALIVISATOS, A.P., GU, W., and LARABELL, C. (2005). Quantum dots as cellular probes. Annu Rev Biomed Eng **7**, 55-76.

ANDERSON, W.F. (1998). Human gene therapy. Nature **392**, 25-30.

AUDOUY, S., and HOEKSTRA, D. (2001). Cationic lipid-mediated transfection in vitro and in vivo (review). Mol Membr Biol **18**, 129-143.

AUSTIN, C.P. (2004). The impact of the completed human genome sequence on the development of novel therapeutics for human disease. Annu Rev Med **55**, 1-13.

BAREFORD, L.M., and SWAAN, P.W. (2007). Endocytic mechanisms for targeted drug delivery. Adv Drug Deliv Rev **59**, 748-758.

BATCHELOR, R.H., SARKEZ, A., COX, W.G., and JOHNSON, I. (2007). Fluorometric assay for quantitation of biotin covalently attached to proteins and nucleic acids. Biotechniques **43**, 503-507.

BELTING, M., SANDGREN, S., and WITTRUP, A. (2005). Nuclear delivery of macromolecules: barriers and carriers. Adv Drug Deliv Rev **57**, 505-527.

BHADRA, D., BHADRA, S., JAIN, P., and JAIN, N.K. (2002). Pegnology: a review of PEG-ylated systems. Pharmazie **57**, 5-29.

BOECKLE, S., and WAGNER, E. (2006). Optimizing targeted gene delivery: chemical modification of viral vectors and synthesis of artificial virus vector systems. Aaps J **8**, E731-742.

BRANDEN, L.J., CHRISTENSSON, B., and SMITH, C.I. (2001). In vivo nuclear delivery of oligonucleotides via hybridizing bifunctional peptides. Gene Ther **8**, 84-87.

BUBLIL, E.M., and YARDEN, Y. (2007). The EGF receptor family: spearheading a merger of signaling and therapeutics. Curr Opin Cell Biol **19**, 124-134.

C. KIRCHNER, T.L., S. KUDERA, T. PELLEGRINO, A. MUNOZ JAVIER, and H.E. GAUB, S.S., N. FERTIG, W.J. PARAK. (2005). Cytotoxicity of colloidal CdSe and CdSe/ZnS nanoparticles. NanoLetters, 331-338.

CAMBI, A., LIDKE, D.S., ARNDT-JOVIN, D.J., FIGDOR, C.G., and JOVIN, T.M. (2007). Ligand-conjugated quantum dots monitor antigen uptake and processing by dendritic cells. In *Nano Lett. pp.* 970-977.

CHEN, J.T., CHEN, R.M., LIN, Y.L., CHANG, H.C., LIN, Y.H., CHEN, T.L., and CHEN, T.G. (2004). Confocal laser scanning microscopy: I. An overview of principle and practice in biomedical research. Acta Anaesthesiol Taiwan **42**, 33-40.

CHERNY, D.I., FOURCADE, A., SVINARCHUK, F., NIELSEN, P.E., MALVY, C., and DELAIN, E. (1998). Analysis of various sequence-specific triplexes by electron and atomic force microscopies. Biophys J **74**, 1015-1023.

CHOI, J.S., MACKAY, J.A., and SZOKA, F.C., JR. (2003). Low-pH-sensitive PEG-stabilized plasmid-lipid nanoparticles: preparation and characterization. Bioconjug Chem **14**, 420-429.

CHOU, T.H., BISWAS, S., and LU, S. (2004). Gene delivery using physical methods: an overview. Methods Mol Biol **245**, 147-166.

CIVIN, C.I. (2000). Gene therapy in clinical applications: overview: how do we translate gene therapy to clinical trials? Stem Cells **18**, 150-151.

COHEN, E.E. (2006). Role of epidermal growth factor receptor pathway targeted therapy in patients with recurrent and/or metastatic squamous cell carcinoma of the head and neck. J. Clin. Oncol. **24**, 2659–2665.

CORNETTA K, R.L., CROSS S. (2008). Production of retroviral vectors for clinical use. Methods Mol Biol., 17-32.

COSTES, S.V., DAELEMANS, D., CHO, E.H., DOBBIN, Z., PAVLAKIS, G., and LOCKETT, S. (2004). Automatic and quantitative measurement of protein-protein colocalization in live cells. Biophys J **86**, 3993-4003.

CRUT, A., GERON-LANDRE, B., BONNET, I., BONNEAU, S., DESBIOLLES, P., and ESCUDE, C. (2005). Detection of single DNA molecules by multicolor quantum-dot end-labeling. Nucleic Acids Res **33**, e98.

DAHAN, M., LEVI, S., LUCCARDINI, C., ROSTAING, P., RIVEAU, B., and TRILLER, A. (2003). Diffusion dynamics of glycine receptors revealed by single-quantum dot tracking. Science **302**, 442-445.

DANIELE GERION, F.P., SHARA C. WILLIAMS, WOLFGANG J. PARAK, DANIELA ZANCHET, SHIMON WEISS, AND A. PAUL ALIVISATOS. (2001). Synthesis and properties of biocompatible water-soluble silicacoated CdSe/ZnS semiconductor quantum dots. Journal of Physical Chemistry B **105**.

DEMIDOV, V.V., KUHN, H., LAVRENTIEVA-SMOLINA, I.V., and FRANK-KAMENETSKII, M.D. (2001). Peptide nucleic acid-assisted topological labeling of duplex dna. Methods **23**, 123-131.

DOS SANTOS, N., ALLEN, C., DOPPEN, A.M., ANANTHA, M., COX, K.A., GALLAGHER, R.C., KARLSSON, G., EDWARDS, K., KENNER, G., SAMUELS, L., WEBB, M.S., and BALLY, M.B. (2007). Influence of poly(ethylene glycol) grafting density and polymer length on liposomes: relating plasma circulation lifetimes to protein binding. Biochim Biophys Acta **1768**, 1367-1377.

EDELSTEIN, M.L., ABEDI, M.R., and WIXON, J. (2007). Gene therapy clinical trials worldwide to 2007--an update. J Gene Med **9**, 833-842.

FELGNER, P.L., GADEK, T.R., HOLM, M., ROMAN, R., CHAN, H.W., WENZ, M., NORTHROP, J.P., RINGOLD, G.M., and DANIELSEN, M. (1987). Lipofection: a highly efficient, lipid-mediated DNA-transfection procedure. Proc Natl Acad Sci U S A **84**, 7413-7417.

FELGNER, P.L., and RINGOLD, G.M. (1989). Cationic liposome-mediated transfection. Nature **337**, 387-388.

FENSKE, D.B., and CULLIS, P.R. (2005). Entrapment of small molecules and nucleic acid-based drugs in liposomes. Methods Enzymol **391**, 7-40.

FENSKE, D.B., MACLACHLAN, I., and CULLIS, P.R. (2002). Stabilized plasmid-lipid particles: a systemic gene therapy vector. Methods Enzymol **346**, 36-71.

GRUENBERG, J., GRIFFITHS, G., and HOWELL, K.E. (1989). Characterization of the early endosome and putative endocytic carrier vesicles in vivo and with an assay of vesicle fusion in vitro. J Cell Biol **108**, 1301-1316.

GUO, X., MACKAY, J.A., and SZOKA, F.C., JR. (2003). Mechanism of pH-triggered collapse of phosphatidylethanolamine liposomes stabilized by an ortho ester polyethyleneglycol lipid. Biophys J **84**, 1784-1795.

GUO, X., and SZOKA, F.C., JR. (2001). Steric stabilization of fusogenic liposomes by a low-pH sensitive PEG--diortho ester--lipid conjugate. Bioconjug Chem **12**, 291-300.

GUPTA, B., LEVCHENKO, T.S., and TORCHILIN, V.P. (2005). Intracellular delivery of large molecules and small particles by cell-penetrating proteins and peptides. Adv Drug Deliv Rev **57**, 637-651.

GUY, J., DRABEK, D., and ANTONIOU, M. (1995). Delivery of DNA into mammalian cells by receptor-mediated endocytosis and gene therapy. In *Mol Biotechnol*. *pp*. 237-248.

HAFEZ, I.M., and CULLIS, P.R. (2001). Roles of lipid polymorphism in intracellular delivery. Adv Drug Deliv Rev **47**, 139-148.

HANOVER, J.A., WILLINGHAM, M.C., and PASTAN, I. (1984). Kinetics of transit of transferrin and epidermal growth factor through clathrin-coated membranes. Cell **39**, 283-293.

HARRIS, J.M., and CHESS, R.B. (2003). Effect of pegylation on pharmaceuticals. Nat Rev Drug Discov **2**, 214-221.

HARVIE, P., WONG, F.M., and BALLY, M.B. (2000). Use of poly(ethylene glycol)-lipid conjugates to regulate the surface attributes and transfection activity of lipid-DNA particles. J Pharm Sci **89**, 652-663.

HEATH, F., HARIA, P., and ALEXANDER, C. (2007). Varying polymer architecture to deliver drugs. Aaps J **9**, E235-240.

HICKS, J. (2003). Genome, proteome, and metabolome: where are we going? Ultrastruct Pathol **27**, 289-294.

HILGENBRINK, A.R., and LOW, P.S. (2005). Folate receptor-mediated drug targeting: from therapeutics to diagnostics. J Pharm Sci **94**, 2135-2146.

HOEKSTRA, D., REJMAN, J., WASUNGU, L., SHI, F., and ZUHORN, I. (2007). Gene delivery by cationic lipids: in and out of an endosome. Biochem Soc Trans **35**, 68-71.

HOFLAND, H.E., MASSON, C., IGINLA, S., OSETINSKY, I., REDDY, J.A., LEAMON, C.P., SCHERMAN, D., BESSODES, M., and WILS, P. (2002). Folate-targeted gene transfer in vivo. Mol Ther **5**, 739-744.

HOFLAND, H.E., SHEPHARD, L., and SULLIVAN, S.M. (1996). Formation of stable cationic lipid/DNA complexes for gene transfer. Proc Natl Acad Sci U S A **93**, 7305-7309.

HOPKINS, C.R., GIBSON, A., SHIPMAN, M., and MILLER, K. (1990). Movement of internalized ligand-receptor complexes along a continuous endosomal reticulum. Nature **346**, 335-339.

HOPKINS, C.R., MILLER, K., and BEARDMORE, J.M. (1985). Receptor-mediated endocytosis of transferrin and epidermal growth factor receptors: a comparison of constitutive and ligand-induced uptake. J Cell Sci Suppl **3**, 173-186.

JEAN-LOUIS RIGAUD, D.L., GERVAISE MOSSER, OLIVER LAMBERT. (1998). Detergent removal by non-polar polystyrene beads. Applications to membrane protein reconstitution and two-dimensional crystallization. Eur Biophys J, 305–319.

JOHNSTON, J.B., NAVARATNAM, S., PITZ, M.W., MANIATE, J.M., WIECHEC, E., BAUST, H., GINGERICH, J., SKLIRIS, G.P., MURPHY, L.C., and LOS, M. (2006). Targeting the EGFR pathway for cancer therapy. Curr Med Chem **13**, 3483-3492.

KAKUDO, T., CHAKI, S., FUTAKI, S., NAKASE, I., AKAJI, K., KAWAKAMI, T., MARUYAMA, K., KAMIYA, H., and HARASHIMA, H. (2004). Transferrin-modified liposomes equipped with a pH-sensitive fusogenic peptide: an artificial viral-like delivery system. Biochemistry **43**, 5618-5628.

KATO, Y., and SUGIYAMA, Y. (1997). Targeted delivery of peptides, proteins, and genes by receptor-mediated endocytosis. Crit Rev Ther Drug Carrier Syst **14**, 287-331.

KIRPOTIN, D., HONG, K., MULLAH, N., PAPAHADJOPOULOS, D., and ZALIPSKY, S. (1996). Liposomes with detachable polymer coating: destabilization and fusion of dioleoylphosphatidylethanolamine vesicles triggered by cleavage of surface-grafted poly(ethylene glycol). FEBS Lett **388**, 115-118.

KNEUER, C., EHRHARDT, C., BAKOWSKY, H., KUMAR, M.N., OBERLE, V., LEHR, C.M., HOEKSTRA, D., and BAKOWSKY, U. (2006). The influence of physicochemical parameters on the efficacy of non-viral DNA transfection complexes: a comparative study. J Nanosci Nanotechnol **6**, 2776-2782.

KRAMER, M., STUMBE, J.F., GRIMM, G., KAUFMANN, B., KRUGER, U., WEBER, M., and HAAG, R. (2004). Dendritic polyamines: simple access to new materials with defined treelike structures for application in nonviral gene delivery. Chembiochem **5**, 1081-1087.

KREFT, M., MILISAV, I., POTOKAR, M., and ZOREC, R. (2004). Automated high through-put colocalization analysis of multichannel confocal images. Comput Methods Programs Biomed **74**, 63-67.

KULLBERG, E.B., NESTOR, M., and GEDDA, L. (2003). Tumor-cell targeted epiderimal growth factor liposomes loaded with boronated acridine: uptake and processing. Pharm Res **20**, 229-236.

KULLBERG, E.B., WEI, Q., CAPALA, J., GIUSTI, V., MALMSTROM, P.U., and GEDDA, L. (2005). EGF-receptor targeted liposomes with boronated acridine: growth inhibition of cultured glioma cells after neutron irradiation. Int J Radiat Biol **81**, 621-629.

LAMAZE, C., BABA, T., REDELMEIER, T.E., and SCHMID, S.L. (1993). Recruitment of epidermal growth factor and transferrin receptors into coated pits in vitro: differing biochemical requirements. Mol Biol Cell **4**, 715-727.

LASIC, D.D., MARTIN, F.J., GABIZON, A., HUANG, S.K., and PAPAHADJOPOULOS, D. (1991). Sterically stabilized liposomes: a hypothesis on the molecular origin of the extended circulation times. Biochim Biophys Acta **1070**, 187-192.

LASIC, D.D., and PAPAHADJOPOULOS, D. (1995). Liposomes revisited. Science **267**, 1275-1276.

LASIC, D.D., VALLNER, J.J., and WORKING, P.K. (1999). Sterically stabilized liposomes in cancer therapy and gene delivery. Curr Opin Mol Ther **1**, 177-185.

LECHARDEUR, D., VERKMAN, A.S., and LUKACS, G.L. (2005). Intracellular routing of plasmid DNA during non-viral gene transfer. Adv Drug Deliv Rev **57**, 755-767.

LI, W., HUANG, Z., MACKAY, J.A., GRUBE, S., and SZOKA, F.C., JR. (2005). Low-pH-sensitive poly(ethylene glycol) (PEG)-stabilized plasmid nanolipoparticles: effects of PEG chain length, lipid composition and assembly conditions on gene delivery. J Gene Med **7**, 67-79.

LI, Z.B., CAI, W., and CHEN, X. (2007). Semiconductor quantum dots for in vivo imaging. J Nanosci Nanotechnol **7**, 2567-2581.

LIDKE, D.S., LIDKE, K.A., RIEGER, B., JOVIN, T.M., and ARNDT-JOVIN, D.J. (2005). Reaching out for signals: filopodia sense EGF and respond by directed retrograde transport of activated receptors. J Cell Biol **170**, 619-626.

LIDKE, D.S., NAGY, P., HEINTZMANN, R., ARNDT-JOVIN, D.J., POST, J.N., GRECCO, H.E., JARES-ERIJMAN, E.A., and JOVIN, T.M. (2004). Quantum dot ligands provide new insights into erbB/HER receptor-mediated signal transduction. Nat Biotechnol **22**, 198-203.

LIDKE, D.S., NAGY, P., JOVIN, T.M., and ARNDT-JOVIN, D.J. (2007). Biotin-ligand complexes with streptavidin quantum dots for in vivo cell labeling of membrane receptors. Methods Mol Biol **374**, 69-79.

LUO, D., and SALTZMAN, W.M. (2000). Synthetic DNA delivery systems. Nat Biotechnol **18**, 33-37.

MAMOT, C., DRUMMOND, D.C., NOBLE, C.O., KALLAB, V., GUO, Z., HONG, K., KIRPOTIN, D.B., and PARK, J.W. (2005). Epidermal growth factor receptor-targeted immunoliposomes significantly enhance the efficacy of multiple anticancer drugs in vivo. Cancer Res **65**, 11631-11638.

MARMOR, M.D., SKARIA, K.B., and YARDEN, Y. (2004). Signal transduction and oncogenesis by ErbB/HER receptors. Int J Radiat Oncol Biol Phys **58**, 903-913.

MAURER, N., MORI, A., PALMER, L., MONCK, M.A., MOK, K.W., MUI, B., AKHONG, Q.F., and CULLIS, P.R. (1999). Lipid-based systems for the intracellular delivery of genetic drugs. Mol Membr Biol **16**, 129-140.

MAXFIELD, F.R., and YAMASHIRO, D.J. (1987). Endosome acidification and the pathways of receptor-mediated endocytosis. Adv Exp Med Biol **225**, 189-198.

MAYER, L.D., TAI, L.C., KO, D.S., MASIN, D., GINSBERG, R.S., CULLIS, P.R., and BALLY, M.B. (1989). Influence of vesicle size, lipid composition, and drug-to-lipid ratio on the biological activity of liposomal doxorubicin in mice. Cancer Res **49**, 5922-5930.

MEHIER-HUMBERT, S., and GUY, R.H. (2005). Physical methods for gene transfer: improving the kinetics of gene delivery into cells. Adv Drug Deliv Rev **57**, 733-753.

MERKLEB, R.T.A.H.P. (2004). Chances and pitfalls of cell penetrating peptides for cellular drug delivery. European Journal of Pharmaceutics and Biopharmaceutics **58**, 209-223.

MICHALET, X., PINAUD, F.F., BENTOLILA, L.A., TSAY, J.M., DOOSE, S., LI, J.J., SUNDARESAN, G., WU, A.M., GAMBHIR, S.S., and WEISS, S. (2005). Quantum dots for live cells, in vivo imaging, and diagnostics. Science **307**, 538-544.

MOK, K.W., LAM, A.M., and CULLIS, P.R. (1999). Stabilized plasmid-lipid particles: factors influencing plasmid entrapment and transfection properties. Biochim Biophys Acta **1419**, 137-150.

MONCK, M.A., MORI, A., LEE, D., TAM, P., WHEELER, J.J., CULLIS, P.R., and SCHERRER, P. (2000). Stabilized plasmid-lipid particles: pharmacokinetics and plasmid delivery to distal tumors following intravenous injection. J Drug Target **7**, 439-452.

MOUSAVI, S.A., MALEROD, L., BERG, T., and KJEKEN, R. (2004). Clathrin-dependent endocytosis. Biochem J **377**, 1-16.

NIELSEN, P.E., and EGHOLM, M. (1999). An introduction to peptide nucleic acid. Curr Issues Mol Biol **1**, 89-104.

PARK, J.W., KIRPOTIN, D.B., HONG, K., SHALABY, R., SHAO, Y., NIELSEN, U.B., MARKS, J.D., PAPAHADJOPOULOS, D., and BENZ, C.C. (2001). Tumor targeting using anti-her2 immunoliposomes. J Control Release **74**, 95-113.

PAYNE, C.K. (2007). Imaging gene delivery with fluorescence microscopy. Nanomed **2**, 847-860.

PECORA, R., and ARAGON, S.R. (1974). Theory of light scattering from hollow spheres. Chem Phys Lipids **13**, 1-10.

PELKMANS, L., BURLI, T., ZERIAL, M., and HELENIUS, A. (2004). Caveolin-stabilized membrane domains as multifunctional transport and sorting devices in endocytic membrane traffic. Cell **118**, 767-780.

PROVENCHER, S.W. (1982). CONTIN: A general purpose constrained regularization program for inverting noisy linear algebraic and integral equations. Comp. Phys. Commun., 229-242.

REJMAN, J., OBERLE, V., ZUHORN, I.S., and HOEKSTRA, D. (2004). Size-dependent internalization of particles via the pathways of clathrin- and caveolae-mediated endocytosis. Biochem J **377**, 159-169.

RUBIN GRANDIS, J.M., M. F.; GOODING, W. E.; DAY, R.; HOLST, and V. A.; WAGENER, M.M.D., S. D.; TWEARDY, D. J. (1998). Levels of TGF-alpha and EGFR protein in head and neck squamous cell carcinoma and patient survival. J. Natl. Cancer Inst. **90**, 824–832.

RUOZI, B., TOSI, G., FORNI, F., FRESTA, M., and VANDELLI, M.A. (2005). Atomic force microscopy and photon correlation spectroscopy: two techniques for rapid characterization of liposomes. Eur J Pharm Sci **25**, 81-89.

SHEPHERD, V.L. (1989). Intracellular pathways and mechanisms of sorting in receptor-mediated endocytosis. Trends Pharmacol Sci **10**, 458-462.

SHI, F., and HOEKSTRA, D. (2004). Effective intracellular delivery of oligonucleotides in order to make sense of antisense. J Control Release **97**, 189-209.

SHI, F., WASUNGU, L., NOMDEN, A., STUART, M.C., POLUSHKIN, E., ENGBERTS, J.B., and HOEKSTRA, D. (2002). Interference of poly(ethylene glycol)-lipid analogues with cationic-lipid-mediated delivery of oligonucleotides; role of lipid exchangeability and non-lamellar transitions. Biochem J **366**, 333-341.

SHIR, A., OGRIS, M., WAGNER, E., and LEVITZKI, A. (2006). EGF receptor-targeted synthetic double-stranded RNA eliminates glioblastoma, breast cancer, and adenocarcinoma tumors in mice. PLoS Med **3**, e6.

SIMOES, S., FILIPE, A., FANECA, H., MANO, M., PENACHO, N., DUZGUNES, N., and DE LIMA, M.P. (2005). Cationic liposomes for gene delivery. Expert Opin Drug Deliv **2**, 237-254.

SIMONSON, O.E., SVAHN, M.G., TORNQUIST, E., LUNDIN, K.E., and SMITH, C.I. (2005). Bioplex technology: novel synthetic gene delivery pharmaceutical based on peptides anchored to nucleic acids. Curr Pharm Des **11**, 3671-3680.

SMITH, A.M., GAO, X., and NIE, S. (2004). Quantum dot nanocrystals for in vivo molecular and cellular imaging. Photochem Photobiol **80**, 377-385.

SOFOU, S., and SGOUROS, G. (2008). Antibody-targeted liposomes in cancer therapy and imaging. Expert Opin Drug Deliv **5**, 189-204.

SONG, L.Y., AHKONG, Q.F., RONG, Q., WANG, Z., ANSELL, S., HOPE, M.J., and MUI, B. (2002). Characterization of the inhibitory effect of PEG-lipid conjugates on the intracellular delivery of plasmid and antisense DNA mediated by cationic lipid liposomes. Biochim Biophys Acta **1558**, 1-13.

SPERLING, R., ET AL. (2006). Electrophoretic Separation of Nanoparticles with a Discrete Number of Functional Groups. Advanced Functional Materials **26**, 943-948.

SVAHN, M.G., LUNDIN, K.E., GE, R., TORNQUIST, E., SIMONSON, E.O., OSCARSSON, S., LEIJON, M., BRANDEN, L.J., and SMITH, C.I. (2004). Adding functional entities to plasmids. J Gene Med **6 Suppl 1**, S36-44.

SZOKA, F., JR., and PAPAHADJOPOULOS, D. (1980). Comparative properties and methods of preparation of lipid vesicles (liposomes). Annu Rev Biophys Bioeng **9**, 467-508.

TORCHILIN, V.P. (2005). Recent advances with liposomes as pharmaceutical carriers. Nat Rev Drug Discov **4**, 145-160.

TORCHILIN, V.P. (2006). Recent approaches to intracellular delivery of drugs and DNA and organelle targeting. Annu Rev Biomed Eng **8**, 343-375.

TORCHILIN, V.P., LEVCHENKO, T.S., RAMMOHAN, R., VOLODINA, N., PAPAHADJOPOULOS-STERNBERG, B., and D'SOUZA, G.G. (2003). Cell transfection in vitro and in vivo with nontoxic TAT peptide-liposome-DNA complexes. Proc Natl Acad Sci U S A **100**, 1972-1977.

UDENFRIEND, S., STEIN, S., BOHLEN, P., DAIRMAN, W., LEIMGRUBER, W., and WEIGELE, M. (1972). Fluorescamine: a reagent for assay of amino acids, peptides, proteins, and primary amines in the picomole range. Science **178**, 871-872.

VIVES, R.R., LORTAT-JACOB, H., and FENDER, P. (2006). Heparan sulphate proteoglycans and viral vectors: ally or foe? Curr Gene Ther **6**, 35-44.

VONDERHEIT, A., and HELENIUS, A. (2005). Rab7 associates with early endosomes to mediate sorting and transport of Semliki forest virus to late endosomes. PLoS Biol **3**, e233.

WAGNER, E. (2007). Advances in cancer gene therapy: tumor-targeted delivery of therapeutic pDNA, siRNA, and dsRNA nucleic acids. J Buon **12 Suppl 1**, S77-82.

WASUNGU, L., and HOEKSTRA, D. (2006). Cationic lipids, lipoplexes and intracellular delivery of genes. J Control Release **116**, 255-264.

WEEKE-KLIMP, A.H., BARTSCH, M., MORSELT, H.W., VAN VEEN-HOF, I., MEIJER, D.K., SCHERPHOF, G.L., and KAMPS, J.A. (2007). Targeting of stabilized plasmid lipid particles to hepatocytes in vivo by means of coupled lactoferrin. J Drug Target **15**, 585-594.

WEI, Q., KULLBERG, E.B., and GEDDA, L. (2003). Trastuzumab-conjugated boron-containing liposomes for tumor-cell targeting; development and cellular studies. Int J Oncol **23**, 1159-1165.

WEIJUN LI, F.C.S.J. (2007). Lipid-based Nanoparticles for Nucleic Acid Delivery. Pharmaceutical Research **24**.

WHEELER, J.J., PALMER, L., OSSANLOU, M., MACLACHLAN, I., GRAHAM, R.W., ZHANG, Y.P., HOPE, M.J., SCHERRER, P., and CULLIS, P.R. (1999). Stabilized plasmid-lipid particles: construction and characterization. Gene Ther **6**, 271-281.

WOODLE, M.C., and LASIC, D.D. (1992). Sterically stabilized liposomes. Biochim Biophys Acta **1113**, 171-199.

XIAOHU GAO, Y.C., RICHARD M LEVENSON, LELAND W K CHUNG AND SHUMING NIE. (2004). In vivo cancer targeting and imaging with semiconductor quantum dots. Nature Biotechnology **22**, 969-976.

YARDEN, Y. (2001). The EGFR family and its ligands in human cancer. signalling mechanisms and therapeutic opportunities. Eur J Cancer **37 Suppl 4**, S3-8.

ZHANG, X., and GODBEY, W.T. (2006). Viral vectors for gene delivery in tissue engineering. Adv Drug Deliv Rev **58**, 515-534.

ZHANG, Y., KAJI, N., TOKESHI, M., and BABA, Y. (2007). Nanobiotechnology: quantum dots in bioimaging. Expert Rev Proteomics **4**, 565-572.

ZHANG, Y.P., REIMER, D.L., ZHANG, G., LEE, P.H., and BALLY, M.B. (1997). Self-assembling DNA-lipid particles for gene transfer. Pharm Res **14**, 190-196.

ZHANG, Y.P., SEKIROV, L., SARAVOLAC, E.G., WHEELER, J.J., TARDI, P., CLOW, K., LENG, E., SUN, R., CULLIS, P.R., and SCHERRER, P. (1999). Stabilized plasmid-lipid particles for regional gene therapy: formulation and transfection properties. Gene Ther **6**, 1438-1447.

ZUHORN, I.S., BAKOWSKY, U., POLUSHKIN, E., VISSER, W.H., STUART, M.C., ENGBERTS, J.B., and HOEKSTRA, D. (2005). Nonbilayer phase of lipoplex-membrane mixture determines endosomal escape of genetic cargo and transfection efficiency. Mol Ther **11**, 801-810.

ZUIDAM, N.J., and BARENHOLZ, Y. (1999). Characterization of DNA-lipid complexes commonly used for gene delivery. Int J Pharm **183**, 43-46.

ZUMBUEHL, O., and WEDER, H.G. (1981). Liposomes of controllable size in the range of 40 to 180 nm by defined dialysis of lipid/detergent mixed micelles. Biochim Biophys Acta **640**, 252-262.

Acknowledgments

In first place, I would like to thank Dr. Thomas Jovin, for teaching me the art of critical scientific thinking and for his outstanding and multiples ideas during the supervision of this study. I also gratefully acknowledge the essential suggestions and discussions from Dr. Donna Arndt-Jovin that allowed the accomplishment of this thesis.

I am indebted to Prof. Dr. Hans-Joachim Fritz and Prof. Dr. Hardeland for being the referent and co-referent of this thesis work, respectively.

I particularly acknowledge Dr. Dietmar Riedel for performing the Electron Microscopy analysis.

Many people were involved at different points of this thesis project and the outcome of this work would have not been possible without such contributions. Special thanks to Reinhard Klement for his continuous support with computers and softwares. Technical assistance has been essential at many stages of this work, special thanks for Joachim Dichter for his expertise in flow cytometry, Danny in assistance with cell cultures, Gudrun Heim for introducing me into the AFM field and Annelies Zechel for her kind help and patience at the beginning of this work. *Vielen Dank Monika und Ingrid* for silent and efficient technical support but personally I will never forget their patient German lessons and never-ending smiles.

Special 'Vielen Dank' for Secretary Renate Jenssen who always surprised me with her efficiency and for appropiate words of advice but above all for her personal and generous care with situations many times beyond her duties.

I greatly acknowledge the help from Guy Hagen and Anthony Devries for helping me with the microscopes and camera settings and thanks to Wouter Caarls for quantitative image analysis. I gratefully acknowledge the suggestions from Elizabeth Jares-Erijman during her short visits to the lab.

Many warm thanks to my colleagues and friends at the Lab of Cellular Dynamics for creating such an 'international' environment, thanks to it I never learnt proper German: Carlos, Julia, Guy, Avishay, Wouter, Shyamala, Anthony, Atul, Alessandra, Cornelia, Wolfgang, Bernd, Gaby, Vlad, Diane, Keith, Rolf and Yanine.

Very special and warm thanks for Michelle, always ready to help and cook! and for Sole who greatly contributed in the last taugh part of the writting process, both great researchers but above all my great friends.

Finally, this work would not have been possible without the endless support from 'mi amado Fito' who greatly helped me through the hopeless times of this work and the long chats on the phone with my parents and brothers who always cheered me up.

Publications related to this thesis project

- *Elizabeth A. Jares-Erijman, Avishay Pelah, María Julia Roberti,* ***Valeria Sigot****, Lia Pietrasanta, Guillermo Menendez, Maria H. Etchehon, and Thomas M. Jovin.* USE OF LUMINESCENT QUANTUM DOTS TO IMAGE AND INITIATE BIOLOGICAL FUNCTIONS.
Chapter for book Inorganic Nanoprobes for Biological Sensing and Imaging Editors: Jinwoo Cheon & Hedi Mattoussi. Artech House Publisher. In press.

- ***V. Sigot*** *and T. Jovin* "Quantum Dots, torch bearers into cells" (2008) *GIT Imaging & Microscopy* 10 (1): 40-43.

- *M.G. Svahn, M. Hasan,* ***V. Sigot****, J.J. Valle-Delgado, M.W. Rutland, K. E. Lundin and C.I. Edvard Smith* "Self-Assembling Supramolecular Complexes by Single-Stranded Extension from Plasmid DNA" (2007) *Oligonucleotides* 17:80-94

Scientific Meetings and Simposia

- *Poster presentation: "Quantum dots-tagged liposomes: stable fluorescent nanoparticles with multivalent binding sites for targeted cell delivery".* ***V. Sigot*** *and T. M. Jovin. FOM2007 Conference, Focus on Microscopy. April 10th-13th, 2007, Valencia, Spain.*

- *Poster presentation: "Quantum dots labeled liposomes for targeted delivery".* ***V. Sigot****, D.J. Arndt-Jovin and T. M. Jovin. 3th International PhD Student Symposium 'Horizons'. September 14th-16th, 2006, Göttingen, Germany.*

- *Oral presentations: "Strategy for plasmid based gene delivery in cells through ligand-receptor interaction".* ***V. Sigot,*** *D.J. Arndt-Jovin and T. M. Jovin. EURO GENE DRUG PROJECT Meeting Reports; June 10th, 2004, Zurich, Switzerland; November 12th-13th, 2004, Göttingen, Germany; May 5th-6th, 2005, Stockholm, Sweden.*

Lebenslauf

Name: *Valeria Sigot*

Geburtsdatum: *19. Mai 1972*

Geburtsort: *Santa Fe, Argentinien*

Nationalität: *argentinisch*

Adresse: *12 Rue Dominique Villars, 38000 Grenoble (Frankreich)*

Bildungsweg:

1978 – 1984: *Grundschule „ Escuela N° 88 Juana Manso“, Rosario, Argentinien.*

1985-1989: *Gymnasium „Escuela Nacional Normal Superior en Lenguas Vivas N°1 de Rosario”, Argentinien.*

1990-1999: *Studium der Biotechnologie an der „Universidad Nacional de Rosario“, Rosario, Argentinien, mit einem Diplomabschluss in Biotechnologie.*

1999-2000: *Wissenschaftlerin am Instituto de Estudios Bioquimicos IDEB, Rosario, Argentinien.*

2000-2004: *Wissenschaftlerin an der „Universidad Nacional de Rosario“, Argentinien.*

Seit 2004: *Promotion an der Georg-August Universität, Göttingen, Doktorarbeit am Max-Planck-Institut für Biophysikalische Chemie, Göttingen, mit dem Thema „Receptor mediated gene delivery using Quantum Dots and liposomes“ bei Prof. Dr. Thomas Jovin.*